MICROCOPY RESOLUTION TEST CHART

NATIONAL BUREAU OF STANDARDS 1963 A

79- 0 5 3 5

DTIC
ELECTE
DEC 1 3 1984
B

84 12 05 096

CAMBRIDGE HYDRODYNAMICS REPORT NO. 10

TRANSITION TO TURBULENCE IN PLANE POISEUILLE
AND PLANE COUETTE FLOW

STEVEN A. ORSZAG AND LAWRENCE C. KELLS

REVISED SEPTEMBER 1978

DTIC
ELECTE
DEC 1 3 1984

B

Abstract

Direct numerical solutions of the three-dimensional
time-dependent Navier-Stokes equations are presented for the
evolution of three-dimensional finite-amplitude disturbances
of plane Poiseuille and plane Couette flows. Spectral methods
using Fourier series and Chebyshev polynomial series are used.
It is found that plane Poiseuille flow can sustain neutrally
stable two-dimensional finite-amplitude disturbances at
Reynolds numbers larger than about 2800. No neutrally stable
two-dimensional finite amplitude disturbances of plane
Couette flow were found.

Three-dimensional disturbances are shown to have a strongly
destabilizing effect. It is shown that finite-amplitude
disturbances can drive transition to turbulence in both plane
Poiseuille flow and plane Couette flow at Reynolds numbers
of order 1000. Details of the resulting flow fields are
presented. It is also shown that plane Poiseuille flow can not
sustain turbulence at Reynolds numbers below about 500.

1

1. Introduction

One of the oldest unsolved problems of fluid mechanics is the theoretical description of the inception and growth of instabilities in laminar shear flows that lead to transition to turbulence. The behavior of small amplitude disturbances on a laminar flow is reasonably well understood, but understanding of the behavior of finite amplitude disturbances is in a much less satisfactory state. There is as yet no close agreement between theoretical and experimental studies of transition flows.

In the laboratory, Davies & White (1928), Kao & Park (1970), and Patel & Head (1969) have shown that plane Poiseuille flow is unstable to finite amplitude disturbances at Reynolds numbers as low as 1000 and that initially turbulent flow remains turbulent at slightly lower Reynolds numbers. Here the Reynolds number is $R = Uh/\nu$, where U is the maximum downstream velocity, h is the half-channel depth and ν is the kinematic viscosity. On the other hand, Nishioka, Iida & Ichikawa (1975) performed experiments in a low-turbulence wind-tunnel in which they were able to maintain laminar plane Poiseuille flow at Reynolds numbers as large as 8000. In order to postpone transition to $R = 8000$, Nishioka et al had to reduce the background turbulence level to less than 0.05%. At larger disturbance levels, instabilities were obtained at lower (subcritical) Reynolds numbers. The experiments of Nishioka et al were performed in a channel with aspect ratio (ratio of width to depth of

channel) of 27.4. At lower aspect ratios,

the channel geometry may induce significant three-dimen-
sionality that may drive transition at lower R . This latter
effect may influence the results of Kao & Park but
should not affect those of Davies & White and Patel & Head.
Thus, it appears that the transition Reynolds number
observed experimentally depends on both the spectrum and
amplitude of the initial two and three-dimensional dist-
urbances to the flow. Typically, transition is observed
at Reynolds numbers of about 1000.

The experimental situation with regard to plane Couette
flow is far less satisfactory. Reichardt (1959) showed that
a turbulent flow is obtained at Reynolds numbers
(based on half-channel depth and wall velocity) as low as
750. Mollo-Christensen (private communication) has obtained
similar results. These experimental findings may be subject to
dispute because of end effects which ,it seems, are difficult to remove.
In summary, the only experimental evidence available to
date suggests that plane Couette flow undergoes transition
at Reynolds numbers similar to those of plane Poiseuille
flow.

Some insight into the mechanism of transition in planar
shear flows was given by the pioneering experiments of
Klebanoff, Tidstrom, & Sargent (1962) who studied the

evolution of a controlled three-dimensional disturbance
in a laminar boundary layer. They found that prod-
uction of longitudinal vorticity by the three-dimensional
disturbance gives a secondary motion that creates local
inflectional profiles; the resulting highly unstable profiles lead
almost instantaneously to turbulent spots. The key result obtained by
Klebanoff et al is that initially weak three-dimensional
disturbances may control the nonlinear development of the
flow and its transition to turbulence. In this paper we
expand on this idea by studying whether a similar effect
can control the transition to turbulence in plane Poiseuille
and plane Couette flow.

Let us begin by reviewing theoretical approaches to
these problems. The equations of motion are the Navier-
Stokes equations

$$\frac{\partial \underset{\sim}{v}(\underset{\sim}{x},t)}{\partial t} + \underset{\sim}{v}(\underset{\sim}{x},t) \cdot \underset{\sim}{\nabla} \underset{\sim}{v}(\underset{\sim}{x},t) = - \underset{\sim}{\nabla} p(\underset{\sim}{x},t) + \nu \nabla^2 \underset{\sim}{v}(\underset{\sim}{x},t) \qquad (1.1)$$

$$\underset{\sim}{\nabla} \cdot \underset{\sim}{v}(\underset{\sim}{x},t) = 0 \qquad (1.2)$$

where $\underset{\sim}{v}(\underset{\sim}{x},t) = (u,v,w)$ is the velocity field at location
$\underset{\sim}{x} = (x,y,z)$ and time t, $p(\underset{\sim}{x},t)$ is the pressure (divided
by density), and ν is the kinematic viscosity. To date there
is no compelling evidence that the Navier-Stokes equations are

4

in any way inadequate on the space- and time-scales involved in transition and turbulence.

The flows discussed in the present paper are confined between rigid walls at $z = \pm 1$ and extend to infinity in the horizontal directions x, y. The boundary conditions at the rigid walls $z = \pm 1$ are that the velocity of the fluid must equal the velocity of the wall. In plane Poiseuille flow, the undisturbed fluid motion is given by

$$\underset{\sim}{v}(\underset{\sim}{x}, t) = (1 - z^2, 0, 0) \ , \quad p(\underset{\sim}{x}, t) = -2\nu x \ ; \tag{1.3}$$

this flow is driven by a pressure gradient. In plane Couette flow, the undisturbed fluid motion is given by

$$\underset{\sim}{v}(\underset{\sim}{x}, t) = (z, 0, 0) \ , \quad p(\underset{\sim}{x}, t) = 0 \ ; \tag{1.4}$$

this flow is driven by the motion of the walls at $z = \pm 1$. For these flows the maximum velocity of the undisturbed flow is 1, so the Reynolds number based on half-channel width is

$$R = \frac{1}{\nu} \tag{1.5}$$

The evolution of a small disturbance on a plane-parallel shear flow is governed by the Orr-Sommerfeld equation, which is

$$\left(\frac{d^2}{dz^2} - \alpha^2 - \beta^2\right)^2 w = iR\left[(\alpha U - \omega)\left(\frac{d^2}{dz^2} - \alpha^2 - \beta^2\right) w - \alpha U'' w\right] \qquad (1.6)$$

with boundary conditions

$$w = w' = 0 \quad \text{at} \quad z = \pm 1. \qquad (1.7)$$

Here the unperturbed velocity is $(U(z), 0, 0)$ and the small disturbance is assumed to have the form

$$w(x, t) = \text{Re}[w(z) e^{i\alpha x + i\beta y - i\omega t}] \qquad (1.8)$$

where α and β are the wave numbers in the x and y directions, respectively, and ω is the (complex) frequency of the disturbance. If α and β are real and $\text{Im}\,\omega > 0$, then the small disturbance is linearly unstable. On the other hand if all such small disturbances to a plane-parallel shear flow have $\text{Im}\,\omega < 0$, then the shear flow is linearly stable.

The critical Reynolds number R_c is defined as the lowest value of R at which there is any solution of the Orr-Sommerfeld equation with $\text{Im}\,\omega = 0$. For $R > R_c$, linearly unstable solutions of the Orr-Sommerfeld equation may exist. In a unidirectional plane-parallel shear flow $[v(x,y,z)/u(x,y,z)$ is independent of x, y, z and $w(x,y,z) = 0$], Squire's theorem (see Lin 1955) implies that if, at some Reynolds number R, there exists an unstable three-dimensional disturbance $[\beta \neq 0$ in (1.8)] then

6

there exists an unstable two-dimensional disturbance [$\beta = 0$] at a lower Reynolds number. Therefore, the mode that becomes unstable at R_c must be a two-dimensional mode. [We emphasize for later reference that at Reynolds numbers larger than R_c, the most unstable solution of the Orr-Sommerfeld equation may be three-dimensional (see Michael 1961).]

Asymptotic analysis of the Orr-Sommerfeld equation for plane Poiseuille flow using recently improved WKB techniques leads to the estimate $R_c \approx 5769.7$ (Lakin, Ng & Reid 1978); earlier asymptotic analysis had given $R_c \approx 5360$ (see Lin 1955). Direct numerical solution of the Orr-Sommerfeld equation gives $R_c \approx 5772.22$ (Orszag 1971b). The mode that becomes unstable at R_c has wavenumbers $\alpha \approx 1.02055$ and $\beta = 0$. Thus the theory of small amplitude disturbances suggests that plane Poiseuille flow is unstable only for Reynolds numbers greater than 5772, in contrast with the experimental observation of possible transition to turbulence at Reynolds numbers as low as 1000.

In plane Couette flow, all numerical evidence suggests that all modes of the Orr-Sommerfeld equation are stable at all Reynolds numbers (Davey 1973). The absence of any critical Reynolds number R_c for plane-Couette flow is in conflict with the available experimental evidence that this flow undergoes transition at modest Reynolds numbers.

Meksyn & Stuart (1951) suggested that finite-amplitude nonlinear effects may permit the growth of disturbances at

subcritical Reynolds numbers. Meksyn & Stuart introduced the so-called mean field equations in which only the interaction of the mean flow with the primary disturbance wave is retained and higher harmonics are neglected. They found that finite-amplitude two-dimensional disturbances to plane Poiseuille flow are unstable at Reynolds numbers larger than about 2900 with a threshold amplitude of about 8% of the centerline velocity. Numerical work by Grohne (1969) solving the mean field equations gave a critical Reynolds number of about 2500 (based on the perturbed centerline velocity).

Stuart (1960) and Watson (1960, 1962) extended the Meksyn-Stuart theory to include the second harmonic of the two-dimensional primary wave. Their results for plane Poiseuille flow are close to those of Meksyn & Stuart. Further work using the Stuart-Watson method by Reynolds & Potter (1967) has confirmed that velocity fluctuations of a few percent can drive two-dimensional finite-amplitude instabilities at Reynolds numbers above 2900. The original Stuart-Watson method involves expansions in both small amplitude and small $Im(\omega)$ about the neutrally stable modes at R_c. Recently, Itoh (1977) has extended the method of Eckhaus (1965) in order to reformulate the theory in a manner that he claims avoids the restriction to the neighborhood of R_c; a critique of Itoh's theory is given by Davey (1978).

8

A slightly different approach to the two-dimensional finite-amplitude instability problem has been given by Pekeris & Shkoller (1967,1969,1971), Zahn, Toomre, Spiegel & Gough (1974), and Herbert (1976,1977). In these investigations, the two-dimensional Navier-Stokes equations are solved using periodic boundary conditions in x by expanding the solution in a highly truncated Fourier series in x. Pekeris & Shkoller (1971) found two dimensional instabilities of plane Poiseuille flow at Reynolds numbers as low as 1000; at R = 1000, instability is achieved with a 6% perturbation, while at R = 3000 instability is achieved with a 0.4% perturbation. Hart (1971) faults the accuracy of the Pekeris-Shkoller (1967,1969) calculations. Our numerical solutions of the Navier-Stokes equations reported in Sec. 3 give no evidence of two-dimensional finite-amplitude instabilities in the vicinity of those predicted by Pekeris & Shkoller (1971) on the basis of nonlinear stability calculations using expansions in eigenfunctions of the Orr-Sommerfeld equation.

Zahn et al solved the Navier-Stokes equations for plane Poiseuille flow by retaining only two Fourier modes in x and using an unequally spaced finite difference grid in z. They found a minimum critical Reynolds number for two-dimensional finite-amplitude instability of 2707. The instability at this Reynolds number is achieved with a value of $\alpha = 1.3126$.

Herbert (1976,1977) performed a similar calculation using up to eight Fourier harmonics in x and 41 Chebyshev polynomials in the z direction. He found a critical Reynolds number of 2935 with a corresponding $\alpha = 1.3231$. Herbert's calculations

are directly comparable to ours in that he used essentially the same numerical technique as we do. The principal differences are that: (i) Herbert seeks neutrally stable finite-amplitude two-dimensional modes by solving time-independent equations while we solve the time-dependent problem; and (ii) Herbert uses up to eight Fourier harmonics in x while we use up to 32. Our two-dimensional calculations are in good agreement with those of Herbert.

In summary, the best available evidence to date suggests that two-dimensional disturbances are unstable only for Reynolds numbers larger than about 2800. Our numerical solutions reported in Sec. 3 confirm this result.

Direct numerical calculations of the two-dimensional Navier-Stokes equation were performed by George, Hellums & Martin (1974). They obtained instability only for Reynolds numbers larger than about 3500. Further discussion of their results is given in Sec. 3.

The current state of understanding of the effect of three-dimensional disturbances on plane Poiseuille flow is less well settled. Meksyn (1964) applied the mean field equations for plane Pouiselle flow and found three-dimensional finite-amplitude instability at $R = 1260$, but he also found two-dimensional instability at $R = 1270$. The inconsistency of these results with other numerical calculations of the mean field equations and the Stuart-Watson equations remains unexplained, but, in any case, they do not show a large effect of three-dimensionality.

10

Zahn et al (1974) examined some three-dimensional modes
and found them to be at least as stable as the two-
dimensional ones. Most recently, Itoh (1978) has extended
the Stuart-Watson-Eckhaus theory to three-dimensional disturbances
for Reynolds numbers close to the linear stability limit
of 5772. Itoh found that three-dimensional disturbances
are strongly destabilizing, but Davey's (1978) criticism may
still apply; in any case, Itoh's theory does not apply
to strongly subcritical Reynolds numbers. Also,
Hocking, Stewartson & Stuart (1972) and Davey,
Hocking & Stewartson (1974) studied the evolution of three-
dimensional finite amplitude disturbances to plane Pouiselle
flow at supercritical Reynolds numbers. They found that three-
dimensional effects are destabilizing above the linear stability
limit.

Theoretical investigations of the finite-amplitude
stability of plane Couette flow are also incomplete at this
time. Kuwabara (1967) applied the mean field equations of
Meksyn & Stuart and found that the minimum critical Reynolds
number for finite-amplitude instability of plane Couette flow
to two-dimensional disturbance to be R = 45212 with the
unstable mode having wavevector $\alpha = 13.565$, $\beta = 0$. Ellingsen,
Gjevik & Palm (1970) Davey & Nguyen (1971), and Coffee (1977)
used the Stuart-Watson method to study two-dimensional finite-
amplitude instability. They found instability to low-amplitude
disturbances down to Reynolds numbers of 1000 and below. However,

11

the absence of neutrally stable linear eigenmodes of plane Couette flow casts some doubt on the applicability of the Stuart-Watson method which involves an expansion about neutral stability (Rosenblat & Davis 1978). Lessen & Cheifetz (1975) also studied the nonlinear evolution of two-dimensional disturbances of plane Couette flow. Their calculations cast doubt that any unstable two-dimensional disturbances exist. Herbert (1977) reports inability to find neutrally stable finite amplitude solutions of plane Couette flow using highly truncated Fourier expansions in x. Our numerical solutions of the Navier-Stokes equations reported in Sec. 3 give no evidence yet of two-dimensional finite-amplitude instabilities in the neighborhood of those predicted by Ellingsen et al, Davey & Nguyen, and Coffee. In summary, there are some significant disagreements on the existence and strength of two-dimensional finite amplitude instabilities of plane Couette flow.

In this paper, we solve the Navier-Stokes equations numerically to study quantitatively the instability and transition to turbulence of plane Poiseuille and plane Couette flows. Since the resulting turbulence is strongly three-dimensional and since two-dimensional nonlinear disturbances of these laminar shear flows do not seem to be able to explain observed experimental results, we concentrate on the study of possible three-dimensional mechanisms.

Some insight is given by results for transition in boundary

layer flows where the experiments of Klebanoff et al (1962) and the theory of Benney and Lin (Benney & Lin 1960, Benney 1961, 1964) suggest that the secondary motions produced by the interaction of three-dimensional modes with two-dimensional modes can produce velocity profiles that are highly inflectional and unstable. Numerical calculations of the Benney-Lin equations by Antar & Collins (1975) have shown that this kind of theoretical approach is in some agreement with experiments. Direct numerical calculations of the three-dimensional Navier-Stokes equation for boundary-layer flow have shown quantitatively the strength of these three-dimensional effects in producing transition (Orszag 1976). On the other hand, direct numerical calculations of the two-dimensional Navier-Stokes equations for boundary layer flow (Fasel 1976, Fasel, Bestek & Schefenacker 1977, Murdock 1977, Murdock & Taylor 1977) do not exhibit explosively strong physical instabilities and the small scale excitation and apparent randomness characteristic of transition.

Because of the limited spatial resolution of our calculations, we do not address in detail the nature of the small scale flow structures that result from flow breakdown. Our goal is to explain the mechanisms by which flows develop that break down to turbulence. The development of very small scale structures in these flows, as studied by Landahl (1972), is beyond the scope of the present work.

In Sec. 2, we discuss briefly the numerical methods used in the present study. Then, in Sec. 3, we present

13

results for two-dimensional linear and nonlinear disturbances of plane Poiseuille and plane Couette flow. In Sec. 4, we present results of calculations of three-dimensional finite-amplitude instabilities of these flows and the resulting transition to turbulence. Finally, in Sec. 5, we summarize our results.

2. Numerical Methods

We solve the Navier-Stokes equations (1.1)-(1.2)
expressed in rotation form

$$\frac{\partial \underset{\sim}{v}(\underset{\sim}{x},t)}{\partial t} = \underset{\sim}{v}(\underset{\sim}{x},t) \times \underset{\sim}{\omega}(\underset{\sim}{x},t) - \underset{\sim}{\nabla}\Pi(\underset{\sim}{x},t) + \nu\nabla^2\underset{\sim}{v}(\underset{\sim}{x},t), \qquad (2.1)$$

where $\underset{\sim}{\omega}(\underset{\sim}{x},t) = \underset{\sim}{\nabla}\times\underset{\sim}{v}(\underset{\sim}{x},t)$ is the vorticity and
$\Pi(\underset{\sim}{x},t) = p(\underset{\sim}{x},t) + \frac{1}{2}|\underset{\sim}{v}(\underset{\sim}{x},t)|^2$ is the pressure head.
The flow is assumed to take place in the three-dimensional
box $0 \le x \le X$, $-\frac{1}{2}Y \le y \le \frac{1}{2}Y$, $-1 \le z \le 1$. At
$z = \pm 1$ we impose the boundary conditions that the fluid
velocity match the wall velocity. In the horizontal
directions, we impose periodic boundary conditions so that

$$\underset{\sim}{v}(x+mX, y+nY, z,t) = \underset{\sim}{v}(x,y,z,t) \qquad (2.2)$$

for all integers m, n. These periodic boundary conditions
are consistent with the Navier-Stokes equations and the
laminar solutions (1.3) for Poiseuille flow and (1.4) for
Couette flow.

The choice of periodic boundary conditions in horizontal
planes does cause some problem with respect to comparison
with experiment since these boundary conditions are not
realized in the laboratory. There are two justifications

15

for their use: (a) The instabilities of laminar flows that lead to turbulence are of small spatial scale so that boundary conditions should have little effect; and (b) the spatial growth of a disturbance in a laboratory coordinate frame appears in an advected coordinate frame as temporal growth, similar to that observed with the boundary conditions (2.2). Transition experiments in a flat plate boundary layer have been performed (Orszag 1976) with proper inflow-outflow boundary conditions applied and the results are qualitatively the same as in the present work. Also, Fasel et al (1977) have used inflow-outflow boundary conditions in their numerical simulations of two-dimensional disturbances to plane Poiseuille flow with results similar to those obtained using periodic boundary conditions. We offer no more excuses for the boundary conditions (2.2) used here and urge further study of their effect by future investigators.

We solve the Navier-Stokes equations in Eulerian coordinates using the pseudospectral method suggested by Orszag (1971a). An introduction to the theory of spectral methods is given in the monograph by Gottlieb & Orszag (1977). Here we summarize the implementation of spectral methods for the present channel flow simulations.

The velocity field is represented using Fourier series in x and y and a Chebyshev polynomial series expansion in z . Thus, the velocity field is represented as

$$\underline{v}(x,t) = \sum_{|m|<M} \sum_{|n|<N} \sum_{p=0}^{P} \underline{u}(m,n,p,t) e^{2\pi i(mx/X + ny/Y)} T_p(z)$$

(2.3)

16

where m, n, p are integers and $T_p(z) = \cos(p\cos^{-1}z)$ is the Chebyshev polynomial of degree p.

Equations for the spectral components $\underset{\sim}{u}(m,n,p,t)$ are obtained using a pseudospectral method to evaluate the non-linear terms of the Navier-Stokes equation. Thus, the rotation term $\underset{\sim}{v} \times \underset{\sim}{\omega}$ in (2.1) is evaluated as

$$\underset{\sim}{v} \times \underset{\sim}{\omega}(x_j,y_k,z_\ell) = \underset{\sim}{v}(x_j,y_k,z_\ell) \times \underset{\sim}{\omega}(x_j,y_k,z_\ell)$$

(2.4)

$$(0 \le j < 2M, \quad 0 \le k \le 2N, \quad 0 \le \ell \le P$$

where the collocation points x_j, y_k, z_ℓ are

$$x_j = jX/(2M), \quad y_k = (k-N)Y/(2N), \quad z_\ell = \cos\pi\ell/P \quad .$$

The values of $\underset{\sim}{v}(x_j,y_k,z_\ell)$ are obtained from (2.3) using fast Fourier transform algorithms [improved to take advantage of the reality of $\underset{\sim}{v}$ and the cosine (Chebyshev) transform in z as described in the appendix to Orszag (1971a)]. Similarly, $\underset{\sim}{\omega}(x_j,y_k,z_\ell)$ is evaluated using fast Fourier transforms applied to the curl of (2.3); for this purpose it is helpful to note that

$$\frac{\partial \underset{\sim}{v}}{\partial z} = \sum_{|m|<M} \sum_{|n|<N} \sum_{p=0}^{P} \underset{\sim}{u}^{(1)}(m,n,p)\,e^{2\pi i(mx/X+ny/Y)}T_p(z)$$

(2.5)

where $\underset{\sim}{u}^{(1)}$ is given in terms of $\underset{\sim}{u}$ by the recurrence relation

$$c_{p-1}\underset{\sim}{u}^{(1)}(m,n,p-1) - \underset{\sim}{u}^{(1)}(m,n,p+1) = 2p \underset{\sim}{u}(m,n,p) \quad (1 \leq p \leq P);$$

(2.6)

where $c_q = 1$ if $q \geq 1$ and $c_0 = 2$, and $\underset{\sim}{u}^{(1)}(m,n,P+1) = \underset{\sim}{u}^{(1)}(m,n,P) = 0$ for all m,n. Also, we apply a special circular truncation to the spectral representation of $\underset{\sim}{v} \times \underset{\sim}{\omega}$ in the x-y plane in order to minimize aliasing effects (Orszag 1971a, Sec.6).

The evaluation of $\underset{\sim}{v} \times \underset{\sim}{\omega}$ by this algorithm requires 9 Fourier transforms on $2MNP$ complex data points [three transforms each to get $\underset{\sim}{v}$ in physical space, $\underset{\sim}{\omega}$ in physical space, and $\underset{\sim}{v} \times \underset{\sim}{\omega}$ back in transform (Fourier-Chebyshev) space (which is the resident representation through most of our computer code)]. With $M=N=16$ and $P = 32$, each component of the velocity field is represented by 33,792 real degrees of freedom (before the circular truncation in the x-y plane is applied); evaluation of $\underset{\sim}{v} \times \underset{\sim}{\omega}$ by the above pseudospectral algorithm requires about 2.5s on the CDC 7600. In contrast, direct evaluation of the convolution-like sums that would be obtained by formulating equations for $\partial \underset{\sim}{u}(m,n,p,t)/\partial t$ using a Galerkin approximation procedure would require about 1000 times more computer time. It is

18

noteworthy that of this speedup by a factor 1000, the fast

Fourier transform contributes only roughly a factor 2; most

of the speedup is due to the reorganization of the calculation

in terms of transforms (which factor into a sequence of one-

dimensional transforms) be they fast or not. This latter

result and the result noted by Gottlieb & Orszag (1977)

that Legendre polynomial expansions are especially accurate

may suggest that Legendre polynomials be used in place of

Chebyshev polynomials in future studies. We also note that

one of us (S.A.O) has recently developed a 'fast' Legendre

transform that requires $0(N(\log_2 N)^2/\log_2 \log_2 N)$ operations

to transform an N term Legendre polynomial or surface

harmonic series to or from physical space.

Four additional features of our numerical methods

deserve comment: time stepping, determination of the

pressure, viscous dissipation, and initial conditions. A

fractional step method is used in time so that we shall

first discuss a time step of the inviscid equation, then

the imposition of the incompressibility constraint,

then viscous effects, and finally initial conditions.

In order that time steps not be unduly restricted

by convective stability conditions due to the relatively

large unperturbed (laminar) flow we use a semi-implicit

scheme in which the largest effects of this parallel flow

are handled implicitly. If the (x-component of the)

unperturbed parallel flow is denoted by $U(z)$, then the terms

in (1.1) responsible for convective stability restrictions

that trace to $U(z)$ are just $U(z)\partial y/\partial x$. This term is best

evaluated in the mixed spectral-physical space representation in which x and y are represented as Fourier modes while z is kept in physical space; in this representation $U(z) \partial \underset{\sim}{v} / \partial x \to i(2\pi m/X) U(z) \underset{\sim}{u}(m,n,z)$, which is diagonalized.

With the semi-implicit treatment of $U(z)$, it is a little tricky to obtain an efficient time-stepping procedure for (2.1) and (1.2) that is high-order accurate in time.[†] We use an Adams-Bashforth-Crank-Nicholson (ABCN) method with global error of order $O(\Delta t^2) + O(\nu \Delta t)$, where we tolerate first-order accuracy on the viscous terms because our calculations are done with very small values of ν. If ν is large, the semi-implicit treatment of $U(z)$ should be sacrificed for better accuracy in time. The ABCN scheme for the nonlinear terms in (2.1) is derived by writing $\partial \underset{\sim}{v} / \partial t + U \partial \underset{\sim}{v} / \partial x = \underset{\sim}{v} \times \underset{\sim}{\omega} + U \partial \underset{\sim}{v} / \partial x$ and applying the Crank-Nicolson scheme on the left and the second-order Adams-Bashforth scheme on the right; the result is

$$\frac{\hat{\underset{\sim}{u}}^{n+1} - \underset{\sim}{u}^n}{\Delta t} = \frac{3}{2} \underset{\sim}{F}^n - \frac{1}{2} \underset{\sim}{F}^{n-1} - \frac{i}{2} \frac{2\pi m}{X} U(z) [\hat{\underset{\sim}{u}}^{n+1} - 2\hat{\underset{\sim}{u}}^n + \hat{\underset{\sim}{u}}^{n-1}] \qquad (2.7)$$

in the mixed spectral-physical space representation. Here $\underset{\sim}{F} = \underset{\sim}{v} \times \underset{\sim}{\omega} + \underset{\sim}{f}$ in the mixed representation where we have generalized the problem slightly by introducing an external force (mean pressure gradient) denoted by $\underset{\sim}{f}$; the superscripts label the time step and no boundary conditions (except

---

† Orszag & Deville (to be published) have recently shown how to obtain unconditionally stable, easily implementable schemes of arbitrary order accuracy in time for the Navier-Stokes equations. Comparisons with the results reported in the present paper show no appreciable errors due to the lower order scheme used here.

periodicity are applied yet. Eq. (2.7) is formulated

for constant time steps Δt; for nonconstant time steps

[as for the first few time steps (we use a slow start

to minimize initial truncation errors)], the coefficients in

(2.7) are different. It is important to emphasize that

the terms multiplying $U(z)$ on the right side of (2.7)

are all <u>intermediate</u> results at time steps $n-1$, n, and

$n+1$; if $\hat{\underset{\sim}{u}}^{n-1}$ and $\hat{\underset{\sim}{u}}^{n}$ are replaced by $\underset{\sim}{u}^{n-1}$ and $\underset{\sim}{u}^{n}$

or $\frac{3}{4}\underset{\sim}{u}^{n} + \frac{1}{4}\hat{\underset{\sim}{u}}^{n}$ (as would be the case if naive application

of the Adams-Bashforth method were made) then the scheme

(2.7) would lead to errors of order $0(\Delta t)$ <u>after</u>

application of the pressure terms in (2.1).

Once the fractional step (2.7) is made, it is

necessary to include the effect of pressure. This is

done by the fractional step

$$\hat{\hat{\underset{\sim}{v}}}^{n+1} - \hat{\underset{\sim}{v}}^{n+1} = - \quad \underset{\sim}{\nabla}\hat{\Pi}^{n+1} \tag{2.8}$$

$$\underset{\sim}{\nabla}\cdot\hat{\hat{\underset{\sim}{v}}}^{n+1} = 0 \tag{2.9}$$

where $\hat{\hat{\underset{\sim}{v}}}^{n+1}$ has global error of order $0(\Delta t^2)$ despite the

fact that $\Delta t \hat{\Pi}^{n+1}$ has global error $0(\Delta t)$ relative to the

pressure head Π. Eqs. (2.8)-(2.9) are solved with the

boundary conditions

$$\hat{\hat{w}}^{n+1} = 0, \ z = \pm 1, \tag{2.10}$$

21

assuming no normal wall motion.

Eqs. (2.8)-(2.10) are best solved in the full
spectral representation using a spectral tau method in
z (Gottlieb & Orszag 1977, Sects. 10, 13). The result-
ing equations for $\hat{\underset{\sim}{u}}$ (dropping the time-step label) are,
in the full spectral representation, given by

$$\hat{\hat{u}}(m,n,p) = \hat{u}(m,n,p) - i\alpha m\hat{\hat{\Pi}}(m,n,p) \quad (0\leq p\leq P) \tag{2.11}$$

$$\hat{\hat{v}}(m,n,p) = \hat{v}(m,n,p) - i\beta n\hat{\hat{\Pi}}(m,n,p) \quad (0\leq p\leq P) \tag{2.12}$$

$$\hat{\hat{w}}(m,n,p) = \hat{w}(m,n,p) - \hat{\Pi}^{(1)}(m,n,p) \quad (0\leq p\leq P-2) \tag{2.13}$$

$$i\alpha m\hat{\hat{u}}(m,n,p) + i\beta n\hat{\hat{v}}(m,n,p) + \hat{\hat{w}}^{(1)}(m,n,p)=0 \quad (0\leq p\leq P) \tag{2.14}$$

$$\sum_{p=0}^{P} \hat{\hat{w}}(m,n,p) = \sum_{p=0}^{P} (-1)^{P}\hat{\hat{w}}(m,n,p) = 0 \tag{2.15}$$

for all retained m,n ($|m|<M, |n|<N$), where[†]
$\alpha = 2\pi/X$, $\beta = 2\pi/Y$ and $\hat{\Pi}^{(1)}$ and $\hat{\hat{w}}^{(1)}$ are related
to $\hat{\Pi}$ and $\hat{\hat{w}}$ as in (2.6).

If $m^2+n^2 \neq 0$, an efficient procedure to solve
(2.11)-(2.15) is to rewrite (2.11)-(2.15) as the nearly
tridiagonal system (see Sec. 10 of Gottlieb & Orszag 1977)

[†] Note that these definitions of α , β are consistent with α , β
used in (1.8) and (2.23)-(2.27) below if the linear
mode in (1.8) is the fundamental mode in the box
$0\leq x\leq X, -\frac{1}{2} Y\leq y\leq \frac{1}{2}Y$.

$$\frac{\gamma c_{p-2}}{4p(p-1)} \hat{\hat{w}}(m,n,p-2) \; - \; (1 + \frac{\gamma e_{p+2}}{2(p^2-1)}) \hat{\hat{w}}(,n,p) \; + \; \frac{\gamma e_{p+4}}{4p(p+1)} \hat{\hat{w}}(m,n,p+2)$$

$$= F(m,n,p) \quad (2 \leq p \leq P) \qquad\qquad (2.16)$$

where $c_0 = 2$, $c_p = 1$ $(p \geq 1)$, $e_p = 1(p \leq P)$, $e_p = 0(p > P)$,

$\gamma = \alpha^2 m^2 + \beta^2 n^2$, and

$$F(m,n,p) = \frac{c_{p-2} f_{p-2}}{4p(p-1)} - \frac{e_{p+2} f_p}{2(p^2-1)} + \frac{e_{p+4} f_{p+2}}{4p(p+1)} \quad (2 \leq p \leq P) \qquad (2.17)$$

with

$$f_p = - \, i\alpha m \hat{u}^{(1)}(m,n,p) \; - \; i\beta n \hat{v}^{(1)}(m,n,p) \; - \gamma \hat{w}(m,n,p)$$

$$(2.18)$$

and $\hat{u}^{(1)}$ and $\hat{v}^{(1)}$ related to $\hat{u}$ and $\hat{v}$ by (2.6).
The system (2.15)-(2.16) is solved for $\hat{\hat{w}}$ by standard
techniques in roughly the same number of operations required
to solve pentadiagonal systems. The equations for $\hat{\hat{w}}$ in
this form are essentially diagonally dominant so no appreciable
accumulation of·roundoff errors occurs.

Once $\hat{\hat{w}}$ is found then $\hat{\Pi}$ is found from

$$\gamma \hat{\Pi}(m,n,p) = - \, i\alpha \hat{u}(m,n,p) - i\beta n \hat{v}(m,n,p) - \hat{\hat{w}}^{(1)}(m,n,p)$$

$$(0 \leq p \leq P) \qquad (2.19)$$

where α, β, γ are given as before in terms of m, n. Then $\hat{\underset{\sim}{u}}$ and $\hat{\underset{\sim}{v}}$ are found directly from (2.11)-(2.12), completing the solution for $\hat{\underset{\sim}{\hat{u}}}$.

If $m = n = 0$, then (2.11)-(2.15) are easily solved by appropriate applications of recurrences like (2.6).

Finally, we use a full implicit fractional step to impose the viscous terms and the boundary conditions:

$$\frac{\underset{\sim}{v}^{n+1} - \hat{\underset{\sim}{v}}^{n+1}}{\Delta t} = \nu \nabla^2 \underset{\sim}{v}^{n+1} \tag{2.20}$$

$$\underset{\sim}{v}^{n+1} = \underset{\sim}{V}_\pm \quad (z = \pm 1) \tag{2.21}$$

where $\underset{\sim}{V}_\pm$ is the wall velocity at $z = \pm 1$, respectively. The full implicit scheme (2.20)-(2.21) is unconditionally stable but it does induce global errors of order $0^{(\nu \Delta t)}$. Eqs. (2.20)-(2.21) are solved efficiently in a full spectral representation using a spectral-tau method; the resulting equations are essentially tridiagonal in the Chebyshev index and diagonal in the Fourier indices (see Sec. 10 of Gottlieb & Orszag 1977). This completes the description of the main part of our computer code.

Initial conditions for the runs reported in Sects. 3-4 usually consist of the unperturbed flow (1.3) or (1.4) on which we superpose finite-amplitude combinations of

two-and three-dimensional eigenmodes of the Orr-Sommerfeld equation (1.6)-(1.8). The Orr-Sommerfeld equation is solved by expanding $w(z)$ in the Chebyshev series (Orszag 1971b)

$$w(z) = \sum_{p=0}^{P} a_p T_p(z),\qquad\qquad (2.22)$$

constructing equations for the expansion coefficients a_p by matrix methods (Metcalfe 1974), finding the eigenvalue by either a global eigenvalue routine based on a matrix QR eigenvalue analysis or a local eigenvalue routine based on an inverse iteration-Rayleigh quotient method, and finally obtaining the eigenfunction by an inverse iteration method. The accuracy of our eigenvalues and eigenfunctions is better than 1 part in 10^6.

Once the complex z-velocity $w(z)$ of an eigenmode of the Orr-Sommerfeld equation is obtained, the x- and y- velocity components, $u(z)$ and $v(z)$, respectively, are obtained as follows. The z-component of the perturbed vorticity, given by $\eta(z)\exp[i\alpha x+i\beta y-i\omega t]$ with

$$\eta(z) = i\beta u(z) - i\alpha v(z),\qquad\qquad (2.23)$$

satisfies the linear inhomogeneous equation

$$(\frac{d^2}{dz^2} - \alpha^2 - \beta^2)\eta(z) = iR[(\alpha U(z)-\omega)\eta(z)+i\beta U'(z)w(z)] \quad (2.24)$$

$$\eta(\pm 1) = 0 , \quad (2.25)$$

where $R = 1/\nu$. Using the incompressibility condition
(1.2), it follows that

$$(\alpha^2+\beta^2)u(z) = -i\beta\eta(z) + i\alpha w'(z) \quad (2.26)$$

$$(\alpha^2+\beta^2)v(z) = i\alpha\eta(z) + i\beta w'(z). \quad (2.27)$$

For two-dimensional disturbances, $\beta = 0$ and $\eta(z) \equiv v(z) \equiv 0$.

In concluding this section we summarize some features
of our computer code. Fourier series representations are
used in x and y and Chebyshev series representations
are used in z . Pseudospectral methods are applied to the
nonlinear terms while tau methods are applied to the
pressure and viscous terms. The resulting scheme is infinite-
order accurate in space, has no phase errors in x and y ,
can resolve boundary layers of thickness $0(1/P^2)$ in z ,
[the collocation points z_1 and z_{P-1} in (2.4) are
located a distance $\pi^2/2P^2$ from the walls at $z = \pm 1$]
and accurately imposes the boundary conditions at the rigid

walls and the incompressibility condition throughout the layer (see Gottlieb & Orszag 1977 for discussion of these features). A fractional time step method is used with global error of order $O(\Delta t^2 + \nu\Delta t)$; time steps are formally restricted only by convective stability restrictions due to the perturbed velocity [although in practice we do not take time steps more than about three times larger than the convective stability limit due to $U(z)$].

A run using $32 \times 32 \times 33$ modes $(M=N=16, P=32)$ to represent each component of velocity requires about 6s (2.5s for evaluation of $\underset{\sim}{v} \times \underset{\sim}{\omega}$) on the CDC 7600 computer per time step, including input-output overhead. The computer time is nearly proportional to MNP. A typical run involves about 1000 time steps. Some runs to validate our code are reported in Sec. 3. We note here that it is our (unpleasant) experience that typical transition calculations require about 10 times as many time steps as typical turbulence decay calculations (see Orszag & Patterson 1972). The reason seems to be the need to maintain accurate phase relations over many linear oscillation times in transition calculations whereas turbulent flows are nearly critically damped and evolve quite rapidly in interesting ways. We also note that less than 15 h

27

of CDC 7600 time was spent on the present series of
computations (including a large number of runs not
reported here). On the newly introduced CRAY-1 computer
the same series of runs requires less than 1.4h, showing
the great strides that can now be made on significant
fluids problems with modest computer resources.

3. Two-Dimensional Finite-Amplitude Disturbances

In this Section, we present results obtained using
the computer code described in Sec. 2 for the evolution of
small and finite-amplitude two-dimensional disturbances of plane
Poiseuille and plane Couette flow. The first series of
runs were made primarily to verify the accuracy of our computer
program in comparison with known results. Two types of
tests have been made: comparison of the evolution of small-
amplitude disturbances with their predicted behavior according
to the Orr-Sommerfeld equation; and comparison of some special
finite-amplitude two-dimensional solutions with the numerical
results of George, Hellums & Martin (1974).

In Table 1, we present results of small-amplitude tests
of the computer code. The values of ω are obtained by
Chebyshev-spectral solution of the Orr-Sommerfeld equation
and represent the least stable eigenmode of the flow for the
given α and β . The predicted amplitude change in the
time interval $0 \leq t \leq T$ is $\exp[(\text{Im } \omega)T]$, while the predicted
phase change in the same time interval is (in radians)
$-(\text{Re } \omega)T$. It seems that most of the small error between
the predicted and computed amplitude and phase changes of
both the two- and three-dimensional modes of plane Pouiseuille
flow and plane Couette flow is due to time differencing
error. Similar tests of the computer code on small-amplitude

29

disturbances have been made for Reynolds numbers up to
.50,000 with similarly good results.

Our next verification run used a large two-dimensional
disturbance studied previously by George et al (1974). George
et al solved the two-dimensional Navier-Stokes equations by
expanding the velocity field into a Fourier series in x
and applying finite-difference methods in z . George et al
did not use initial conditions corresponding to eigenmodes
of the Orr-Sommerfeld equation, but rather chose the initial
velocity field to be that generated by the streamfunction

$$\psi(x,z) = k(\frac{\cosh az}{\cosh a} - \frac{\cos az}{\cos a}) \cos \alpha x. \qquad (3.1)$$

Here $a \approx 2.365$ in order to satisfy the boundary conditions,
and we integrated the neutrally stable case found by George
et al in which $R = 4000$, $\alpha = 1.05$, $k = 0.0599$.   The initial
maximum amplitude of the perturbation of x-velocity is 0.1465.
Using 8 Fourier modes in x and 33 Chebyshev polynomials in
z , the results of our computer code agreed well through late
times with those of George et al. It seems that the reason that
George et al were unable to achieve two-dimensional instability
at Reynolds numbers as low as those predicted by the Stuart-
Watson technique is due to two causes: (a) the initial

condition (3.1) is not a pure mode of the Orr-Sommerfeld equation; and (b) more importantly, the choice $\alpha = 1.05$, while close to the most unstable α for small-amplitude disturbances is far from the most unstable α for finite-amplitude disturbances (see below).

Some characteristics of the two-dimensional finite-amplitude runs discussed below are given in Table 2. Additional details are given by Kells (1978). The results of Herbert (1976) suggest that the critical Reynolds number for finite-amplitude two-dimensional instability of plane Poiseuille flow is roughly 2935 with the unstable mode having a wavenumber $\alpha = 1.3231$. Runs 2-4 present results of our numerical simulations of such a flow.

In Fig. 1 we plot the profile of the x-velocity component of the two dimensional primary disturbance mode [which depends on

x like $\exp(i\alpha x)$] imposed at $t = 0$ in Run 2. The initial disturbance imposed in Runs 3 and 4 has the same shape but is reduced in amplitude. In Fig. 2 we plot the time evolution in Run 2 of the maximum amplitude A of the x-velocity of the primary wave and its harmonic [that depending on x like $\exp(2i\alpha x)$]. After an initial transient period the primary wave settles down into a period of slow growth suggesting that the initial finite-amplitude disturbance does not die out as $t \to \infty$. However, despite the growth of the finite-amplitude disturbance, there is no sign of 'turbulence' in the sense that

31

the flow remains ordered and well behaved. In Fig. 3, we plot
the profile of the primary wave after evolution to t = 120
in Run 2; in this Figure, the x-velocity component u(z) is
plotted as a function of z at a point x at which its phase
relative to the initial perturbation is 0 . Comparision of
Figs. 1 and 3 shows that nonlinear effects tend to move the
maximum perturbation velocity away from the walls at z = ±1

In Fig. 4, we plot the unperturbed velocity profile $1 - z^2$
and the mean velocity profile obtained from Run 2 at t = 120.
In Fig. 5, we plot the curvature of the unperturbed flow
and the mean flow at t = 120. Observe that although the mean
flow is changed only slightly in evolution from t = 0 to
t = 120, there are large changes in the curvature in the wall
regions.

Run 2 has 32 Fourier modes in x and 33 Chebyshev modes
in z. Its numerical accuracy was tested by making other runs
with different values of M and P . A run with 16 Fourier
modes in x and 33 polynomials in z gave nearly identical
results, while a run with 8 Fourier modes indicated faster in-
stability. Increasing the number of Chebyshev polynomials in
z to 65 gave negligible change. In Run 2, higher harmonics
have very small amplitudes; the harmonic $\exp(3i\alpha x)$ has maximum
amplitude 0.01 in z at t = 120 while the harmonic
$\exp(7i\alpha x)$ has amplitude 0.001.

The results of Runs 3 and 4 indicate the effect of chang-
ing the initial amplitude of the finite-amplitude disturbance.
In Run 3 a nearly stationary disturbance is achieved in

evolution to t = 100 (see Fig. 10).   On the other hand,
Run 4 shows that there is a critical amplitude of about
10% below which finite-amplitude disturbances decay at
R = 2935.   In Fig. 6, we plot the maximum amplitude of the
x-velocity of the primary disturbance and its harmonic as
a function of time in Run 4.   After an initial transient period,
both the primary and its harmonic settle down to a state of
steady decay.

In Fig. 7 we plot the primary wave and harmonic wave
amplitude vs. time for Run 1 at R = 2500. The result that
the disturbance decays as t increases for an initial disturb-
ance which is designed to be close to the most unstable finite-
amplitude disturbance at this Reynolds number suggests that all
two-dimensional disturbances decay at R = 2500. We conclude
that the threshold for neutral stability is near R = 2800,
in rough agreement with previous theoretical results.

Run 5 shows that decreasing α to $\alpha = 1$ gives stable
finite-amplitude results even at R = 3500. This result explains
why George et al (1974) were unable to find two-dimensional
instabilities at Reynolds numbers below 3500. George et al
used a disturbance wave number $\alpha = 1.05$ which is close to
the value of α that gives the linearly least stable mode
of plane Poiseuille flow at R = 3500 among all real α ,
but $\alpha = 1.05$ is far from those modes that give unstable
finite-amplitude disturbances. While the amplitudes of the

33

harmonics of the primary wave disturbances in Runs 2 and 3 are quite small, nonlinear effects do cause considerable distortion of the primary wave itself (see Figs. 1 and 3), giving a large effect on the least stable α.

In summary, while there are finite-amplitude two-dimensional instabilities of plane Poiseuille flow at subcritical Reynolds numbers, there are apparently no explosive instabilities that can generate small-scale random flow structures when only two-dimensional interactions are allowed.

Run 6 illustrates the effect of finite-amplitude two-dimensional disturbances on plane Couette flow. In Fig. 8 we plot the profile of the x-velocity component of the initial disturbance in Run 6. This initial disturbance is constructed from a solution of the Orr-Sommerfeld equation as follows. For the given $\alpha = 2$, $\beta = 0$, and $R = 5000$, the least stable eigenmode $\hat{u}(z)$ of plane Couette flow is asymmetric about $z=0$. It is easy to verify from the Orr-Sommerfeld equation (1.6) that if $\hat{u}(z)$ corresponds to the wave vector-frequency α, β, ω, then $\hat{u}^*(-z)$ is the eigenfunction associated with $\alpha, \beta, -Re(\omega)+iIm(\omega)$. Note that the phase velocity of this complex-congugate reflected mode is the negative of the phase velocity of the original mode. The initial conditions for Run 6 are chosen to be the (symmetrized) conditions in which the x-velocity is given by

$$u(x,z,0) = \tfrac{1}{2}Re[\hat{u}(z)+\hat{u}^*(-z)]e^{i\alpha x}. \tag{3.2}$$

In Fig. 9 we plot the time evolution of the maximum amplitude of the primary disturbance and its harmonic as functions of time for Run 6. The decay is quite rapid, in contrast with the

34

predictions of Ellingsen, Gjevik & Palm (1970) and Coffee

(1977) whose theoretical calculations seem to predict that

Run 6 should lead to a finite-amplitude stationary disturbance.

Other runs for plane Couette flow give no indication as yet

of any region of two-dimensional instability [although our

computer code is not capable of resolving the case suggested

by Kuwabara (1967)]. It is not likely that our decay results

for plane Couette flow are due to the low 8×33 resolution

used in Run 6. The 33 Chebyshev polynomials used in z are

more than adequate to resolve the vertical structure. The

8 Fourier modes used in x also seem to be adequate; at

$t = 90$, the primary wave has maximum amplitude 0.0053, its

harmonic has maximum amplitude 0.00034, while its second

harmonic has amplitude 0.000060. In any case, our experience

with increasing the x-resolution is that higher resolution

gives more stable results than low resolution (see Sec. 4).

The high frequency oscillation exhibited by the primary

wave in Fig. 9 is due to the fact that the maximum amplitude

of $u(z)$ appears alternately near $z = \pm 1$; this effect is

a consequence of the symmetrized mode (3.2) in which the two

components have equal and opposite phase velocity. Unsymmetrized

initial conditions do not lead to these rapid oscillations (see Fig. 37).

Our results suggests a serious discrepancy between the

Stuart-Watson-Eckhaus theory predictions of two-dimensional

finite-amplitude instability of plane Couette flow and direct

numerical calculations that indicate decay. One possible explanation is that we have not sought solutions with large enough α. According to Davey & Nguyen (1971), the finite-amplitude disturbances requiring the least energy to excite have $\alpha \approx 0.13R^{1/2}$ or $\alpha \approx 9$ for $R = 5000$. However, the energy required to excite a finite-amplitude mode at this large Reynolds number is a fairly flat function of α and our inability to find instability with $\alpha=2$ is, in our view, a serious criticism of the theory. We are now studying solutions with larger α using a higher resolution computer code in order to resolve the discrepancy between non-linear stability theory and numerical experiments. However, the main point of the present paper is the strength of three-dimensional effects; the possibility that two-dimensional inter-actions may be slightly stronger for much larger α than considered here is, we believe, a secondary issue.

In summary, our direct calculations of the Navier-Stokes equations are in reasonably good agreement with nonlinear stab-ility theory calculations of plane Poiseuille flow. While no transition to turbulence is either observed or predicted due to two-dimensional disturbances, there are finite-amplitude motions that do not decay for Reynolds numbers larger than about 2800. Serious discrepancies do now exist between nonlinear stability theory and direct calculations of two-dimensional finite-amplitude effects in plane Couette flow.

4. Three-Dimensional Finite-Amplitude Disturbances

In this Section, we present results obtained using the computer code described in Sec. 2 for the evolution of finite-amplitude three-dimensional disturbances of plane Poiseuille and plane Couette flow. Some characteristics of the runs discussed in this Section are given in Table 3 for the plane Poiseuille runs and in Table 4 for the plane Couette flow runs.

Run 3A is identical to Run 3 discussed in Sec. 3 except for one interesting three-dimensional feature. The two-dimensional Run 3 was made with the three-dimensional computer code using $8 \times 4 \times 33$ resolution and setting all flow components to be independent of y at $t = 0$. Since we did not reset the flow to be independent of y at later times, round-off error induced a small (order 10^{-14}) three-dimensionality on the flow. This three-dimensional component was rapidly filtered into an unstable three-dimensional mode that grew rapidly on the finite-amplitude two-dimensional background. A plot of the maximum amplitude of the primary two-dimensional disturbance, its two-dimensional harmonic, and the fundamental oblique wave (with wave numbers $\alpha = 1.3231$, $\beta = 1$) is given in Fig. 10. Note that the amplitude of the oblique component is multiplied by 10^8. The results of Run 3A show that the evolved two-dimensional finite-amplitude state is quite susceptible to three-dimensional instabilities.

Run 3A suggests a simple mechanism for transition. Whereas two- and three-dimensional linear instabilities of plane

Poiseuille flow are quite mild and occur only for large
Reynolds numbers ($R \gtrsim 5772$), finite-amplitude two-dimensional
neutrally stable states of plane Poiseuille flow seem to
be explosively unstable to three dimensional perturbations
at subcritical Reynolds numbers.

In Runs 7-16 we investigate the finite-amplitude aspects
of three-dimensional instability of plane Pouiseuille flow.
All of these runs (except Run 16) are made by choosing the
initial condition to consist of a superposition of four
components:

$$\underset{\sim}{v} = (U(z),0,0) + \text{Re}\,[\underset{\sim}{v}_{2D}(z)\,e^{i\alpha x}] + \text{Re}\,[\underset{\sim}{v}_{+,3D}(z)\,e^{i\alpha x + i\beta y}]$$

$$+ \text{Re}\,[\underset{\sim}{v}_{-,3D}(z)\,e^{i\alpha x - i\beta y}] \qquad (4.1)$$

Here $U(z) = 1 - z^2$ is the unperturbed plane Pouiseuille flow,
$\underset{\sim}{v}_{2D}(z)$ is a two-dimensional eigenfunction of the Orr-Sommerfeld
equation, and $\underset{\sim}{v}_{\pm,3D}(z)$ is a three-dimensional eigenfunction
of the Orr-Sommerfeld equation with spanwise wave number
$\pm\beta$. The form of this initial flow field is chosen to corresp-
ond to that suggested by the experiments of Klebanoff, Tidstrom &
Sargent (1962) and the theory of Benney & Lin (1960). The oblique
three-dimensional disturbance is always formed with symmetric
$\pm\beta$ components, so the initial conditions give a standing
wave disturbance with the x-axis an axis of symmetry. For
all runs (except Runs 12 and 13) the Orr-Sommerfeld eigenfunctions

v_{2D} and v_{3D} are chosen to be the least stable eigenfunctions for the given values of α, β. Because of the computational cost of the three-dimensional runs, we have not been able to make a complete survey of the effects of disturbance wave length and amplitude on the strength of the transition process. However, there are indications on the basis of the results reported below that the chosen values of α and β give nearly the most strongly unstable results.

In Figs. 11 and 12 we plot the profiles of the two dimensional disturbance $u_{2D}(z)$ and the three-dimensional disturbance $u_{+,3D}(z)$, respectively, applied initially in Runs 7 and 8. In Figs. 13 and 14, we plot the maximum amplitude of the two-dimensional primary disturbance, its two-dimensional harmonic [depending on x like $\exp(2i\alpha x)$], and the primary oblique wave [depending on x and y like $\exp(i\alpha x + i\beta y)$] for Runs 7 and 8, respectively.

The only difference between Runs 7 and 8 is that Run 7 has twice the x-y resolution. It is apparent from Figs. 13 and 14 that the results are nearly identical through $t = 35$, but the results later diverge. In Run 7, the flow seems to 'break down' at $t \approx 40$, while in Run 8 the 'breakdown' seems to occur for $t \approx 37$. (Part of this difference may be due to time truncation error since Run 7 uses a time step of 0.05 while Run 8 uses a time step of 0.1.) Another run made with the initial conditions of Runs 7 and 8 but increasing the z-resolution to 65 Chebyshev polynomials showed no change from the results with 33 Chebyshev polynomials until well into the breakdown region.

In Tables 5 and 6, we give values of the maximum amplitudes in z of the x-velocity Fourier components $u(m,n,z,t)$, given in terms of the spectral components $u(m,n,p,t)$ in (2.3) by

$$u(m,n,z,t) = \sum_{p=0}^{P} u(m,n,p,t) \, T_p(z) \, .$$

While the convergence of the expansion (2.3) evidently does deteriorate somwehat with time, especially near $t \approx 40$ when the flow breaks down, the decrease of the maximum amplitude with increasing m and n is sufficiently rapid for us to confidently assert that the results of Run 7 are real and not due to numerical instability. Also, while the effects of truncation of the Fourier expansion (2.3) in Run 8 are even more pronounced than for Run 7, the lower resolution results of Run 7, are a faithful predictor of flow breakdown and accurately represent the flow until just before breakdown occurs.

We emphasize the qualitative change in the behavior of the flow brought about by three dimensionality. While the finite amplitude two-dimensional results presented in Sec. 3 show the resulting flow to be smooth, periodic and with no appreciable small-scale excitation, quite the opposite is true in the three-dimensional flows considered here. In three dimensions, the flow develops into a state of apparent randomness with appreciable small-scale excitation. It is this latter state that we claim is representative of the transition to turbulence.

While we cannot claim that our results for Run 7 are in detail accurate for $t > 50$ when the flow is seemingly random and "turbulent", the relative insensitivity to changes in resolution

suggest strongly that our simulations accurately portray the breakdown of the laminar flow and its transition to turbulence. [While the flow after breakdown is almost certainly not being treated in detail accurately, there is some basis for the

assertion that the <u>statistical</u> properties of the resulting flow are in reasonable agreement with real flows. Some further elaboration of this point is given below. However, we do not stress the turbulence aspects of the developed flow in this paper as numerical simulations of turbulence are best done slightly differently.]

The apparent discontinuities in the time-history curves plotted in Figs. 13, 14, and later arise because the maximum amplitude of each of the flow components may come from different local maxima and, hence, quite distinct z locations at different times.

In Fig. 15, we plot x-y averages of the x-component of the velocity field in Run 8 at t = 30-75(15):

$$\bar{u}(z,t) = \frac{1}{XY} \int_0^X dx \int_{-\frac{Y}{2}}^{\frac{Y}{2}} dy \; u(x,y,z,t) \tag{4.2}$$

The results for Run 7 at t = 30 and t = 45 (the only times at which corresponding results are available) are indistinguishable from the plotted curves. The mean velocity profiles plotted in Fig. 15 correspond to profiles in the nonlinear laminar,

early transition, late transition, and turbulent flow regimes.
The mean velocity profile at $t = 75$ is strikingly similar to
mean velocity profiles observed experimentally in turbulent
channel flow (Laufer 1951, Comte-Bellot 1965). In a continuation
of Run 8 to $t > 75$, no change in the mean velocity profile is
found.

While there are no strong inflections appearing in the
mean velocity profiles plotted in Fig. 15, instantaneous
velocity profiles plotted in Figs. 16 and 17 for Run 7 at
$t = 30$ and $t = 45$, respectively, show strong inflections.
These local velocity profiles are strongly unstable and,
presumably, their instability leads to the random behavior
observed at later times.

Contour plots of the x-velocity component for Run 7
in the y-z plane at $x = 0$ are given in Fig. 18 for
$t = 0-45(15)$. At the spanwise-y location of the center of
the 'cat's-eyes' observed in Fig. 18, the velocity
profile is much fuller than the undisturbed plane Poiseuille
profile and the corresponding wall shear is much greater (see
Figs. 16 and 17). In the region between the 'cat's-eyes',
the local velocity profile is highly inflectional (as shown
in Figs. 16 and 17).

Contour plots of the longitudinal vorticity component
for Run 7 in the y-z plane at $x = 0$ are given in Fig. 19 for
$t = 0-45(15)$. Several features of these contour plots should

be observed. First, there is considerable enhancement of
longitudinal vorticity during time evolution of this flow.
In Table 5, we present data on the maximum amplitude of the
transverse waves [m=0 in (2.3)] as a function of time in Run 7.

Through t = 35, the data in Table 5 agrees to within a relative
error of less than 2% with the corresponding data for Run 8.
The primary transverse mode seems to achieve rapidly a nearly
steady value, while the flow breakdown is signaled by rapid
growth of the n=2 harmonic component. Second, the small-
scale structure evident in Fig. 19 at t = 45 indicates the
breakdown of the flow.

In Fig. 20, contour plots are given of the y- and z-
components of the velocity and vorticity for Run 7 in the
y-z plane at x = 0 at t = 30. Examination of these contour
plots (and others made at different locations) show several
interesting features. First, there is evidently a correlation
between the x- and z-velocity components representing enhanced
transfer of momentum towards the walls. Also, the contours of
u in the x-y plane given in Fig. 21 show gusts of high-
velocity fluid moving through the center of an otherwise
slow-moving stream; the leading edges of a gust seem to be
sharper than the trailing edges, implying negative skewness
in velocity derivatives.

In Fig. 22, we plot the profile of the two-
dimensional primary wave at t = 30 and t = 45 , respectively,
for Run 7. In Fig. 23 , we present a similar plot of the
two-dimensional harmonic components at t = 45 in Run 7,
while in Fig. 24 we plot the profile of the primary oblique

43

wave ($\alpha = 1, \beta = 1$) at $t = 45$ in Run 7. Figs. 22-24 show

that, through the period of initial breakdown, the largest

fluctuations occur in the neighborhood of the walls. At later

times, the harmonic components develop slightly stronger activity

near the center of the channel. The spatial structure and amplitude

of these fluctuations is not inconsistent with experimental

observations (Laufer 1951, Comte-Bellot 1965).

Run 9 tests the effect of decreasing the initial amplitude

of the two-dimensional and three-dimensional initial disturbances

in Runs 7 and 8 by 25%. In Fig. 25, the maximum amplitude of the

primary two-dimensional wave, its harmonic, and the primary three-

dimensional wave for Run 9 are plotted as functions of t. The

instability in Run 9 is considerably weaker than in Run 8. In

other runs, we have found that keeping the amplitude of the

two-dimensional disturbance in Run 8 at 0.11, but decreasing

the amplitude of the three-dimensional disturbance to 0.025

stabilizes the flow. Similarly, another run decreasing the

amplitude of the two-dimensional wave to 0.05, but keeping the

amplitude of the three-dimensonal wave disturbance at 0.05 as

in Run 8, stabilized the flow. At R = 1250, there seems to

be a critical amplitude of about 0.08 for the two-dimensional

component and about 0.04 for the three-dimensional component.

Runs 10-13 were designed to test the sensitivity of the

flow to various spanwise wave numbers. The amplitude of the

initial disturbances in these runs is chosen to be close to that

of Runs 7 and 8. Run 10 uses a primary spanwise wave number

$\beta = 0.25$. In this case, the three-dimensional disturbance is

nearly two-dimensional and is barely distinguishable from the primary two-dimensional disturbance. The resulting flow is so nearly two-dimensional that the disturbances die away quickly. Run 11 uses a primary spanwise wave number $\beta = 0.5$; in this case transition was observed but only at the late time $t \approx 120$. (Even though Runs 10-13 use the low spatial resolution $8 \times 8 \times 33$, we believe that the prediction of transition in Runs 11 and 12 is justified because the three-dimensional disturbance remains at large amplitude during the laminar phase. The resolution problems discussed below with regard to Runs 14 and 15 seem to apply only to marginally unstable flows.)

Other runs made with the two- and three-dimensional disturbances detuned from the least stable modes of the Orr-Sommerfeld equation [used in (4.1)] gave significantly less tendency to undergo transition than the runs discussed here.

Runs 12 and 13 introduce a new feature into the calculation. With $\beta = 2$ (Run 12) and $\beta = 4$ (Run 13), the least stable three-dimensional mode of the Orr-Sommerfeld equation is no longer concentrated near the wall like the two-and three-dimensional modes plotted in Figs. 11 and 12. The least stable three-dimensional mode with $\beta = 4$ at $R = 1250$ is plotted in Fig. 26; it is evident that this mode is concentrated near the center of the channel. Runs made using this three-dimensional center mode together with the two-dimensional disturbance mode plotted in Fig. 11 invariably decay, evidently because there is not enough interaction between the center mode and the wall mode disturbances. However, transition to turbulence with these larger spanwise wave numbers β can be achieved by using a three-dimensional wall mode disturbance.

45

The least stable three-dimensional wall mode disturbance with
$\beta = 4$ at $R = 1250$ is plotted in Fig. 27. Runs 12 and 13 use
these least stable wall modes. Run 12 is strongly unstable
and leads quickly to transition. On the other hand, Run 13 is

stable and does not undergo transition, even though the
wall mode disturbance is used. Evidently there is a spanwise
wave number selection mechanism involved in the transition
process. It seems that the most dangerous three-dimensional disturbances
have wavefronts at an angle of about 45°-60° to the mean flow.

Runs 14 and 15 illustrate a possible pitfall of numerical
analysis of these transition problems. The only difference between
these two runs is the horizontal resolution: in Run 14, only
8×8 Fourier modes are used to resolve the x and y directions;
in Run 15, 16×16 Fourier modes are used. Both runs are
made at $R = 750$. In Fig. 28, we plot the maximum amplitudes
of the primary two-dimensional wave, its harmonic, and the
primary three-dimensional wave for Run 14. The disturbances
decay until about $t \approx 100$ and then abruptly erupt into
turbulence. A similar plot for Run 15 is given in Fig. 29.
In this case, the disturbances undergo only a smooth continuous
decay and no 'transition' is observed. We have also made a run
in which the $8 \times 8 \times 33$ resolution of Run 14 is increased to
$16 \times 16 \times 33$ at $t = 90$ in Run 14; in this case, as in Run 15,
no transition is observed. Evidently low-resolution can give
premature predictions of transition. Similar effects of low
resolution have been observed by McLaughlin & Orszag (1979) in
calculations of transition in three-dimensional Bénard

46

convection. It is essential that transition calculations be done with utmost care, in order to avoid these spurious predictions of instability and breakdown in three-dimensional calculations. Our spectral calculations do provide a 'bootstrap' procedure to test internal accuracy of the simulations; if the spectrum obtained by Run 14 is tested for convergence in the same way as the spectrum of Run 7 is tested by the results given in Tables 5 and 6, it is found that the 8×8 truncation in x and y in Run 14 has a large effect.

We are confident that our transition predictions cited earlier in this Section, especially for Run 7, are not affected by these resolution problems of Run 14.

Our final plane Poiseuille flow run is Run 16. Here the initial conditions consist of the output from Run 8. These "turbulent" initial conditions are then run at the lower Reynolds number $R = 500$, in order to test whether an initial field of turbulence can persist at this lower Reynolds number. In Fig. 30, we plot the evolution of the maximum amplitude of the two-dimensional primary wave, its harmonic, and the primary three-dimensional wave. While the results are not conclusive, it seems that the field of turbulence is slowly decaying and that $R = 500$ is not sufficiently high to sustain turbulence.

Runs 17-20 investigate the effect of three-dimensional finite-amplitude disturbances on plane Couette flow. While plane Couette flow is much more stable than plane Poiseuille flow for small-amplitude disturbances and two-dimensional finite-amplitude disturbances (see Sec. 3), the effects of finite-amplitude three-dimensional disturbances at modest

Reynolds numbers are just as dramatic in plane Couette flow as in plane Poiseuille flow.

In Figs. 31 and 32, we plot the profiles of the x-velocity of the two- and three-dimensional primary disturbances, respectively, applied initially in Runs 17 and 18 at R = 1250. These profiles are obtained from the corresponding least stable eigenfunctions of the Orr-Sommerfeld equation for plane Couette flow by forming the symmetric combination (3.2) [with an extra factor $exp(i\beta y)$ for the three-dimensional mode]. (The asymmetry observed in Fig. 31 is due to the complex phase of the mode at the particular value of x at which the plot was made.) In Fig. 33, we plot the maximum amplitude of the two-dimensional primary disturbance, its harmonic, and the primary three-dimensional disturbance vs

t for Run 17. The flow breaks down to turbulence near t = 45 . A similar plot for the lower resolution Run 18 is given in Fig. 34. There is good agreement between the results plotted in Figs. 33 and 34 until beyond the breakdown of the laminar flow. We conclude that this flow does undergo transition to turbulence.

In Fig. 35, we plot the mean-velocity profile $\bar{u}(z)$ for Run 17 at t = 60 . It is apparent that the mean-velocity profile is tending toward the characteristic S-shape expected in turbulent Couette flow.

The effect of the symmetrized initial condition (3.2) on the evolution of the flow is illustrated by Runs 19 and 20 made at R = 1000. The maximum amplitude plot for Run 19 plotted in Fig. 36 suggests possible transition near t = 75 ; we hesitate to

claim that this transition is real because of possible resolution limitations. The maximum mode amplitudes for Run 19 listed in Table 7 show that the transverse $(m = 0)$ modes are likely to be inadequately resolved for $t \gtrsim 60$. An interesting feature of Figs. 33, 34, and 36 for the symmetrized initial disturbances is the high frequency oscillation of the maximum amplitude of the two-dimensional primary wave and its harnomic. Run 20 is made using unsymmetrized Orr-Sommerfeld eigenfunctions as initial conditions. The maximum amplitude plot for this run, made at $R = 1000$, is given in Fig. 37. Two features are noteworthy. First, in contrast with Run 19, the transition in this case can be much more confidently asserted, because the resolution limitations do not appear to be severe until after breakdown occurs. Second, the high frequency oscillations in the two-dimensional disturbances and its harmonic have disappeared.

As for plane Poiseuille flows, the plane Couette flow runs are characterized by very rapid generation of the transverse Fourier components $m = 0$ in (2.3) [see Table 7 for the results of Run 19]. In these flows, it seems that small-scale structures are generated by the strong instability of the flows resulting from superposition of the longitudinal vortices, represented by the transverse $(m = 0)$ Fourier components, on the basic laminar flows (1.3-4).

We have encountered significant difficulty in extending our plane Couette flow runs to later times than initial breakdown. Evidently, the turbulence that develops is of a particularly severe kind that is inadequately resolved using the current codes.

In conclusion, it seems that plane Couette flow undergoes transition at Reynolds numbers at least as low as those for which

plane Poiseuille flow undergoes transition. Three-dimensional effects are crucial in establishing breakdown at Reynolds numbers of order 1000.

5. Conclusions

The results presented in Sects. 3 and 4 show the central role played by the interaction of two-and three-dimensional finite-amplitdue disturbances in the breakdown of plane Poiseuille and plane Couette flows. The basic character of this interaction is qualitatively consistent with the theory developed by Benney & Lin(1960) to explain the experiments of Klebanoff, Tidstrom & Sargent (1962). However, as has been emphasized by Stuart (1961), the Benney-Lin theory can be at

best qualitatively correct. The theory assumes that the phase velocities of the interacting two- and three-dimensional waves are identical, which is not correct (see Tables 3 and 4).

Our calculations show that three-dimensional finite-amplitude effects produce strong inflectional velocity profiles that eventually break down to turbulence. In plane Poiseuille flow, these three-dimensional effects due to initial disturbances with amplitudes of 5-10% of the mean flow explain the experimentally observed transitions at Reynolds numbers of order 1000, whereas arbitrarily large two-dimensional finite-amplitude disturbances seem powerless at Reynolds numbers much below 3000. The most dangerous three-dimensional interactions seem to be between oblique Orr-Sommerfeld modes propagating at about 45° to the unperturbed flow with a wavelength about 3 times larger than the channel depth. In plane Couette flow, our numerical results suggest that three-dimensional effects due to initial disturbances

with amplitudes of order 5-10% can drive transition at Reynolds numbers of order 1000, while two-dimensional effects do not seem strong even at Reynolds numbers an order of magnitude larger. The numerical results also suggest that turbulence can be sustained in these planar shear flows at somewhat lower Reynolds numbers but not as low as 500.

One disturbing feature is the high resolution in both space and time that seems to be necessary to compute these transition flows. To compute transition accurately, it is necessary to calculate relatively weak interactions over many linear oscillation periods. While turbulent flows do require high spatial resolution, they also evolve quickly so that the total computer time may be less than for a transition calculation. Also, in turbulence calculations, only statistical averages need be determined accurately and practice has shown that accurate statistical results can be obtained with relatively low resolution.

It is interesting that we have found, in contrast to some previous investigators, that the accuracy requirements of transition calculations are more severe in the horizontal x- and y-directions than in the z-direction normal to the walls. The Chebyshev expansions used in the z-direction have extraordinarily good resolution near the walls. Our result that low horizontal resolution can give spurious predictions of transition must be considered carefully in future work on these problems. Low horizontal resolution prevents the excitation of small scale motions that can act as an 'eddy' viscosity that damps out instabilities.

References

Antar, B. N. & Collins, F. G. 1975 Numerical calculation of finite amplitude effects in unstable laminar boundary layers. Phys. Fluids 18, 289.

Benney, D. J. 1961 A non-linear theory for oscillations in a parallel flow. J. Fluid. Mech. 10, 209.

Benney, D. J. 1964 Finite amplitude effects in an unstable laminar boundary layer. Phys. of Fluids 7, 319.

Benney, D. J. & Lin, C. C. 1960 On the secondary motion induced by oscillations in a shear flow. Phys. of Fluids 3, 656.

Coffee, T. 1977 Finite amplitude instability of plane Couette flow. J. Fluid Mech. 83, 401.

Comte-Bellot, G. 1965 Écoulement Turbulent Entre Deux Parois Parallèles. Publications Scientifiques et Techniques du Ministère de l'Air 419.

Davey, A. 1973 On the stability of plane Couette flow to infinitesimal disturbances. J. Fluid Mech. 57, 369.

Davey, A. 1978 On Itoh's finite amplitude stability theory for pipe flow. J. Fluid Mech. 86, 695.

Davey, A., Hocking, L. M. & Stewartson, K. 1974 On the nonlinear evolution of three-dimensional disturbances in plane Poiseuille flow. J. Fluid Mech. 63, 529.

Davey, A. & Nguyen, H.P.F. 1971 Finite-amplitude stability of pipe flow. J. Fluid Mech. 45, 701.

Davies, S. J. & White, C. M. 1928 An experimental study of the flow of water in pipes of rectangular section. Proc. Roy. Soc. A119, 92.

Ellingsen, T., Gjevik, B. & Palm, E. 1970 On the non-linear stability of plane Couette flow. J. Fluid Mech. 40, 97.

Eckhaus, W. 1965. Studies in Non-Linear Stability Theory. Springer-Verlag, New York.

Fasel, H. 1976 Investigation of the stability of boundary layers by a finite-difference model of the Navier-Stokes equations. J. Fluid Mech. 78, 355.

Fasel, H., Bestek, H. & Schefenacker, R. 1977 Numerical simulation studies of transition phenomena in incompressible, two-dimensional flows. Laminar-Turbulent Transition, AGARD Conference Proceedings No. 224, p. 14-1.

George, W. D., Hellums, J. D. & Martin, B. 1974 Finite-amplitude neutral disturbances in plane Poiseuille flow. J. Fluid Mech. 63, 765.

Gottlieb, D. & Orszag, S. A. 1977 Numerical Analysis of Spectral Methods: Theory and Applications. NSF-CBMS Monograph 26, Soc. Ind. App. Math., Philadelphia.

Grohne, D. 1969 Die Stabilität der ebenen Kanalstromung gegenüber dreidimensionalen Störungen von endlicher Amplitude. A. V. A. Gottingen Rep. 69-A-30.

Herbert, T. 1976 Periodic secondary motions in a plane channel. Proceedings of the Fifth International Conference on Numerical Methods in Fluid Dynamics, ed. by A. I. van de Vooren and P. J. Zandbergen, Springer-Verlag. New York, p. 235.

Herbert, T. 1977 Finite amplitude stability of plane parallel flows. Laminar-Turbulent Transition, AGARD Conference Proceedings No. 224, p. 3-1.

Hocking, L. M., Stewartson, K. & Stuart, J.T. 1972 A nonlinear instability burst in plane parallel flow. J. Fluid Mech. 51, 705.

Itoh, N. 1977 Nonlinear stability of parallel flows with subcritical Reynolds numbers. Part 1. An asymptotic theory valid for small amplitude disturbances. J. Fluid Mech. 82, 455.

Itoh, N. 1978 Three-dimensional growth of finite wave disturbances in plane Poiseuille flow. To be published.

Kao, T. W. & Park, C. 1970 Experimental investigations of the stability of channel flows. Part 1. Flow of a single liquid in a rectangular channel. J. Fluid Mech. 43, 145.

Kells, L. C. 1978 Numerical calculations of turbulent and transition flows. Ph. D. Thesis, M.I.T., Cambridge, MA.

Klebanoff, P. S., Tidstrom, K. D. & Sargent, L. M. 1962 The three-dimensional nature of boundary-layer instability. J. Fluid Mech. 12, 1.

Kuwabara, S. 1967 Nonlinear instability of plane Couette flow. Phys. of Fluids 10, S115.

Lakin, W. D., Ng, B. S. & Reid, W. H. 1978 Approximations to the eigenvalue relation for the Orr-Sommerfeld problem. Phil. Trans. Roy. Soc. Lond. A289, 347.

Landahl, M. T. 1972 Wave mechanics of breakdown. J. Fluid Mech. 56, 775.

Laufer, J. 1951 Investigation of turbulence in a two-dimensional channel. N.A.C.A. Tech. Rep. no. 1053.

Lessen, M. & Cheifetz, M. G. 1975 Stability of plane Couette flow with respect to finite two-dimensional disturbances. Phys. of Fluids 18, 939.

Lin, C. C. 1955 The Theory of Hydrodynamic Stability. Cambridge University Press.

McLaughlin, J. & Orszag, S. A. 1979. To be published.

Meksyn, D. 1964 Stability of laminar flow between parallel planes for two- and three-dimensional finite disturbances. Z. Phys. 178, 159.

Meksyn, D. & Stuart, J. T. 1951 Stability of viscous motion between parallel planes for finite disturbances. Proc. Roy. Soc. A208, 517.

Metcalfe, R. W. 1974 Spectral methods for boundary value problems in fluid mechanics. Ph. D. Thesis, M.I.T., Cambridge, MA.

Michael, D.H. 1961 Note on the stability of plane parallel flows. J. Fluid Mech. 10, 525.

Murdock, J. 1977 A numerical study of nonlinear effects on boundary-layer stability. AIAA 15th Aerospace Sciences Meeting, Paper 77-127.

Murdock, J. & Taylor, T. D. 1977 Numerical investigation of nonlinear wave interaction in a two-dimensional boundary layer. Laminar-Turbulent Transition, AGARD Conference Proceedings No. 224, p. 4-1.

Nishioka, M., Iida, S. & Ichikawa, Y. 1975 An experimental investigation of the stability of plane Poiseuille flow. J. Fluid Mech. 72, 731.

Orszag, S. A. 1971a Numerical simulation of incompressible flows within simple boundaries. I. Galerkin (spectral) representations. Stud. in Appl. Math. 50, 293.

Orszag, S. A. 1971b Accurate solution of the Orr-Sommerfeld stability equation. J. Fluid Mech. 50, 689.

Orszag, S. A. 1976 Turbulence and transition: a progress report. Proceedings of the Fifth International Conference on Numerical Methods in Fluid Dynamics, ed. by A. I. van de Vooren and P. J. Zandbergen, Springer-Verlag, New York, p. 32.

Orszag, S.A. & Patterson, G. S. 1972 Numerical simulation of three-dimensional homogeneous isotropic turbulence. Phys. Rev. Letters 2_, 76.

Patel, V. & Head, M.R. 1967 Some observations on skin friction and velocity profiles in fully developed pipe and channel flows. J. Fluid Mech. 38, 181.

Pekeris, C. L. & Shkoller, B. 1967 Stability of plane Poiseuille flow to periodic disturbances of finite amplitude in the vicinity of the neutral curve. J. Fluid Mech. 29, 31.

Pekeris, C. L. & Shkoller, B. 1969 Stability of plane Poiseuille flow to periodic disturbances of finite amplitude. J. Fluid Mech. 39, 611.

Pekeris, C. L. & Shkoller, B. 1971 Stability of plane Poiseuille flow to periodic disturbances of finite amplitude. II. Proc. Nat. Acad. Sci. 68, 197.

Reichardt, H. 1959 Gesetzmässigkeiten der geradlinigen turbulenten Couetteströmung. Mitt. Max-Planck-Institut für Strömungsforschung 22, Göttingen.

Reynolds, W. C. & Potter, M. C. 1967 Finite-amplitude instability of parallel shear flows. J. Fluid Mech. 27, 465.

Rosenblat, S. & Davis, S. H. 1978 Bifurcation from infinity. To be published.

Stuart, J. T. 1960 On the non-linear mechanics of wave disturbances in stable and unstable parallel flows. Part 1. The basic behavior in plane Poiseuille flow. J. Fluid Mech. 9, 353.

Stuart, J. T. 1961 On three-dimensional nonlinear effects in the stability of parallel flows. Adv. Aeronaut. Sci. 3, 121.

Stuart, J. T. 1971 Nonlinear stability theory. Ann. Rev. Fluid Mech. 3, 347.

Watson, J. 1960 On the non-linear mechanics of wave disturbances in stable and unstable parallel flows. Part 2. The development of a solution for plane Poiseuille flow and for plane Couette flow. J. Fluid Mech. 9, 371.

Watson, J. 1962 On spatially-growing finite disturbances in plane Poiseuille flow. J. Fluid Mech. 14, 211.

Zahn, J.-P., Toomre, J., Spiegel, E. A. & Gough, D. O. 1974 Nonlinear cellular motions in Poiseuille channel flow. J. Fluid Mech. 64, 319.

Table 1. Behavior of small-amplitude disturbances computed numerically compared with behavior predicted by Orr-Sommerfeld equation.

	Plane Poiseuille flow		Plane Couette flow	
	Two-dimensional disturbance	Three-dimensional disturbance	Two-dimensional disturbance	Three-dimensional disturbance
Reynolds number R	1500	1500	5000	5000
x-wavenumber α	1	1	0.5	0.5
y-wavenumber β	0	1	0	0.5
Re ω	0.3262988	0.4012928	0.3511072	0.3517084
Im ω	-0.0282057	-0.0282305	-0.0413797	-0.0418436
Initial amplitude (x-velocity)	2.198×10^{-5}	4.964×10^{-5}	1.209×10^{-4}	6.338×10^{-4}
Spatial resolution $(2M) \times (P+1)$	8×33	8×33	8×65	8×65
Time step Δt	0.1	0.1	0.1	0.1
Final time T	10	10	6	6
Computed amplitude decay $0 \leq t \leq T$	0.753519	0.756756	0.781904	0.778925
Predicted amplitude decay $\exp[(Im \, \omega)T]$	0.754231	0.754044	0.780143	0.777975
Computed phase change (radians) $0 \leq t \leq T$	-3.25644	-4.00617	-2.10548	-2.10545
Predicted phase change $-(Re \, \omega)T$	-3.26299	-4.01293	-2.10664	-2.11025

Table 2. Finite-amplitude two-dimensional disturbance
characteristics of runs discussed in Sec. 3.

Run number	1	2	3	4	5	6
Undisturbed flow	←————————— Plane Poiseuille —————————→					Plane Couette
Reynolds number R	2500	2935	2935	2935	3500	5000
x-wavenumber $\alpha(=2\pi/X)$	1.3231	1.3231	1.3231	1.3231	1.	2.
Re ω	0.4480553	←—————— 0.4352820 ——————→			0.2848825	1.6314426
Im ω	-0.0192961	←—————— -0.0181933 ——————→			-0.0072171	-0.1093940
Initial amplitude (x-velocity)	0.179	0.182	0.108	0.072	0.217	0.184
Spatial resolution $(2M)\times(P+1)$	32×33	32×33	8×33	8×33	16×33	8×33
Time step Δt	0.05	0.05	0.1	0.1	0.1	0.1
Final time T	150.	150.	100.	100.	100.	150.
Growth or decay?	Decay	Weak Growth	Neutral	Decay	Decay	Decay

Table 3. Finite-amplitude three-dimensional disturbance characteristics of plane Poiseuille flow runs discussed in Sec. 4.

Run number	3A	7	8	9	10	11	12	13	14	15	16
Reynolds number R	2935	1250	1250	1250	1250	1250	1250	1250	750	750	500
Spatial resolution:											
2M	8	32	16	16	8	8	8	8	8	16	16
2N	4	32	16	16	8	8	8	8	8	16	16
P+1	33	33	33	33	33	33	33	33	33	33	33
Two-dimensional disturbance:											
x-wavenumber $\alpha(=2\pi/X)$	1.3231	1	1	1	1	1	1	1	1	1	1
Re ω	0.4353				←———— 0.3353 ————→				←0.3604→		*
Im ω	-0.0182				←———— -0.0348 ————→				←-0.0533→		*
Initial x-velocity amplitude	0.11	0.11	0.11	0.08	0.11	0.11	0.11	0.11	0.11	0.11	*
Three-dimensional disturbance:											
x-wavenumber α	1.3231	1	1	1	1	1	1	1	1	1	1
y-wavenumber $\beta(=2\pi/Y)$	1	1	1	1	0.25	0.5	1	2.	4.	1	1.
Re ω	*		←—— 0.4132 ——→		0.3420	0.3602	0.4823*	0.4635*	←0.4463→		*
Im ω	*		←—— -0.0318 ——→		-0.0328	0.0300	-0.0926*	-0.1607*	←-0.0453→		*
Initial x-velocity amplitude	10^{-14}*	0.05	0.05	0.04	0.05	0.05	0.05	0.05	0.04	0.04	*

* See text

Table 4. Finite-amplitude three-dimensional disturbance characteristics of plane Couette flow runs discussed in Sec. 4.

Run number	17	18	19	20
Reynolds number R	1250	1250	1000	1000
Spatial Resolution:				
2M	16	8	16	8
2N	16	8	16	8
P+1	33	33	33	33
Two-dimensional disturbance:				
x-wavenumber $\alpha(=2\pi/X)$	1	1	1	1
Re ω	←— 0.6324 —→		←— 0.6053 —→	
Im ω	←— −0.1098 —→		←— −0.1192 —→	
Initial x-velocity amplitude	0.10	0.10	0.09	0.09
Three-dimensional disturbance:				
x-wavenumber α	1	1	1	1
y-wavenumber $\beta(=2\pi/Y)$	1	1	1	1
Re ω	←— 0.6380 —→		←— 0.6118 —→	
Im ω	←— −0.1140 —→		←— −0.1241 —→	
Initial x-velocity amplitude	0.06	0.06	0.05	0.05

Table 5.

Maximum amplitude in z of the transverse Fourier components of the x-velocity $u(m=0,n,z,t)$ in the mixed spectral (x-y)-physical (z) space representation for Run 7.

Spanwise Wavenumber   (n)

t	1	2	3	4	6	8
0	0	0	0	0	0	0
10	1.88(-2)	8.29(-3)	6.60(-4)	1.42(-4)	3.40(-6)	1.00(-7)
20	3.24(-2)	2.32(-2)	4.10(-3)	2.40(-3)	4.78(-4)	1.00(-4)
30	3.79(-2)	6.19(-2)	1.56(-2)	8.55(-3)	2.09(-3)	1.57(-3)
35	3.38(-2)	9.56(-2)	2.51(-2)	1.30(-2)	2.32(-3)	1.77(-3)
40	2.76(-2)	1.27(-1)	3.48(-2)	1.73(-2)	4.41(-3)	2.71(-3)
45	3.18(-2)	1.36(-1)	3.04(-2)	2.06(-2)	6.90(-3)	4.34(-3)
50	2.94(-2)	6.84(-2)	1.00(-2)	2.14(-2)	8.17(-3)	2.86(-3)

Table 6.

Maximum Amplitude in z of the Fourier components of the x-velocity u(m,n,z,t) in the mixed spectral (x-y)-physical (z) space representation for Run 7.

	Time (t)			
Component (m,n)	20	30	40	50
Two Dimensional Harmonics				
(1,0)	5.69(-2)	4.11(-2)	2.70(-2)	1.78(-2)
(2,0)	4.50(-3)	4.45(-3)	3.31(-3)	7.66(-3)
(3,0)	1.45(-3)	8.31(-4)	3.05(-4)	5.33(-3)
(4,0)	4.99(-4)	9.63(-5)	2.16(-4)	3.75(-3)
(6,0)	6.08(-5)	3.02(-5)	3.50(-5)	2.26(-3)
(8,0)	1.10(-5)	1.03(-5)	1.28(-5)	5.92(-4)
Oblique Harmonics				
(1,1)	7.61(-2)	8.15(-2)	6.14(-2)	2.31(-2)
(2,1)	6.75(-3)	2.47(-3)	8.71(-4)	9.46(-3)
(4,1)	5.98(-4)	2.80(-4)	2.32(-4)	1.89(-3)
(6,1)	6.35(-5)	4.34(-5)	3.06(-5)	1.20(-3)
(8,1)	1.61(-5)	1.43(-5)	1.35(-5)	4.31(-4)
Diagonal Components				
(2,2)	5.90(-3)	6.37(-3)	3.99(-3)	9.55(-3)
(3,3)	1.12(-3)	1.14(-3)	1.28(-3)	3.09(-3)
(4,4)	1.32(-4)	3.69(-4)	4.05(-4)	2.35(-3)
(6,6)	5.38(-6)	7.00(-5)	9.30(-5)	1.37(-3)
(8,8)	5.64(-7)	2.07(-5)	1.38(-5)	7.94(-4)

Table 7. Maximum amplitude in z of the Fourier components of
the x-velocity u(m,n,z,t) in the mixed spectral
(x-y) - physical (z) space representation for Run 19.

Component (m,n)	Time (t)			
	30	45	60	75
Two-Dimensional Harmonics				
(1,0)	4.87(-3)	2.08(-3	1.40(-3)	2.58(-3)
(2,0)	8.51(-4)	2.57(-4)	1.42(-3)	1.85(-3)
(3,0)	8.53(-5)	2.52(-5)	1.87(-4)	8.56(-4)
(4,0)	1.92(-5)	2.42(-6)	7.07(-5)	2.98(-4)
(6,0)	2.70(-6)	3.29(-7)	1.20(-6)	4.39(-5)
Oblique Harmonics				
(1,1)	2.76(-2)	6.30(-3)	1.11(-3)	4.97(-3)
(2,1)	1.31(-3)	9.32(-5)	3.95(-4)	2.96(-3)
(3,1)	9.69(-5)	4.41(-5)	4.82(-5)	1.37(-3)
(4,1)	2.29(-5)	3.91(-6)	3.30(-5)	3.92(-4)
(6,1)	3.50(-6)	2.47(-7)	1.17(-6)	3.46(-5)
Transverse Components				
(0,1)	1.32(-2)	1.63(-2)	1.95(-2)	1.95(-2)
(0,2)	2.57(-2)	4.19(-2)	4.08(-2)	3.65(-2)
(0,3)	6.14(-3)	9.12(-3)	5.51(-3)	1.14(-2)
(0,4)	1.91(-3)	6.34(-3)	5.62(-3)	7.72(-3)
(0,6)	1.38(-4)	1.53(-3)	3.08(-3)	6.09(-3)
Diagonal Components				
(2,2)	1.30(-3)	3.55(-4)	2.44(-3)	3.55(-3)
(3,3)	1.14(-4)	8.14(-5)	1.45(-4)	1.62(-3)
(4,4)	1.37(-5)	8.86(-6)	2.20(-5)	4.22(-4)

Figure Captions

Fig. 1.   A plot of the profile u(z) of the x-velocity of
the two-dimensional initial disturbance used in Run 2.   This
disturbance is   chosen as the least stable eigenmode of the
Orr-Sommerfeld equation for plane Poiseuille flow with
$R = 2935$ and $\alpha = 1.3231$.   The phase of the initial
perturbation is   chosen so that the maximum velocity
perturbation occurs initially at $x = 0$,   where this plot
is made.   The initial disturbances used in Runs 3 and 4 are
proportional to that imposed in Run 2.

Fig. 2.   A plot of the time evolution of the maximum amplitude
in z of the x-velocity component of the two-dimensional
primary disturbance [that depending on x   like $\exp(i\alpha x)$]
and its harmonic [depending on x   like $\exp(2i\alpha x)$] for
Run 2.   At late times the primary disturbance is undergoing
slow growth.

Fig. 3.   A plot of the z-profile of the x-velocity component
of the primary disturbance in Run 2 at $t = 120$.

Fig. 4.   A plot of the mean velocity $\bar{u}(z)$ in Run 2 at $t = 120$.
For comparison, the undisturbed plane Poiseuille flow profile
$1-z^2$ is also plotted.

Fig. 5.   A plot of the curvature $-\bar{u}''(z)$ of the mean
velocity profile in Run 2 at $t = 120$.   For comparison, the
curvature 2 of the parabolic profile $1-z^2$ is also plotted.

Fig. 6.   A plot of the maximum amplitude A of the primary
disturbance and its harmonic for Run 4.   See Fig. 2.

Fig. 7.   A plot of the maximum amplitude A of the primary
disturbance and its harmonic for Run 1 at $R = 2500$.   The
initial disturbance is   chosen to be the least stable eigen-
mode of the Orr-Sommerfeld equation with $R = 2500$ $\alpha = 1.3231$.
See Fig. 2.

Fig. 8. A plot of the z-profile of the x-velocity component of the two-dimensional primary disturbance u(z) for the plane Couette flow Run 6 at R = 5000, α = 2. The initial conditions are chosen as the symmetrized combination (3.2) of the least stable eigenmode of the Orr-Sommerfeld equation and its complex-conjugate reflected eigenmode.

Fig. 9. A plot of the maximum amplitude A vs t of the x-velocity of the primary disturbance and its harmonic for the two-dimensional plane Couette flow Run 6 at R = 5000.

Fig. 10. A plot of the maximum amplitude A vs t for the two-dimensional primary disturbance and its harmonic and the three-dimensional primary wave [with α = 1.3231 and β = 1] in Run 3A. The two-dimensional part of the initial conditions is the same as in Run 3 of Sec. 3 while the three-dimensional component is introduced initially through round-off error. Note that the amplitude of the three-dimensional component is multiplied by 10^8.

Fig. 11. A plot of the z-profile of the x-velocity of the two-dimensional disturbance used in Runs 7-13. This disturbance is chosen to be the least stable eigenmode of the Orr-Sommerfeld equation for plane Poiseuille flow at R = 1250 with α = 1. The amplitude of this initial perturbation is reduced by 25% in Run 9.

Fig. 12. A plot of the z-profile of the x-velocity of the initial three-dimensional disturbance imposed in Runs 7-9. This disturbance is chosen as the least stable eigenmode of the Orr-Sommerfeld equation at R ≈ 1250 with α = 1 and β = 1. In Run 9, the initial amplitude is decreased by 25%.

Fig. 13. A plot of the maximum disturbance amplitudes A vs t for the three-dimensional plane Poiseuille flow Run 7 at R = 1250. The plotted amplitudes are the maxima in z of x-velocity of the two-dimensional primary disturbance and its harmonic (multiplied by 10) and the three-dimensional primary

disturbance [depending on x like exp($i\alpha x + i\beta y$) with
$\alpha = 1$ and $\beta = 1$].

Fig. 14. Same as Fig. 13 except for Run 8. The amplitude
of the two-dimensional harmonic is not multiplied by the
factor 10 used in Fig. 13.

Fig. 15. Plots of the mean velocity profiles (4.2) for
Run 8. _____ $t = 30$; $-\,-\,-$ $t = 45$; $-----$ $t = 60$;
..... $t = 75$. The corresponding plots for $t = 30$ and
$t = 45$ for Run 7 are indistinguishable from those plotted
in this Figure.

Fig. 16. Plots of the instantaneous x-velocity profiles $\bar{u}(x,y,z,t)$ vs.
z at $t = 30$ for Run 7. _____ $x = 0$, $y = -\pi$; $-\,-\,-\,-$
$x = 0$, $y = -\pi/2$; $-----$ $x = 0$, $y = 0$; ●●●●●●●●
$x = 13\pi/8$, $y = -5\pi/8$.

Fig. 17. Same as Fig. 16, except at $t = 45$. Labeled curves
are plotted at the same values of x and y as in Fig. 16.

Fig. 18. Contour plots of the instantaneous x-velocity $u(x,y,z,t)$
in the y-z plane at $x = 0$ in Run 7. (a) $t = 0$, contours
$0,0.9(0.1)$. (b) $t = 15$, contours $0,1(.1)$. (c) $t = 30$,
contours $0,1(0.1)$. (d) $t = 45$, contours $0,1(0.1)$. Note that
while the tick marks along the y-axis do indicate the available
y-resolution, the tick marks along the z-axis are included for
reference only and do not indicate the available resolution of
the Chebyshev series, especially near the walls.

Fig. 19. Contour plots of the x-vorticity component $\omega_1(x,y,z,t)$
in the y-z plane at $x = 0$ in Run 7. (a) $t = 0$, contours
-0.35, $0.35(0.07)$. (b) $t = 15$, contours $-0.32,0.32(0.08)$.
(c) $t = 30$, contours $-1,1(0.2)$. (d) $t = 45$, contours
$-2,2(0.4)$.

Fig. 20. Contour plots of flow components in Run 7 at $t = 30$
in the y-z plane at $x = 0$. (a) $v(x,y,z)$, contours $-0.06,0.06$
(0.01). (b) w (x,y,z), contours $-0.024,0.012(0.004)$. (c)

$\omega_2(x,y,z)$, contours $-2.5,2(0.5)$. (d) $\omega_3(x,y,z)$, contours $-0.3,0.3(0.06)$.

Fig. 21. Contour plots of the instantaneous x-velocity $u(x,y,z,t)$ in the x-y plane at $z = \cos 3\pi/16$ in Runs 7,8. (a) $t = 0$, contours 0.19, $0.41(0.01)$. (b) $t = 30$, contours 0.21, $0.42(0.01)$ for Run 7. (c) $t = 60$, contours 0.16, $0.84(0.04)$ for Run 8.

Fig. 22. A plot of the z-profile of the two-dimensional primary disturbance $u(1,0,z,t)$ [see (2.3)] in Run 7: (a) $t = 30$; (b) $t = 45$.

Fig. 23. A plot of the x-profile of the two-dimensional harmonic disturbance $u(2,0,z,t)$ [that depends on x and y like $\exp(2i\alpha x)$] at $t = 45$ in Run 7.

Fig. 24. A plot of the z-profile of the primary three-dimensional disturbance $u(1,1,z,t)$ [that depends on x and y like $\exp(i\alpha x+i\beta y)$] at $t = 45$ in Run 7.

Fig. 25. A plot of the maximum disturbance amplitudes vs t in Run 9 at $R = 1250$. This run is the same as Run 8 except that the initial amplitudes of both the two- and three-dimensional disturbances are reduced by 25%.

Fig. 26. A plot of the z-profile of the least stable eigenmode of the Orr-Sommerfeld equation for plane Poiseuille flow at $R = 1250$ with $\alpha = 1$ and $\beta = 4$. Observe that this mode is concentrated near the center of the channel, so it has little opportunity to interact with the least stable two-dimensional disturbance which is concentrated near the walls. This kind of three-dimensional disturbance typically does not lead to transition. The eigenvalue of the·Orr-Sommerfeld equation is $\omega = 0.9076 - i0.0579$. The phase velocity of this mode is about 0.9, in contrast to the phase velocity of wall modes which are usually in the range $0.3-0.4$.

Fig. 27. A plot of the z-profile of the second least stable eigenmode of the Orr-Sommerfeld equation for plane Poiseuille flow at $R = 1250$ with $\alpha = 1$ and $\beta = 4$. This wall mode has eigenvalue $\omega = 0.4635 - i0.1607$. This mode is used as the three-dimensional disturbance in Run 13.

Fig. 28. A plot of the maximum disturbance amplitudes in Run
14 at R = 750. This run uses 8 x 8 x 33 spatial resolution.

Fig. 29. Same as Fig. 28, except for Run 15. The amplitude of
the two-dimensional harmonic components is multiplied by a
factor 10. Run 15 differs from Run 14 only in that the spatial
resolution is 16 x 16 x 33. Observe that the flow no longer
undergoes 'transition'.

Fig. 30. A plot of the maximum disturbance amplitudes vs t
for Run 16 at R = 500. The initial conditions for this run
are the output conditions from Run 8. These initial conditions
are intended to simulate turbulence.

Fig. 31. A plot of the z-profile of the initial two-dimensional
disturbance used in Run 17 and 18. This disturbance is const-
ructed from the least stable eigenmode of the Orr-Sommerfeld
equation for plane Couette flow at R = 1250 with $\alpha = 1$
and $\beta = 0$ by symmetrizing according to (3.2).

Fig. 32. Same as Fig. 31, except that the profile of the
initial three-dimensional disturbance for Run 17 and 18 is
plotted.

Fig. 33. A plot of the maximum disturbance amplitudes A
vs t in Run 17 for plane Couette flow at R = 1250.

Fig. 34. Same as Fig. 33, except for Run 18, also at R = 1250.

Fig. 35. A plot of the mean velocity profile $\bar{u}(z)$ at t = 60
in Run 17.

Fig. 36. Same as Fig. 33, except for the plane Couette flow
Run 19 at R = 1000. Symmetrized initial conditions are used.

Fig. 37. Same as Fig. 33, except for the plane Couette flow
Run 20 at R = 1000. In this case, unsymmetrized initial
conditions are used. Observe that the high frequency time
oscillations in the maximum amplitude of the two-dimensional
primary disturbance and its harmonic disappear.
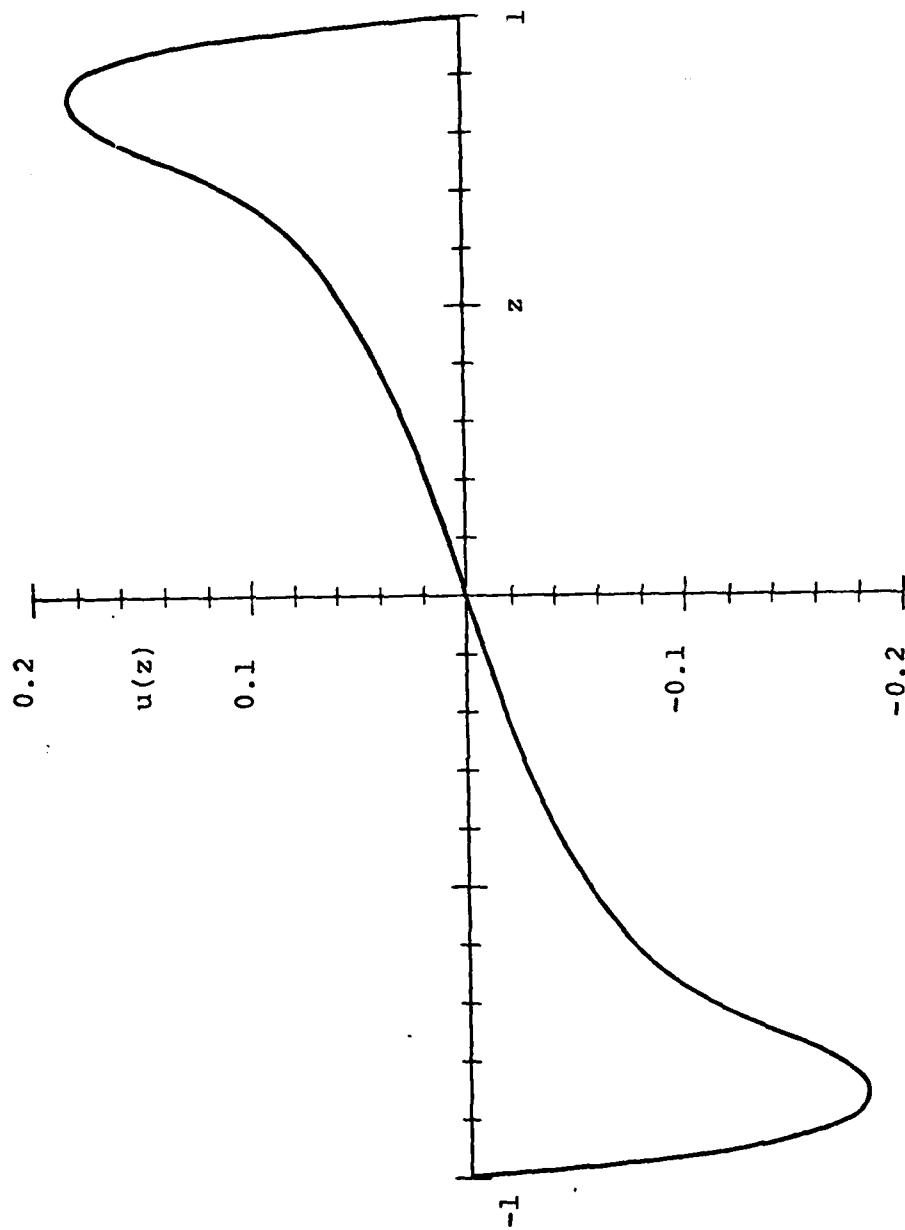
Figure 1

Figure 2

Figure 3

$1-z^2$

$\bar{u}(z)$ ——

Figure 4

$-\overline{u}''(z)$
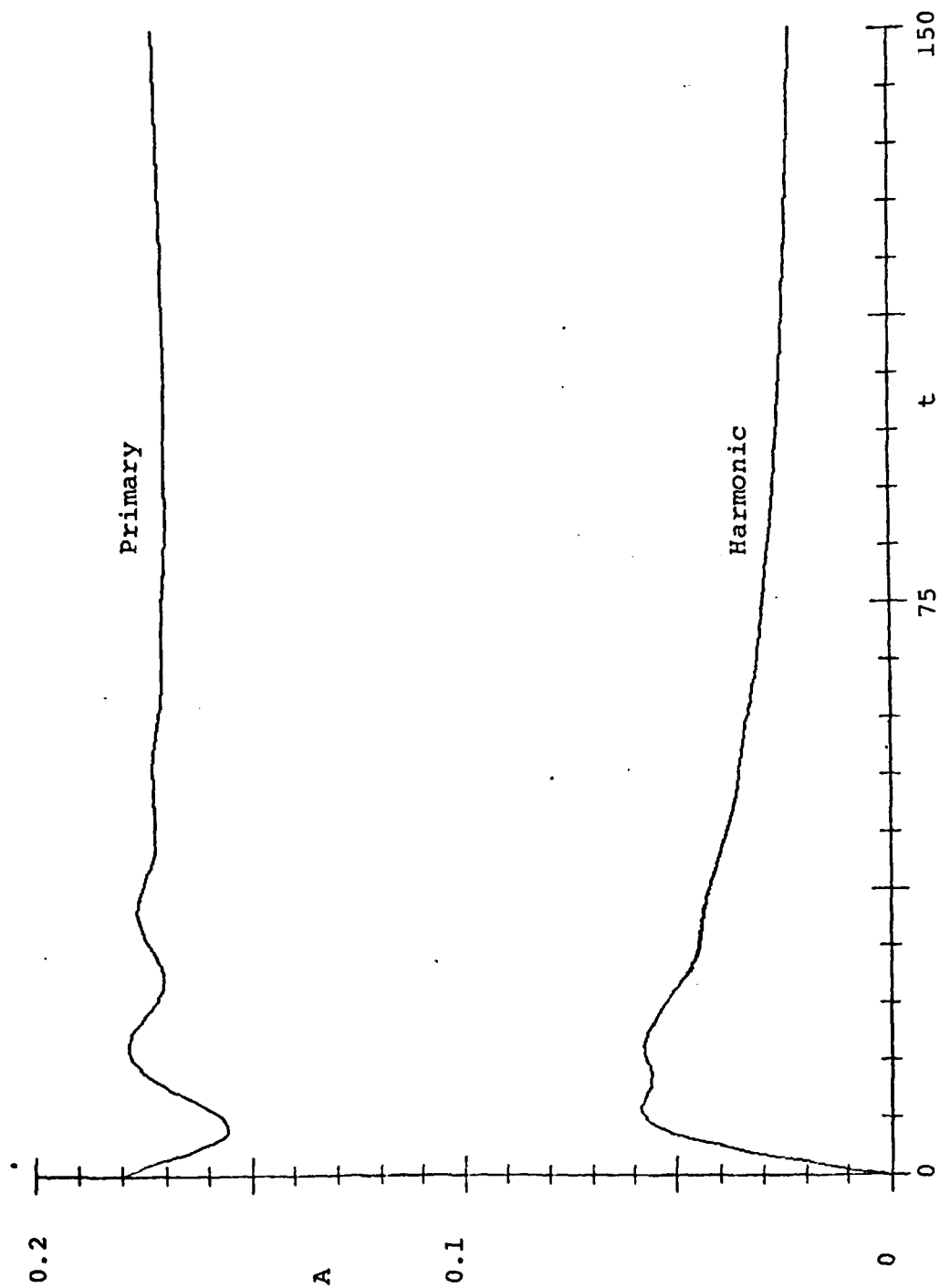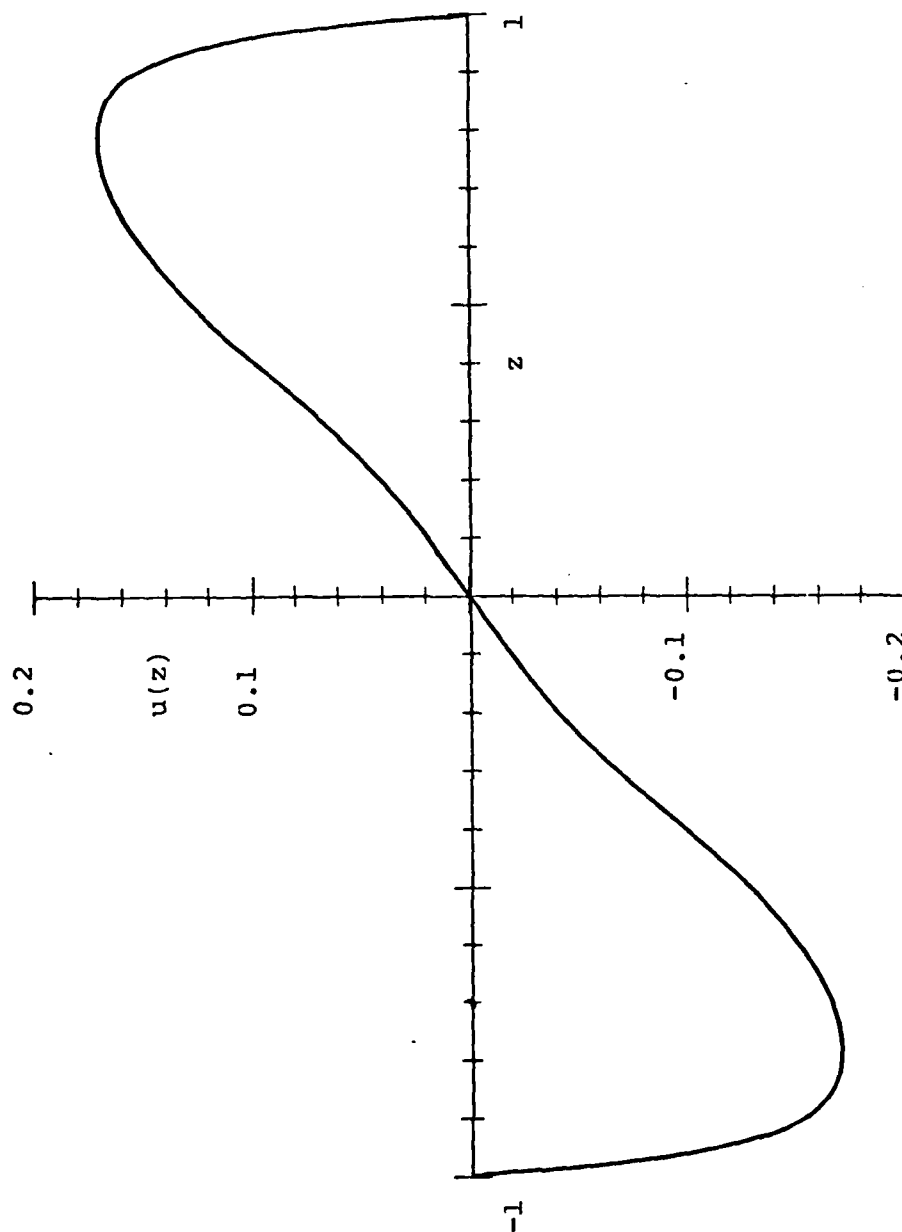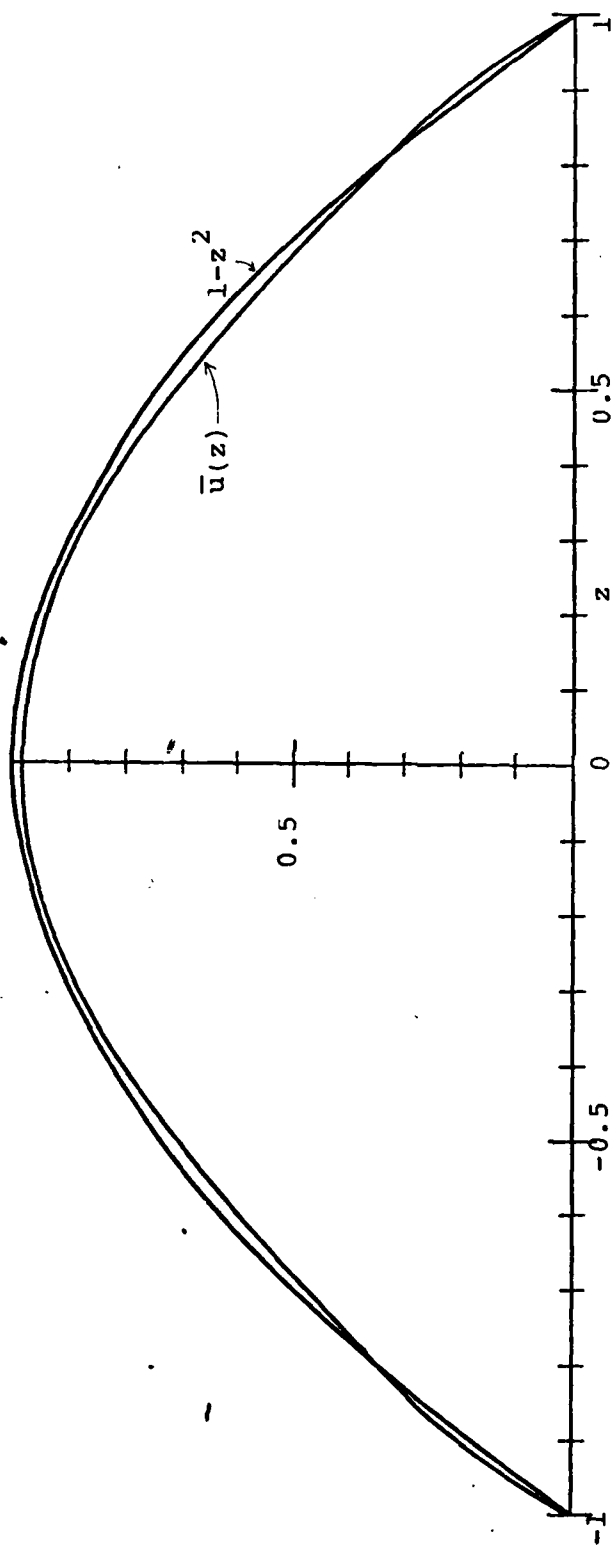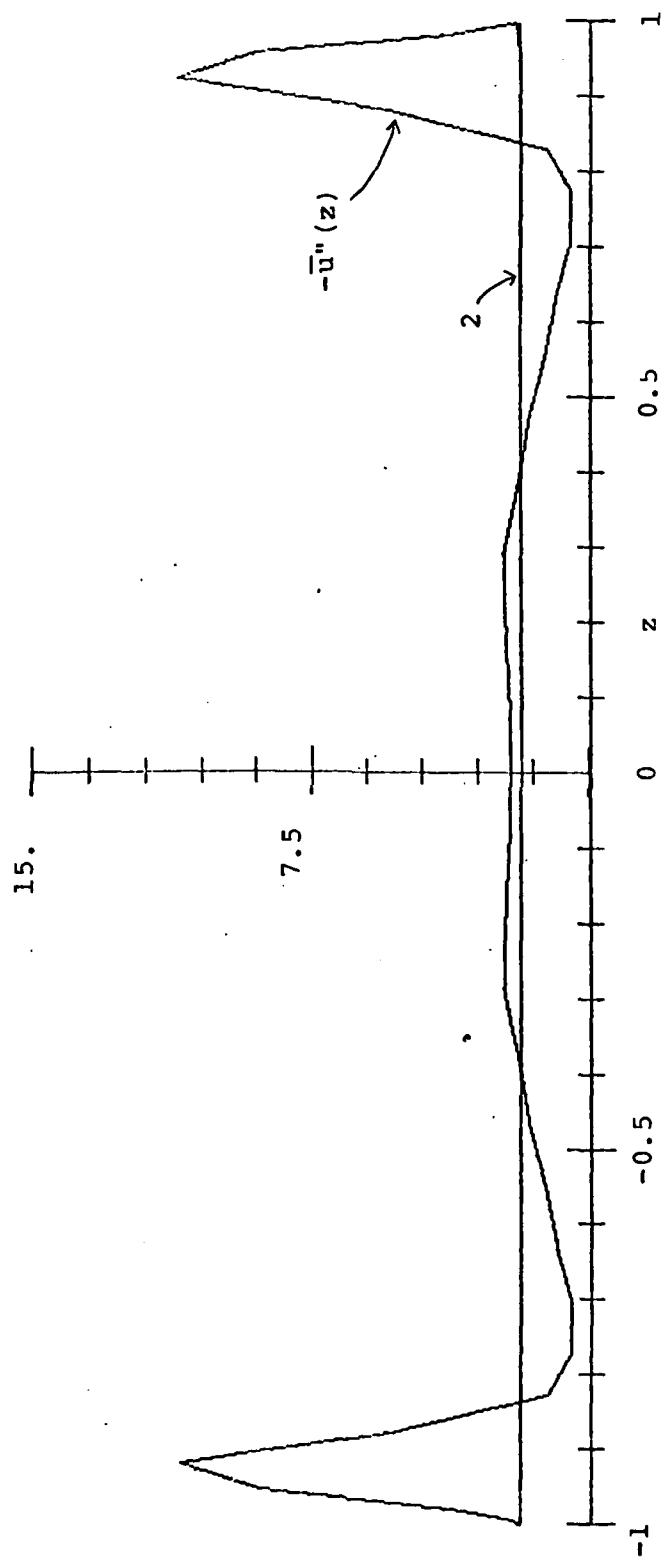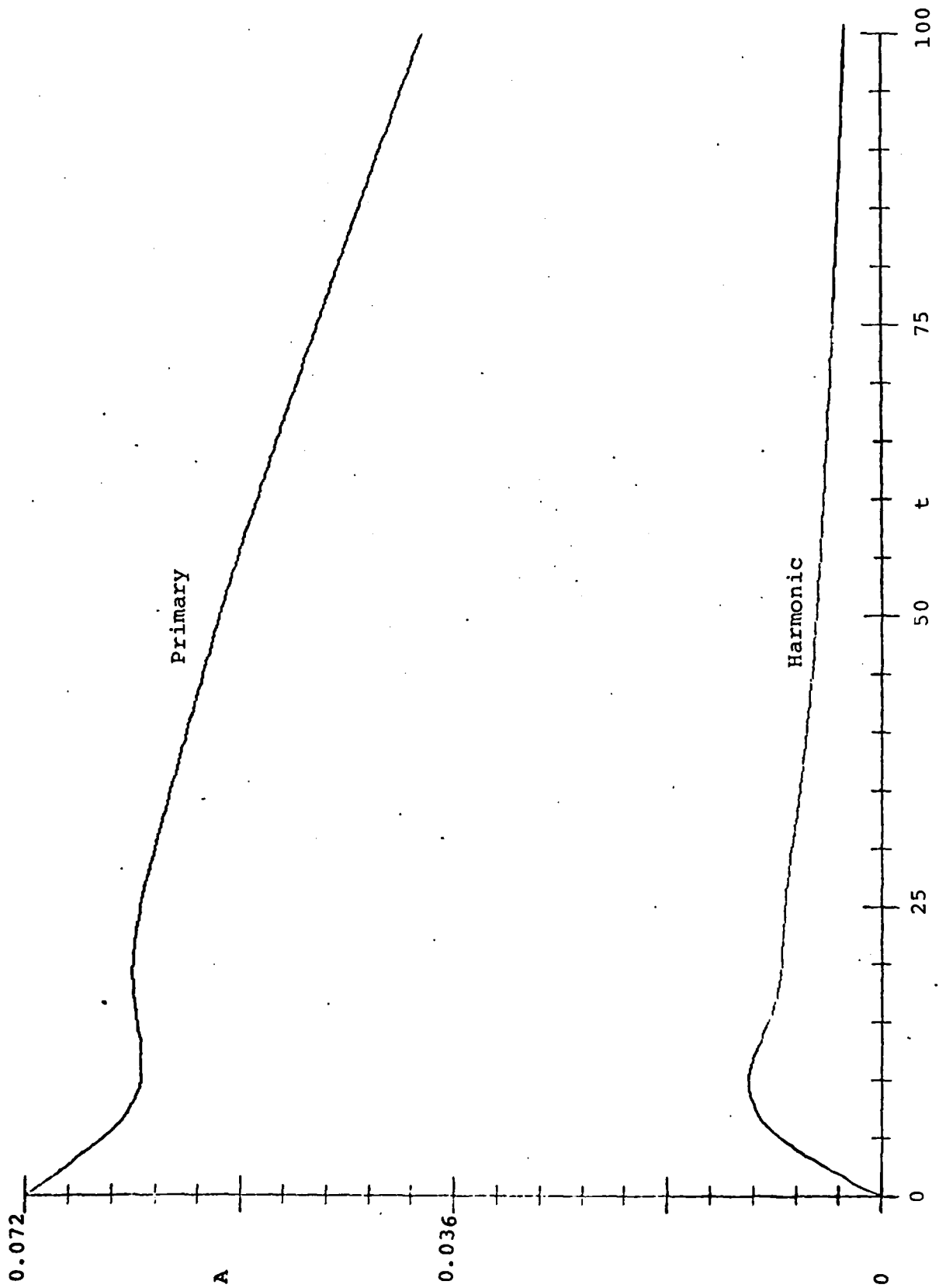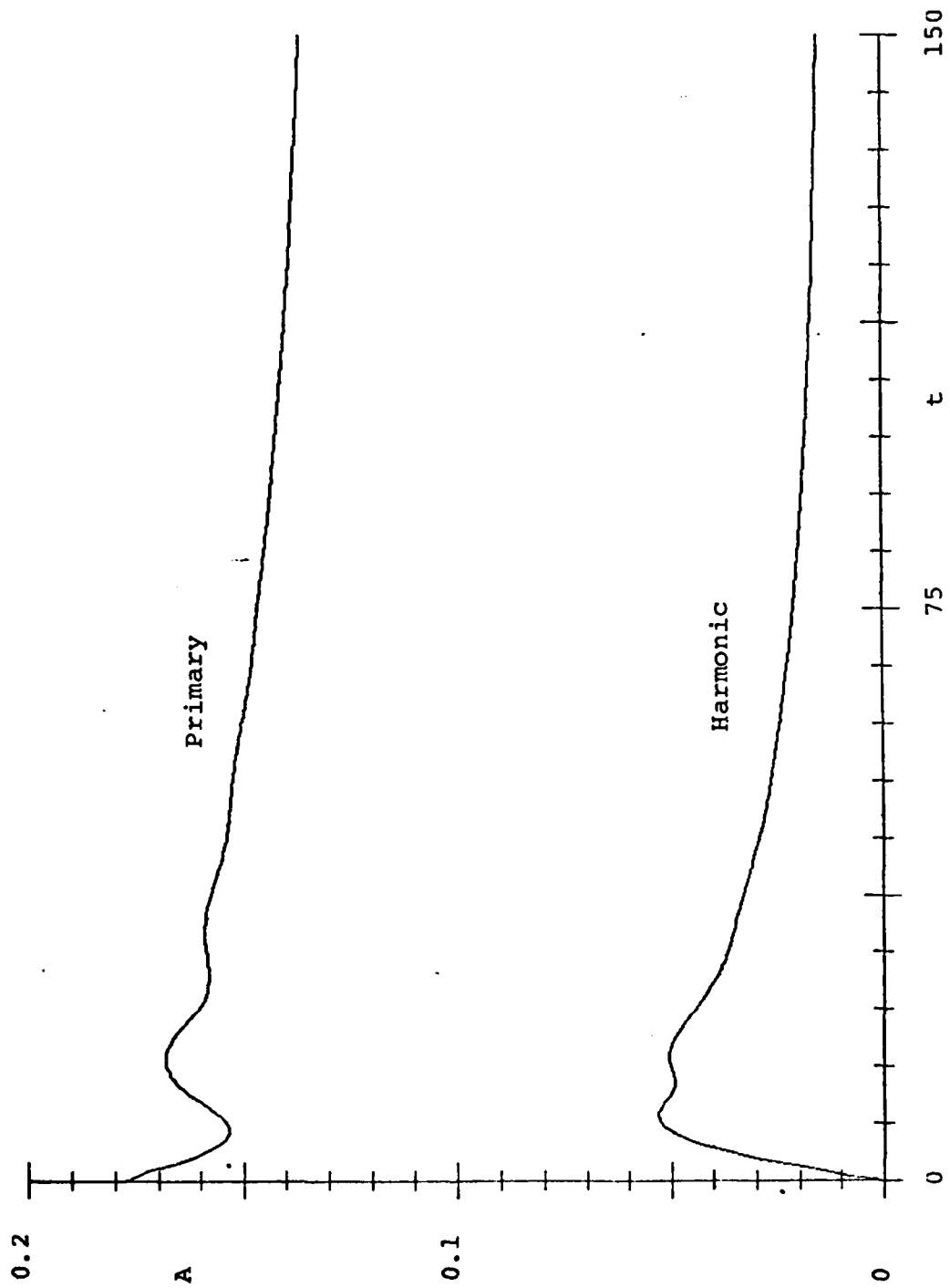
Figure 5
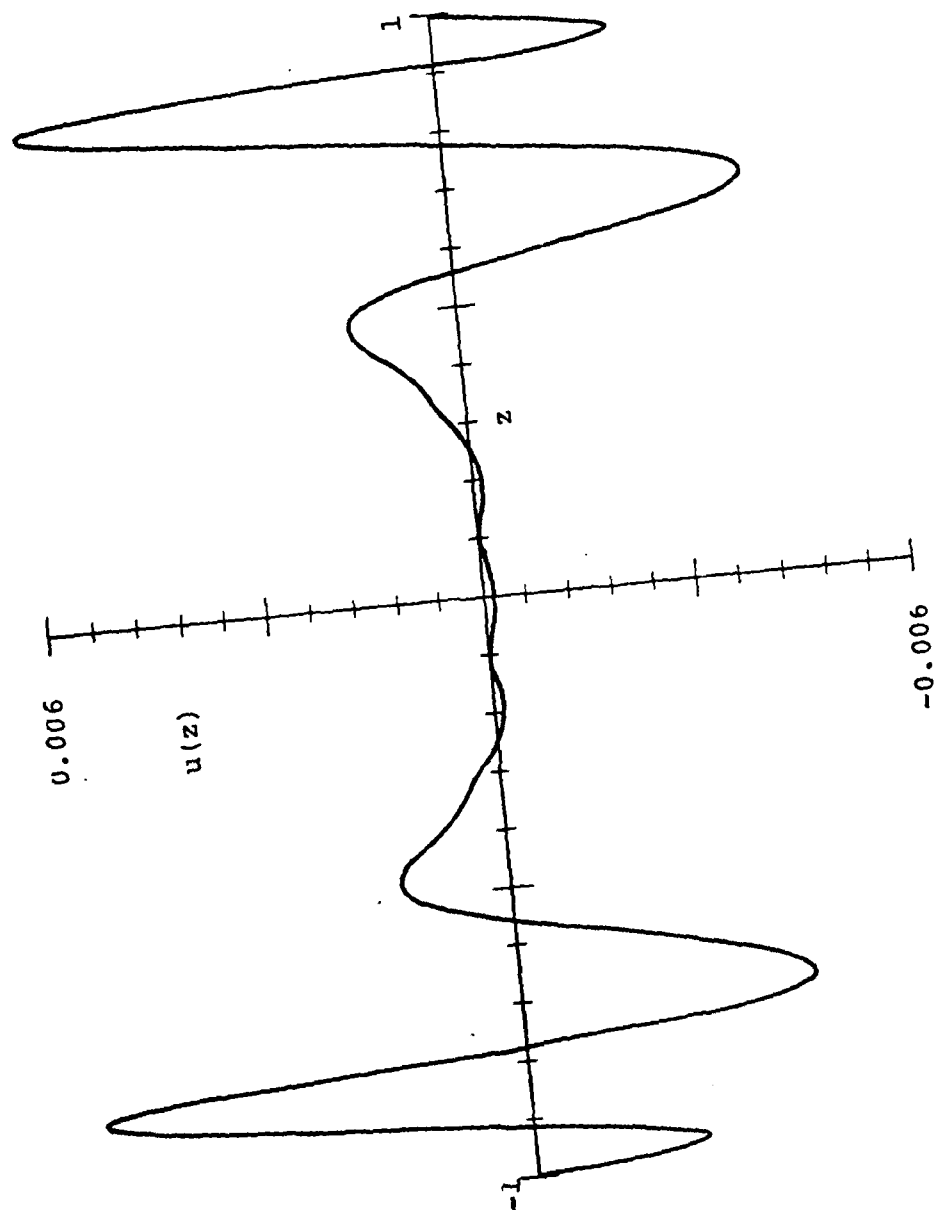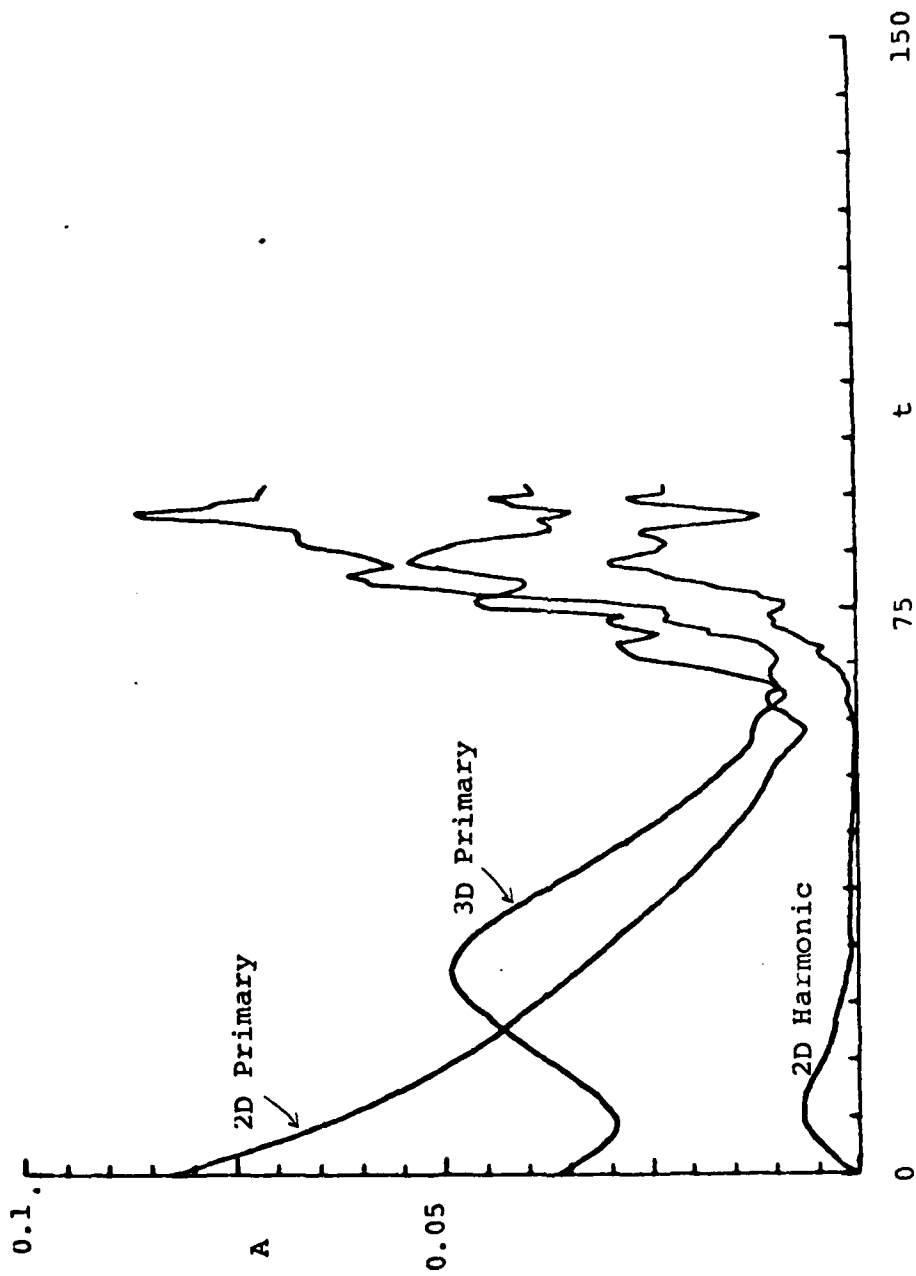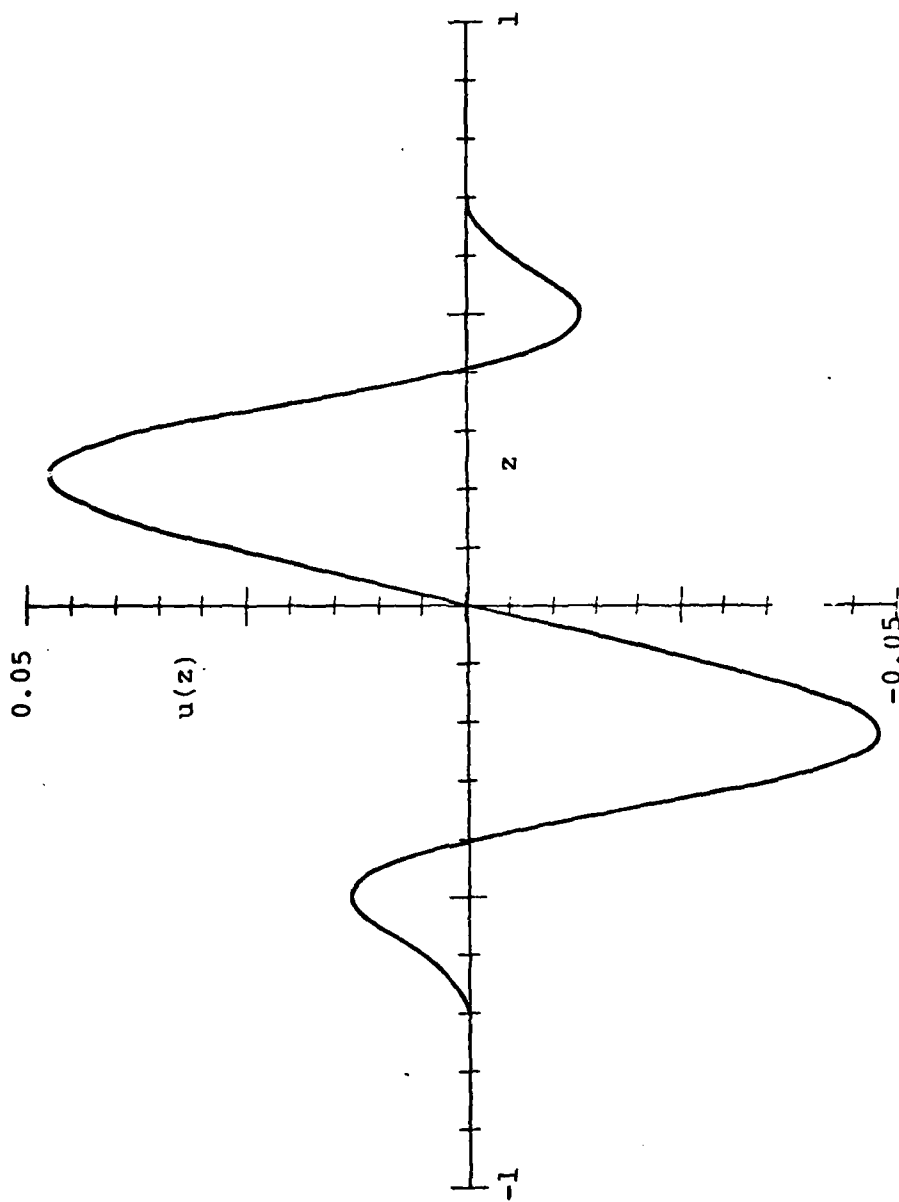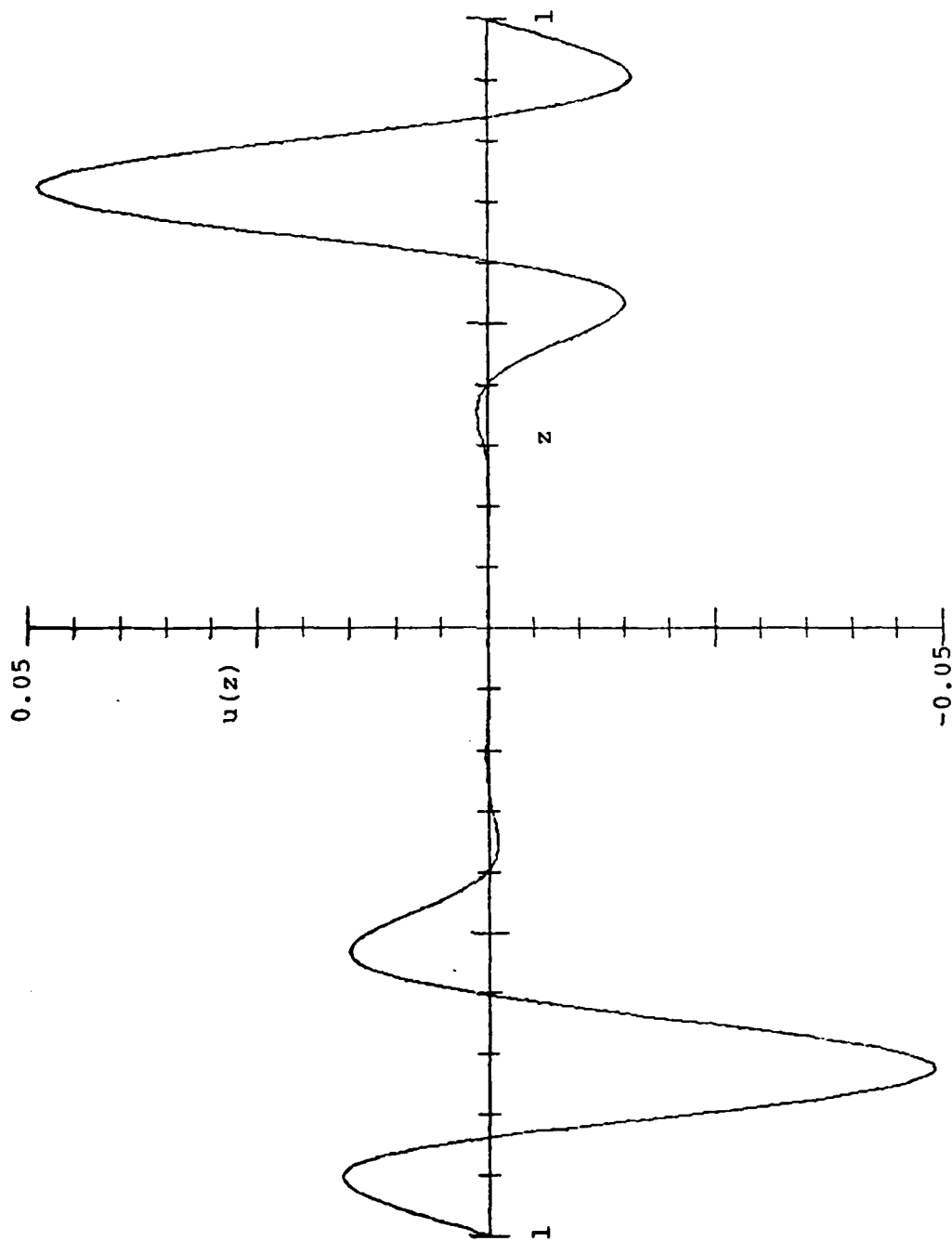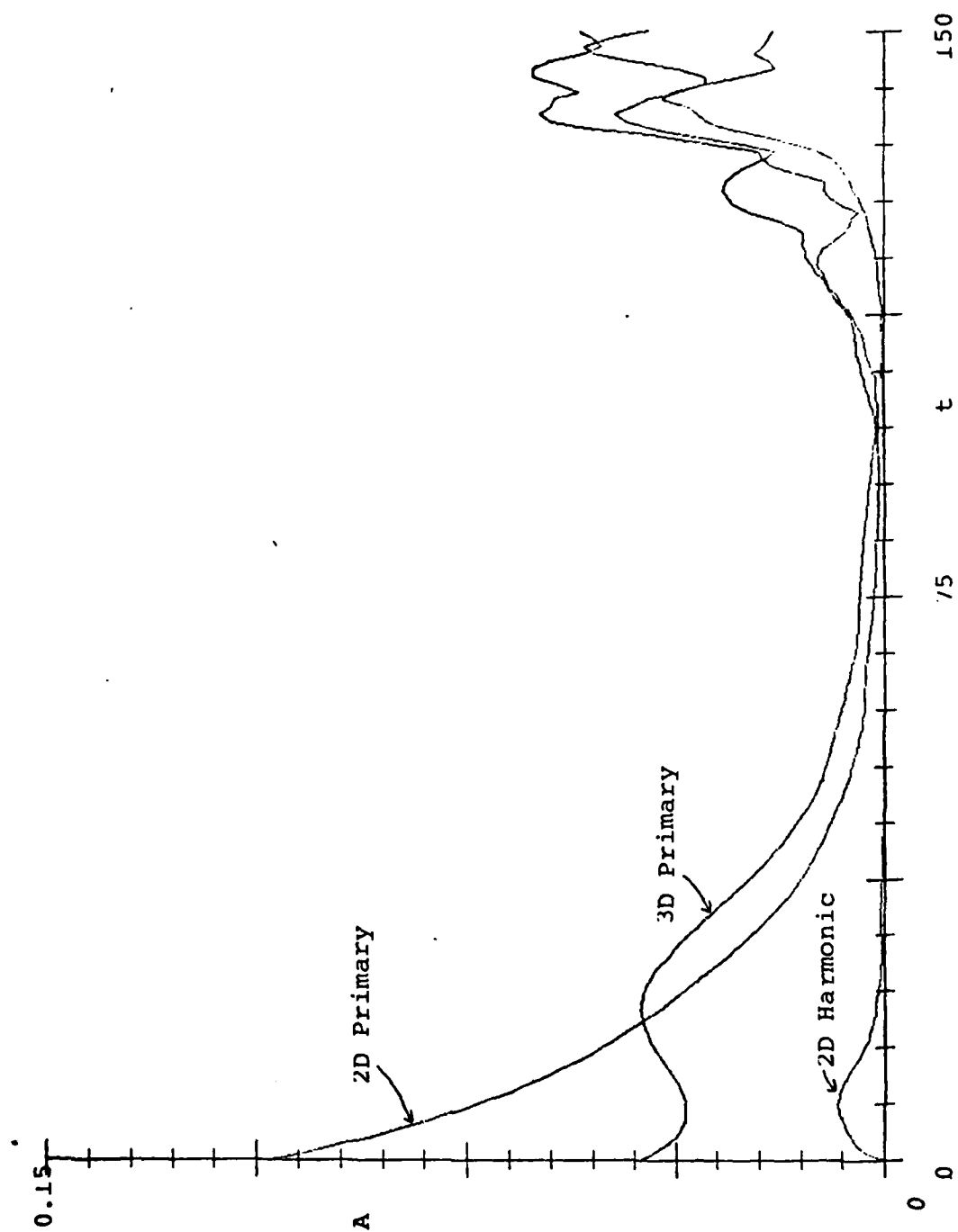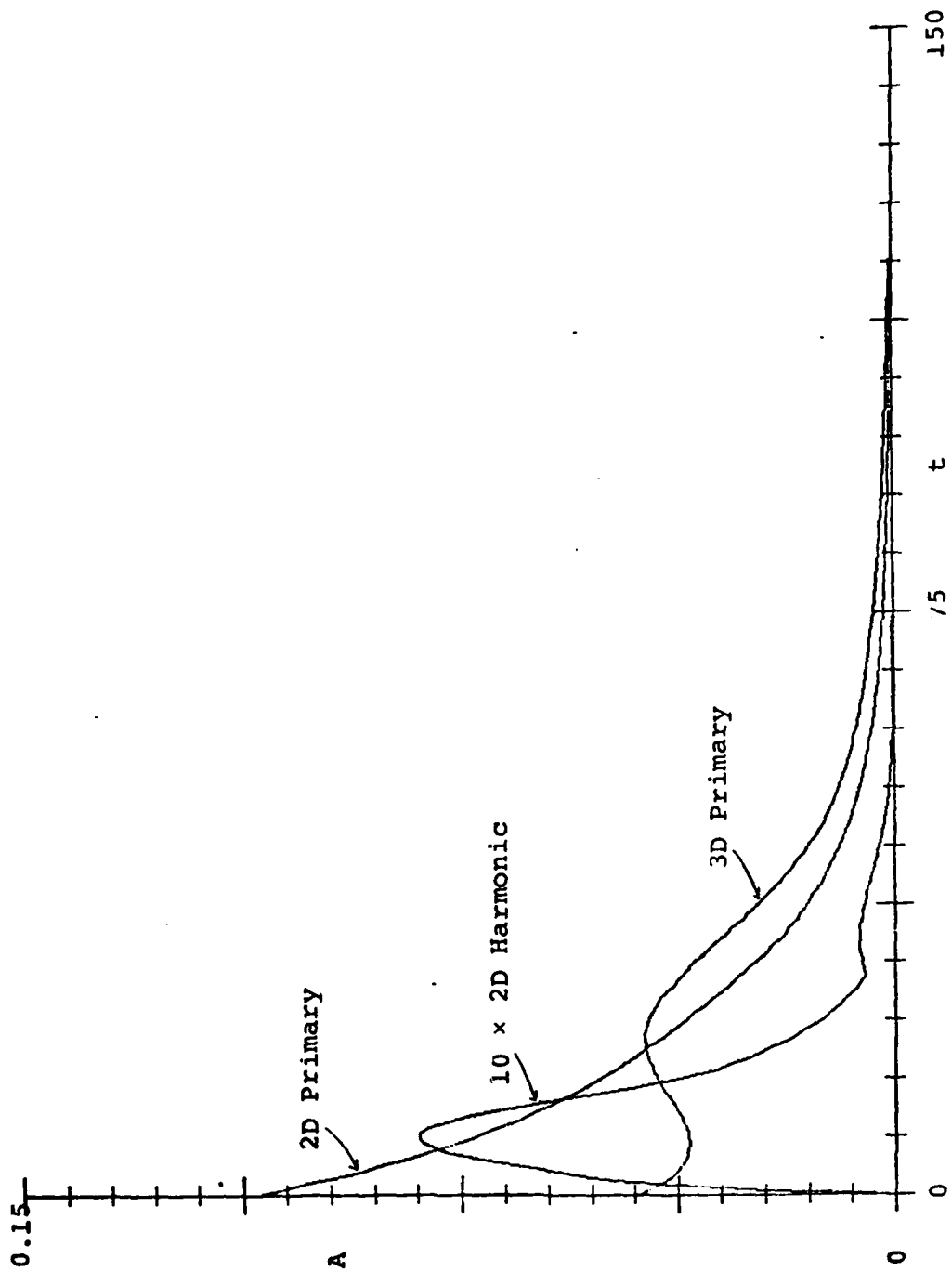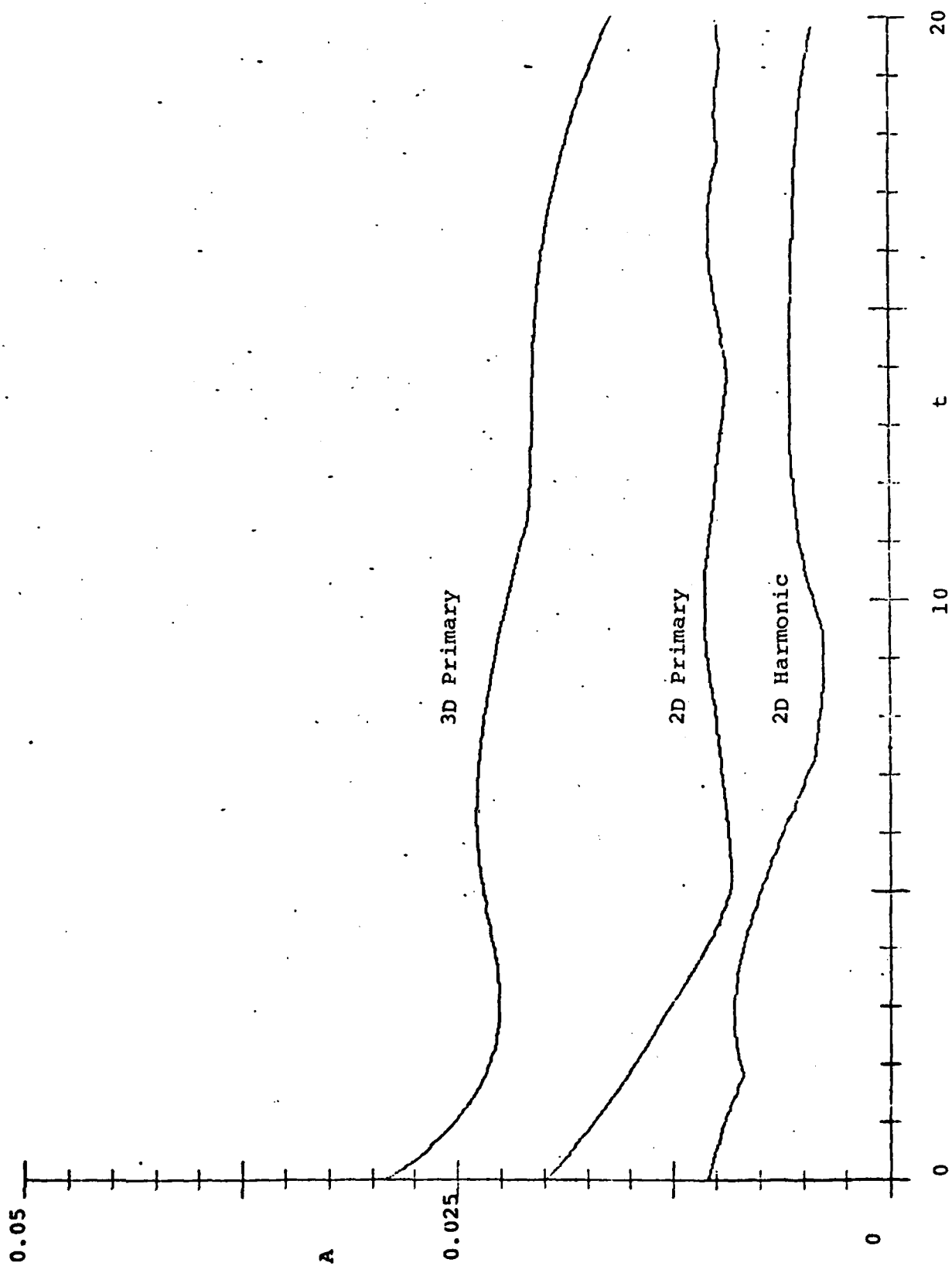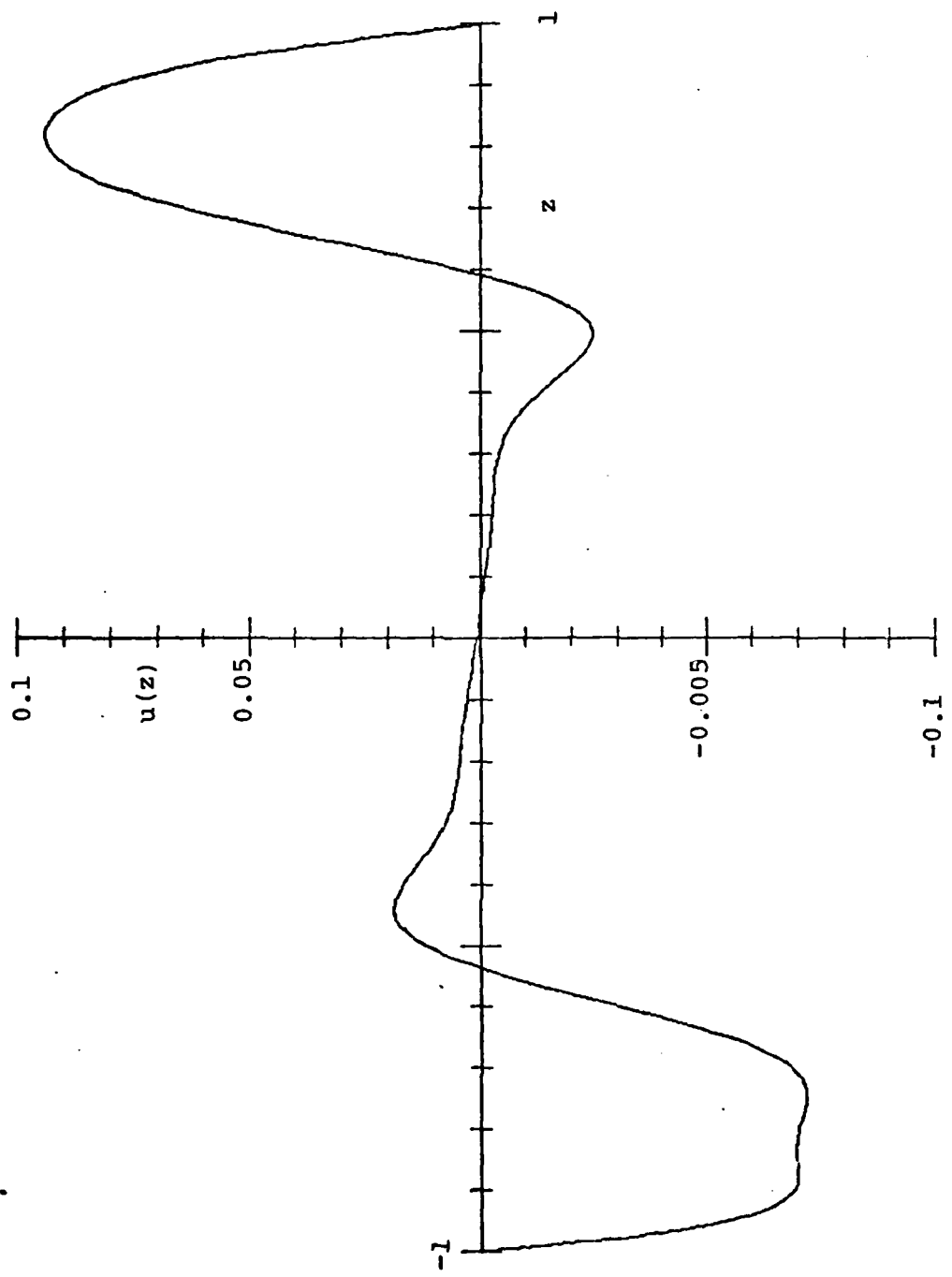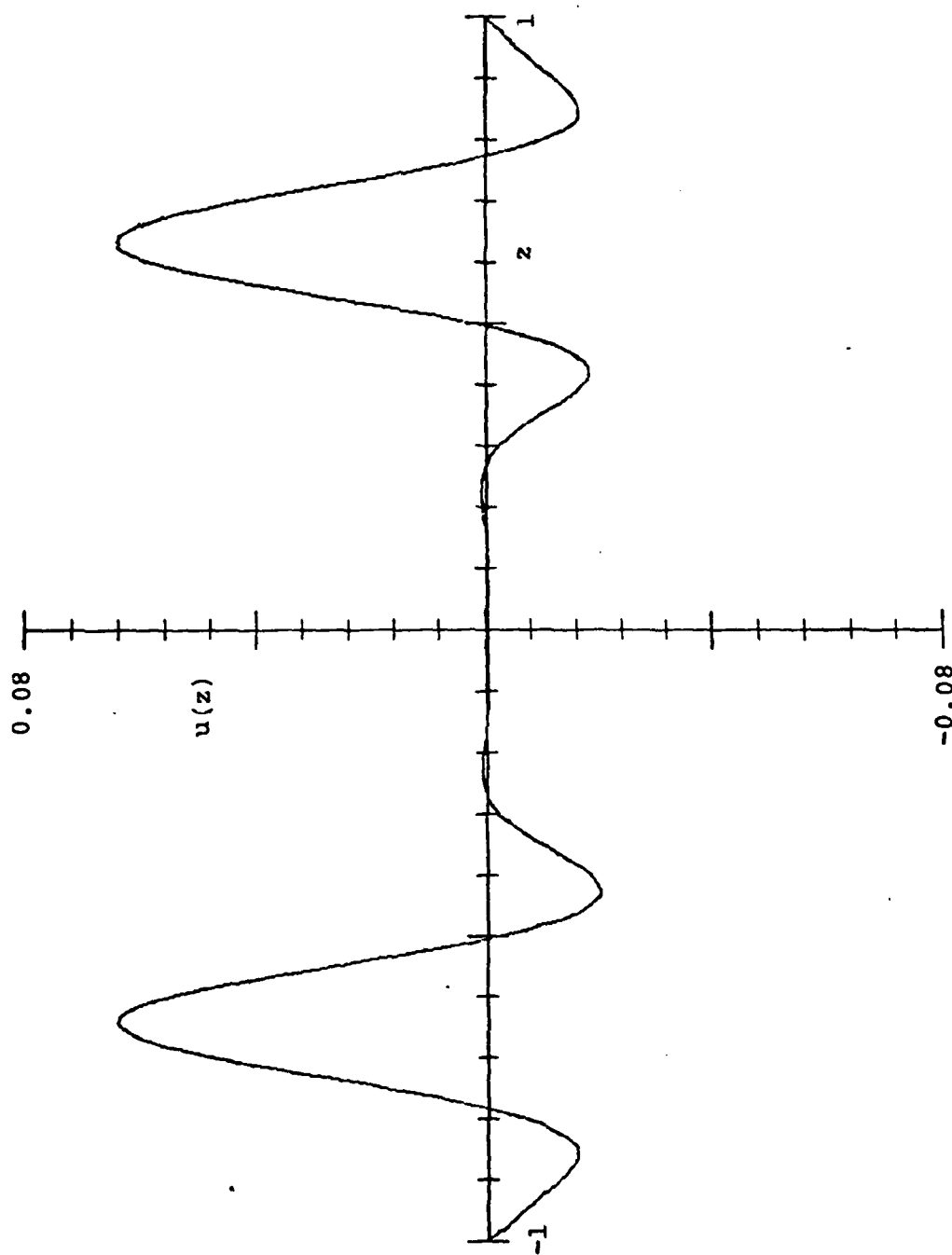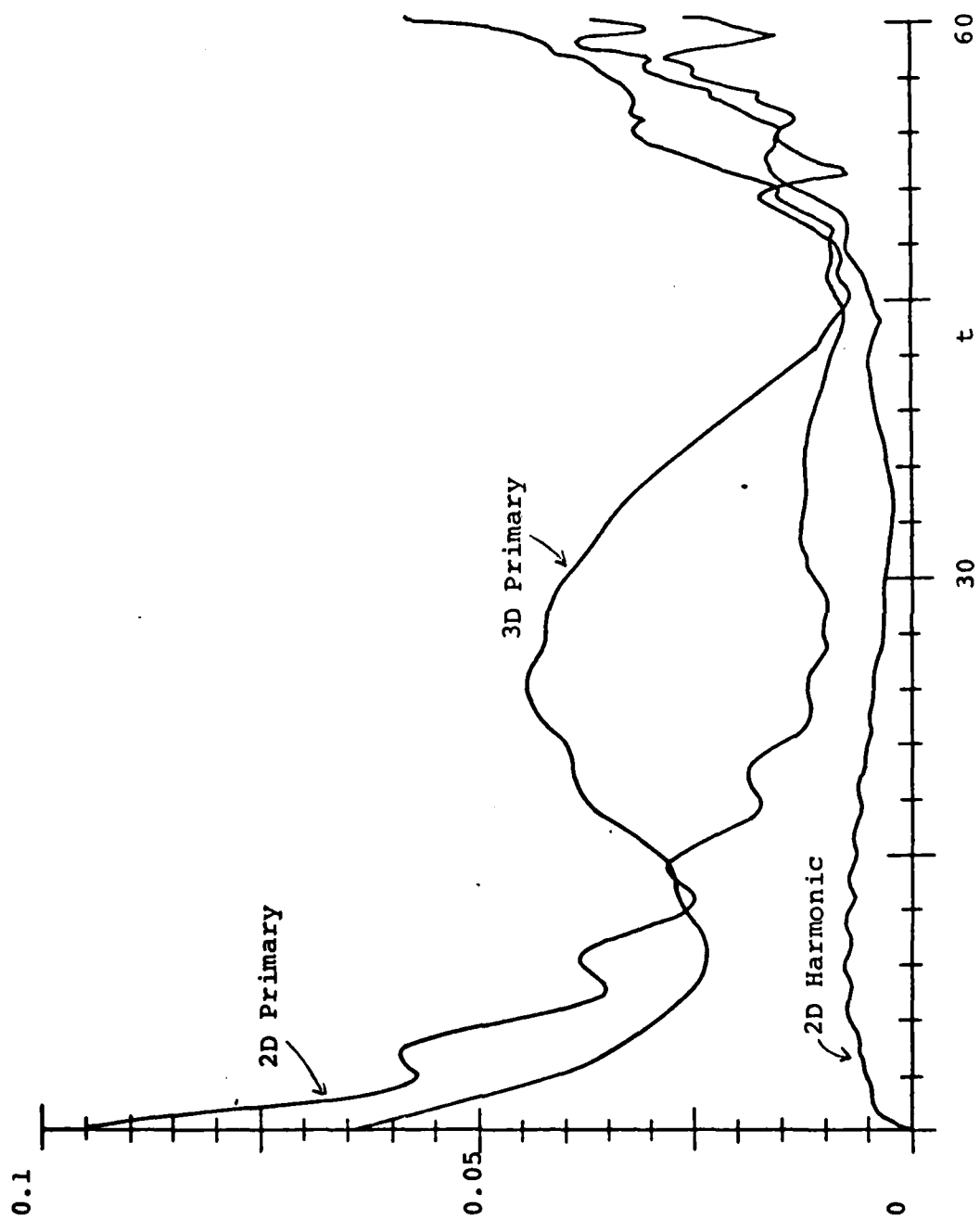
Figure 6

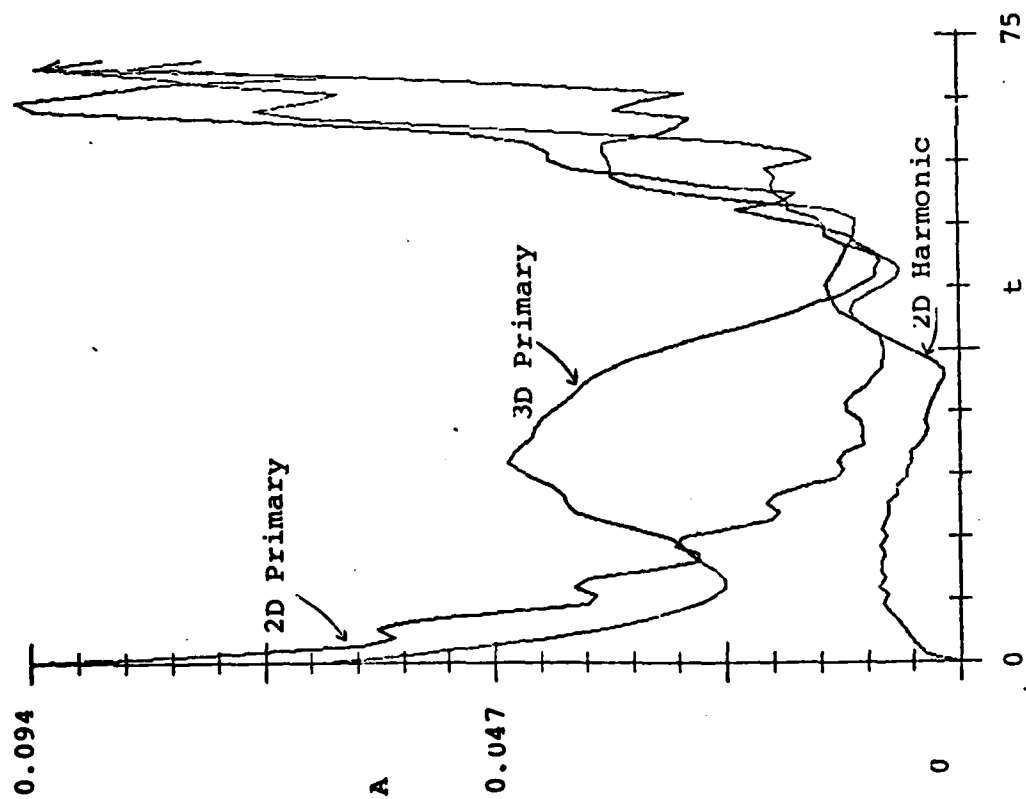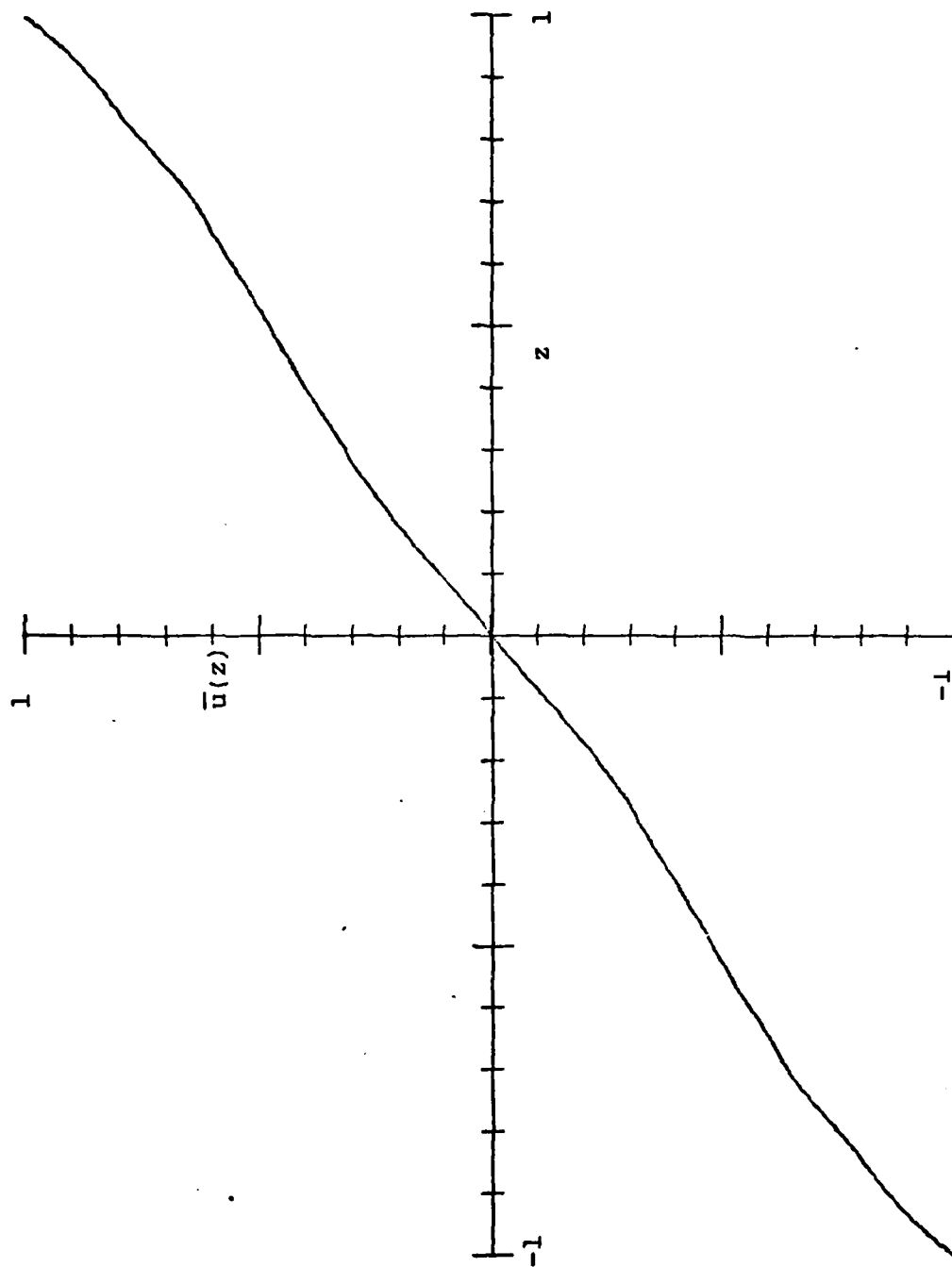Figure 7
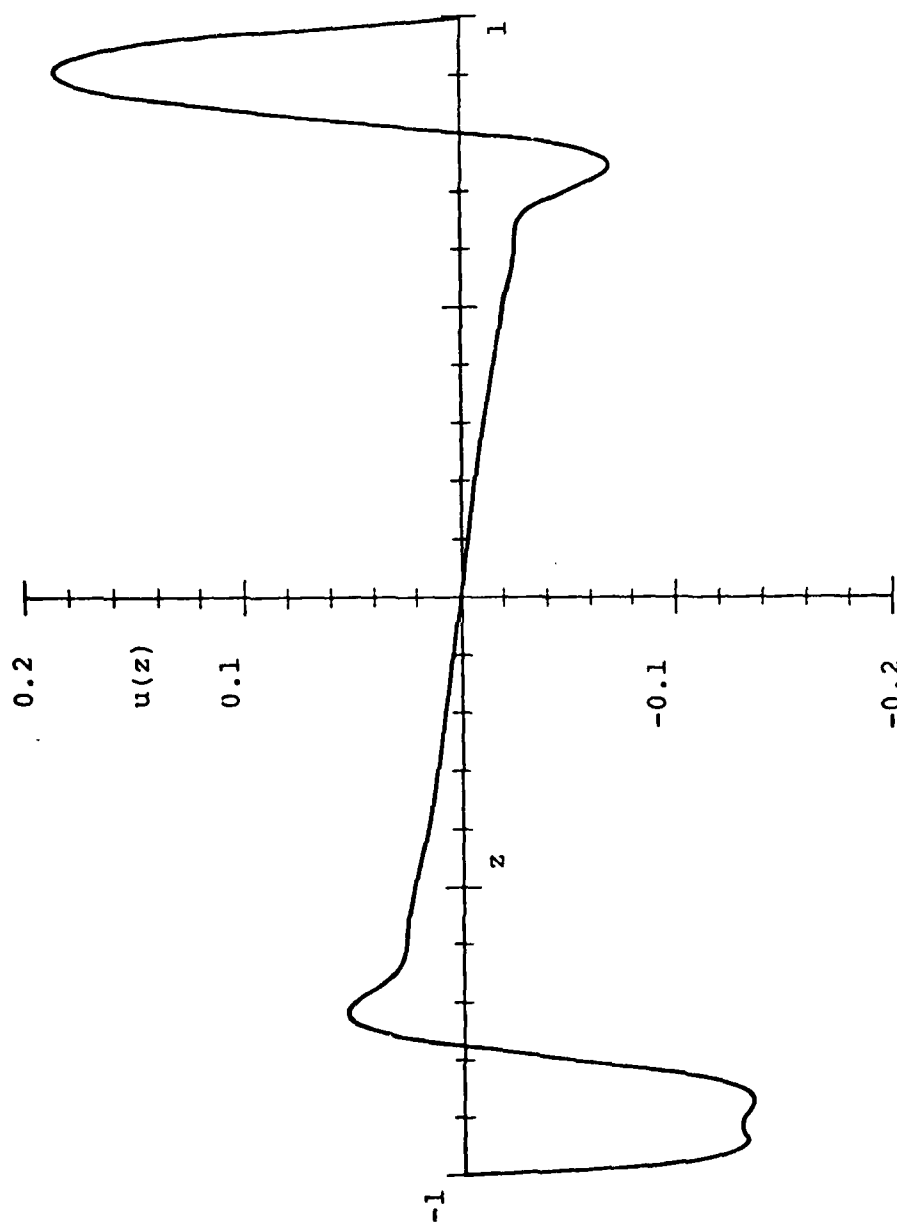
Figure   8
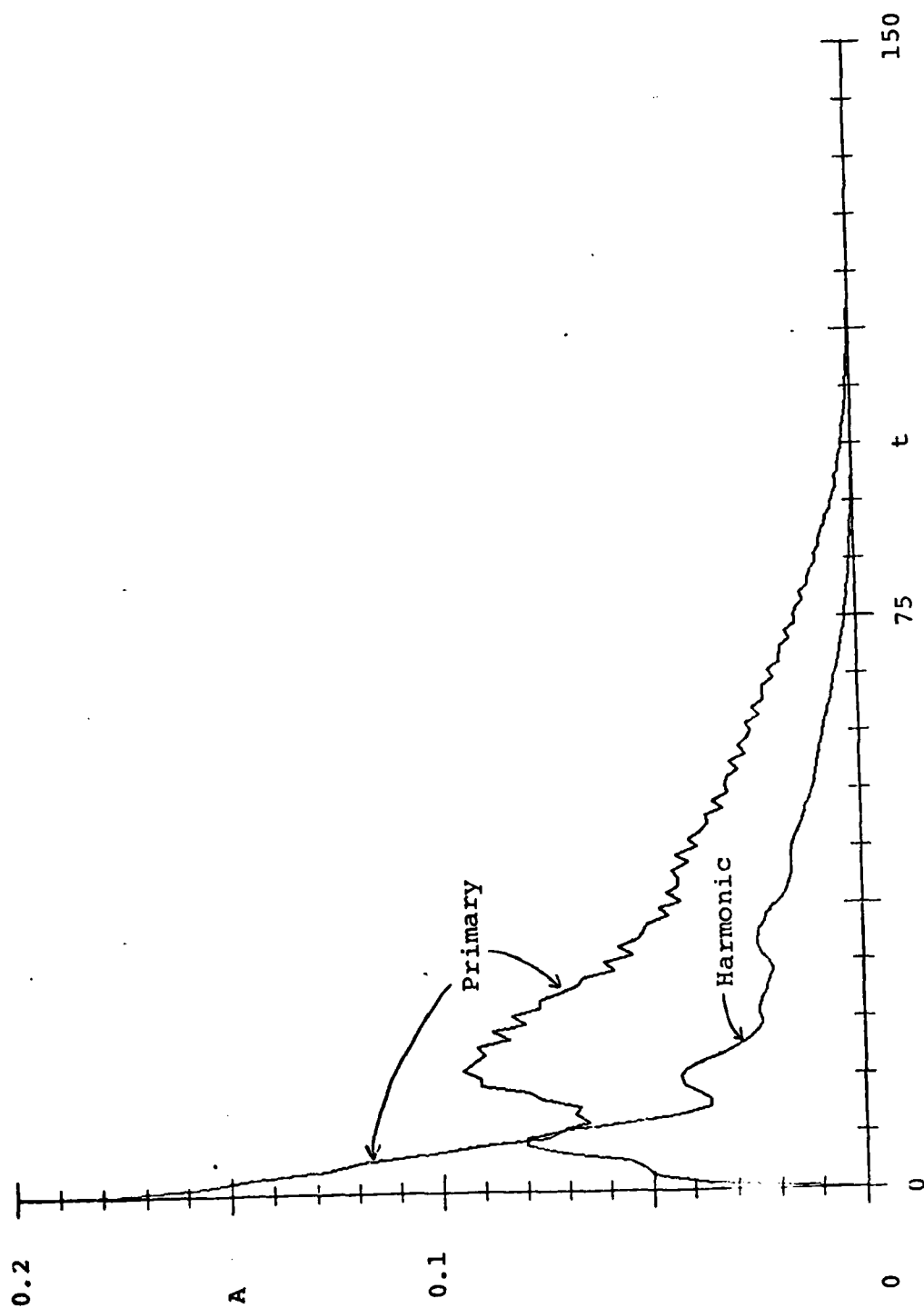
Figure 9
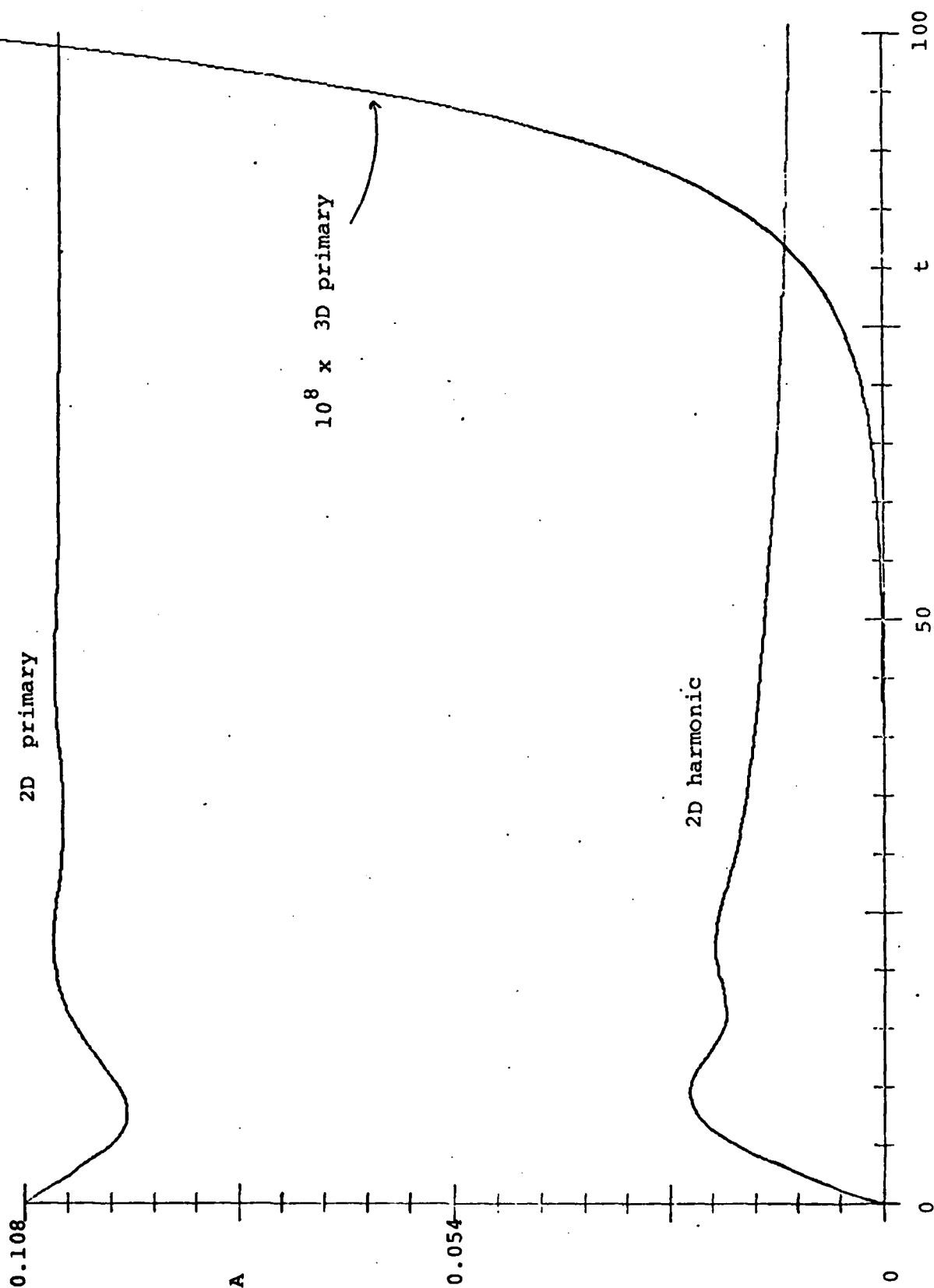
Figure 10
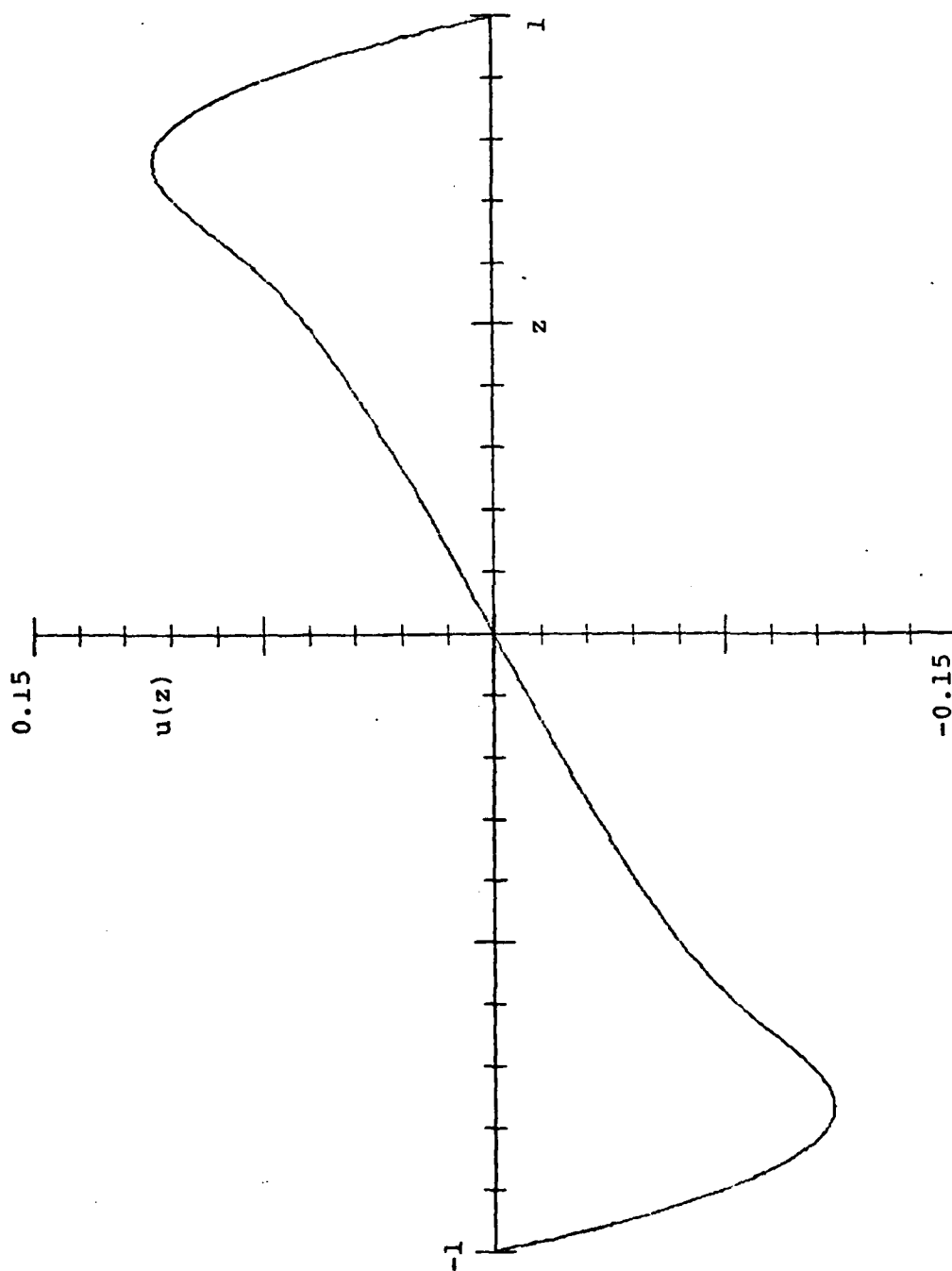
Figure 11
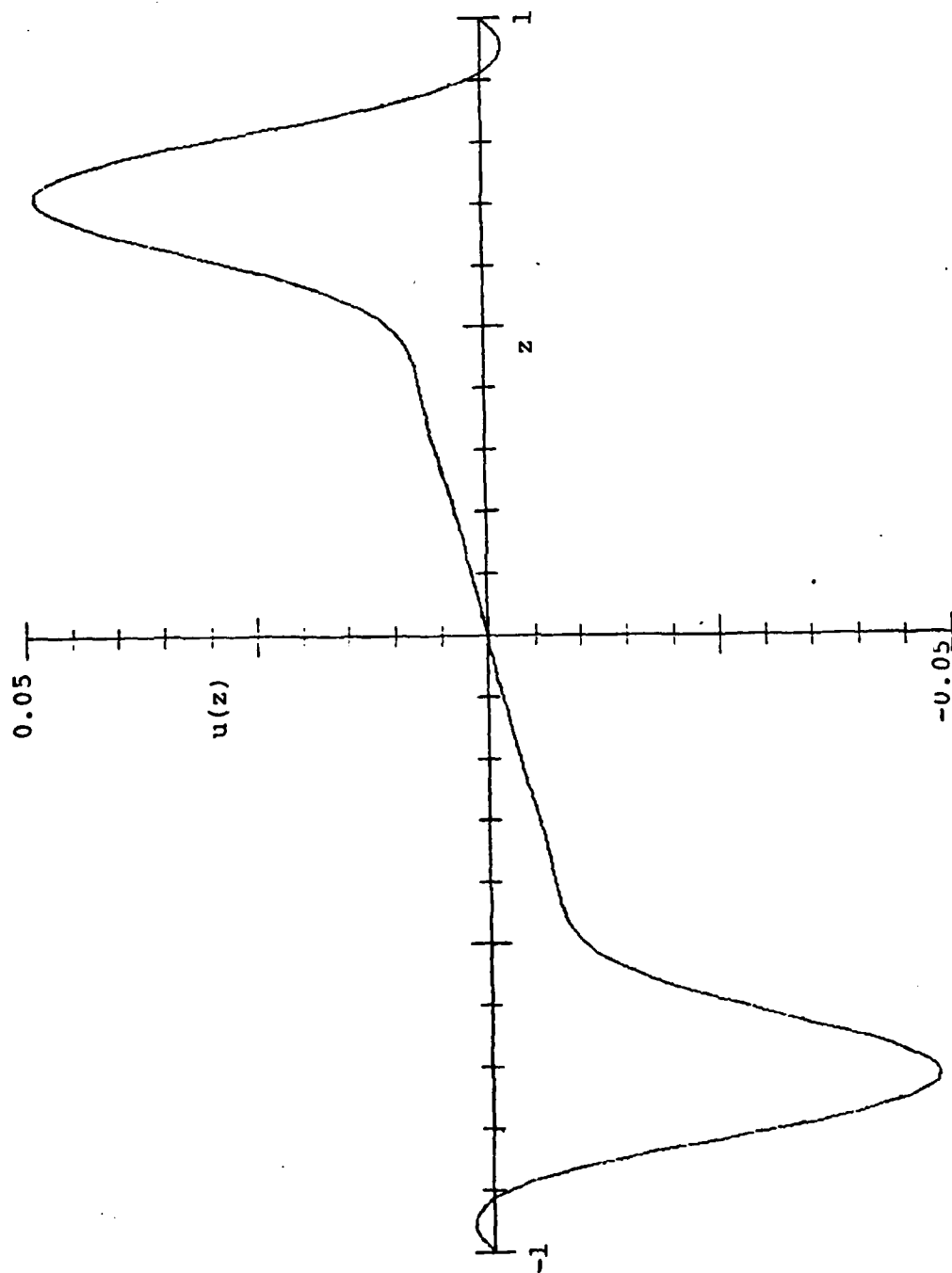
Figure 12
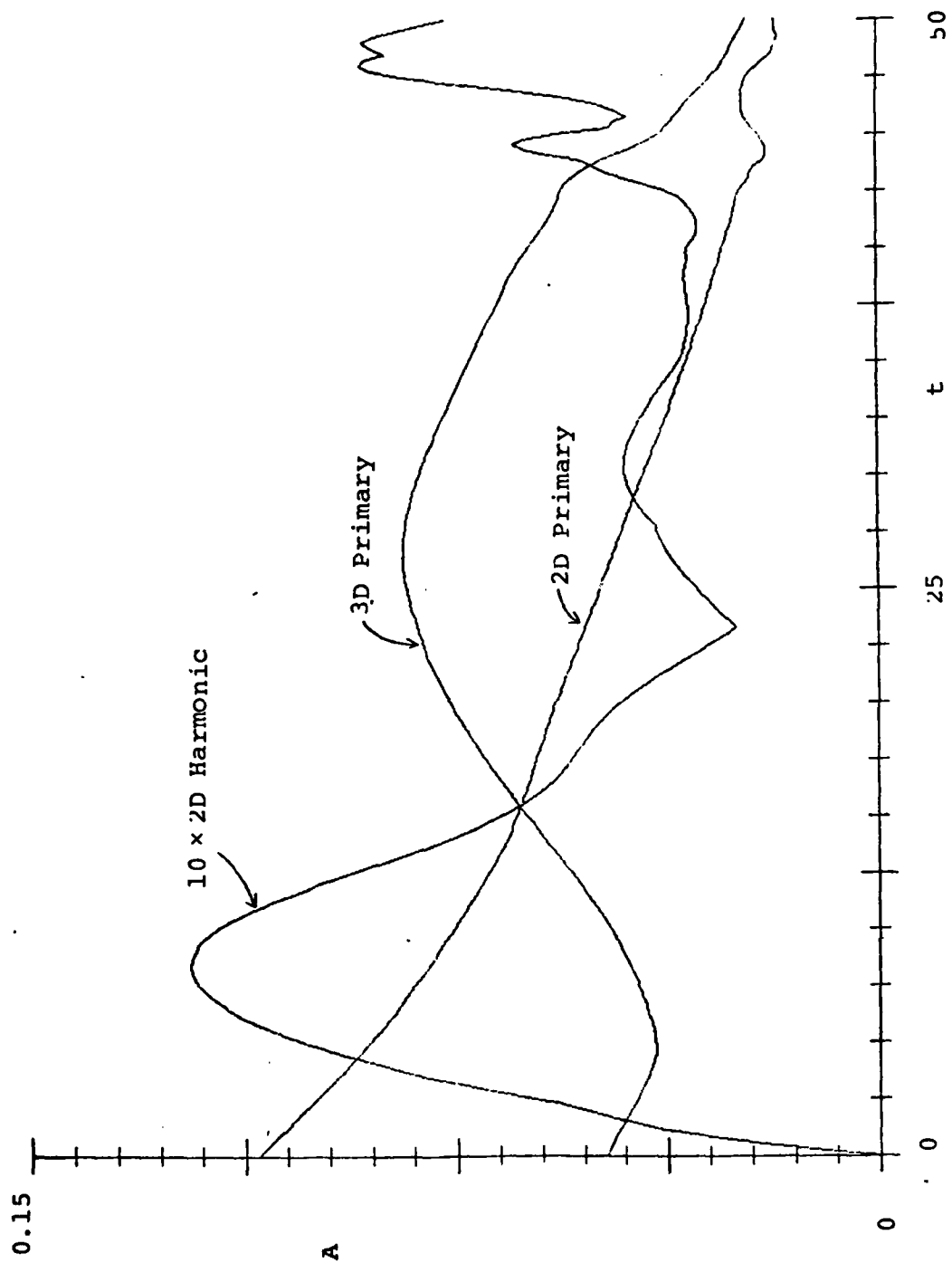
Figure 13
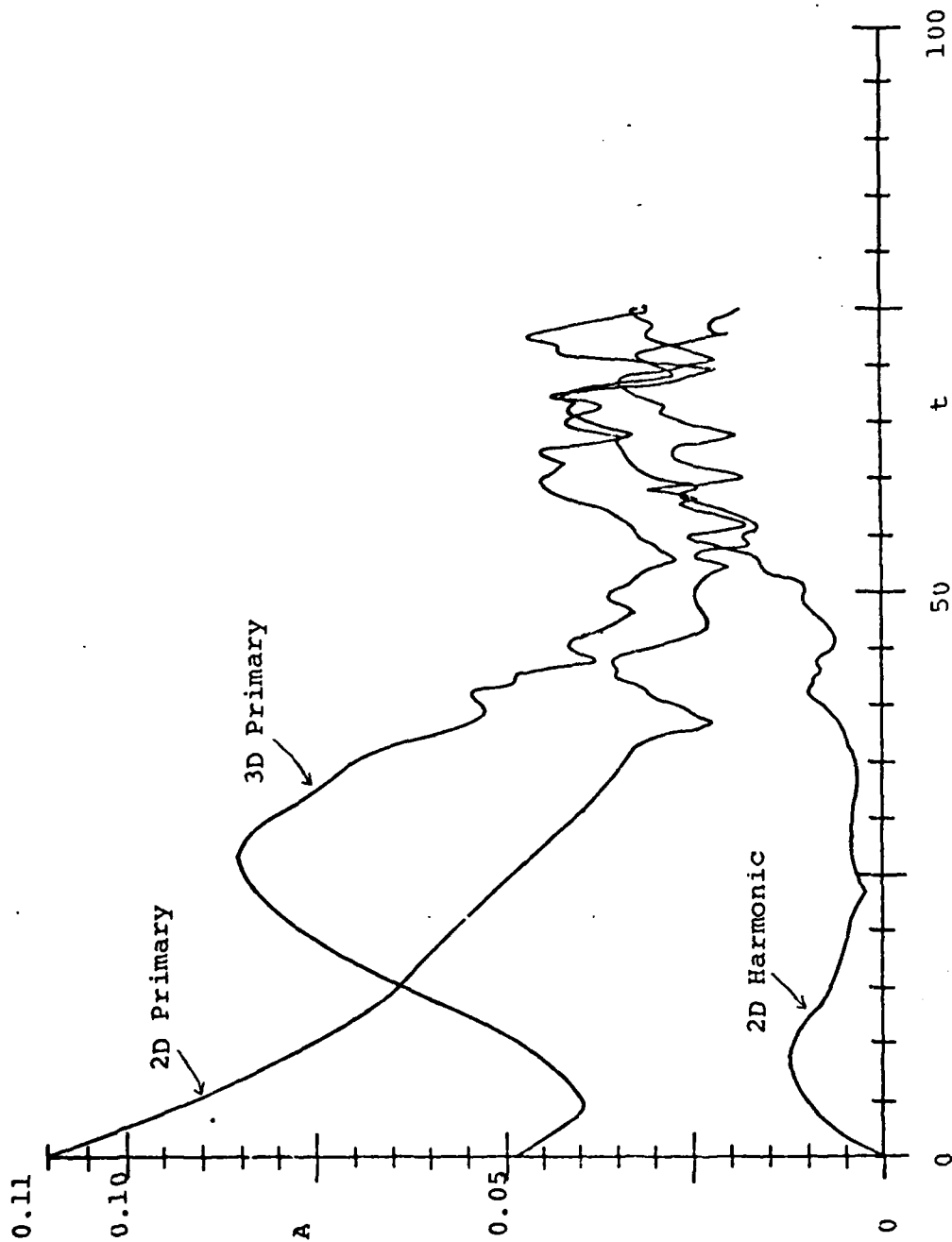
Figure 14
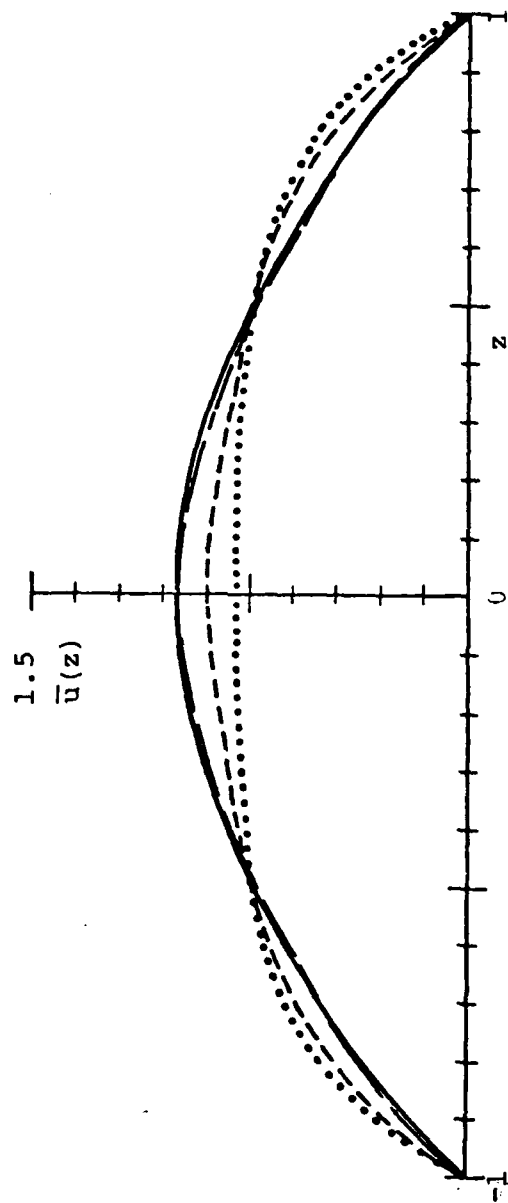
Figure 15
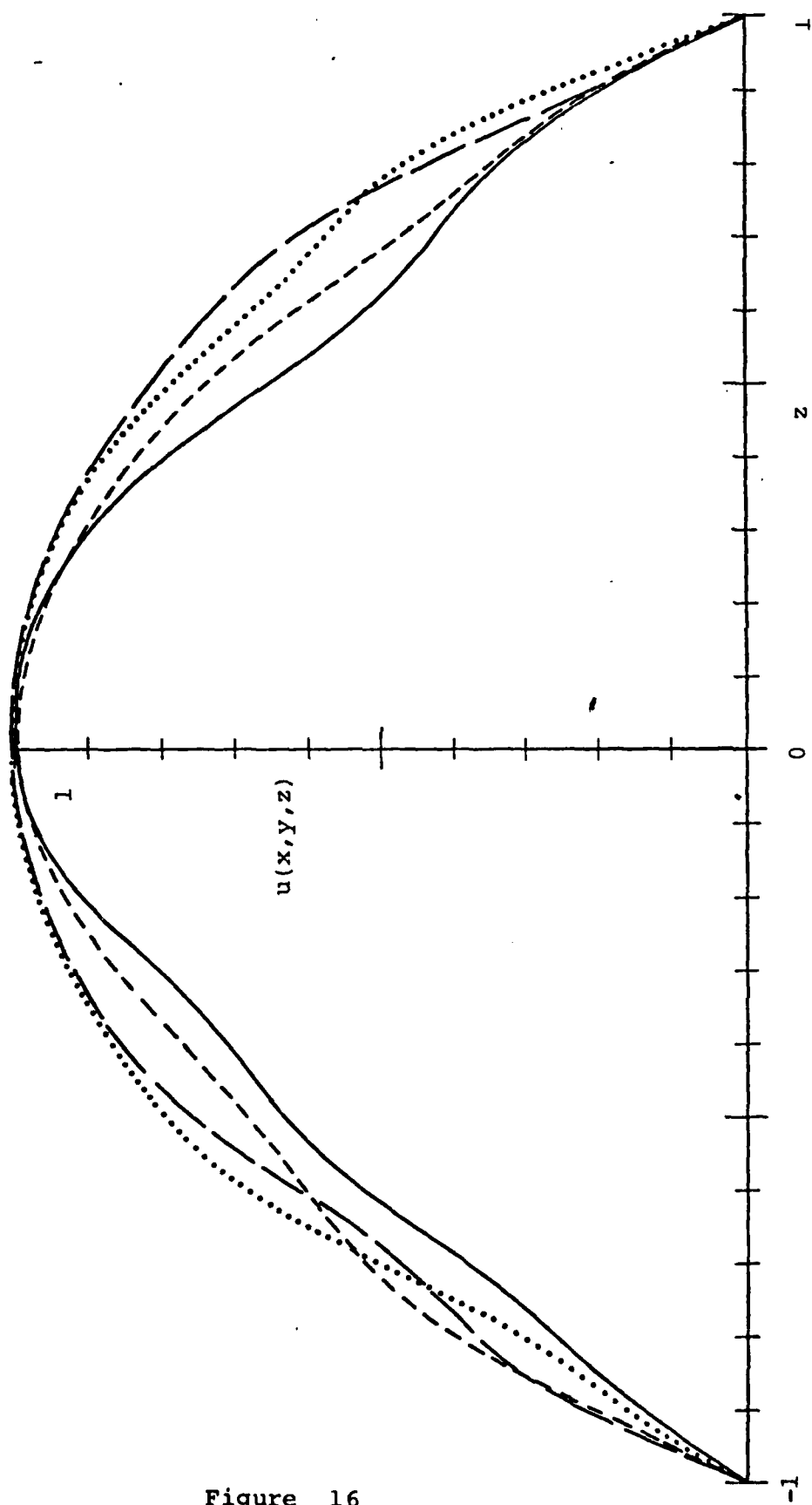
Figure 16
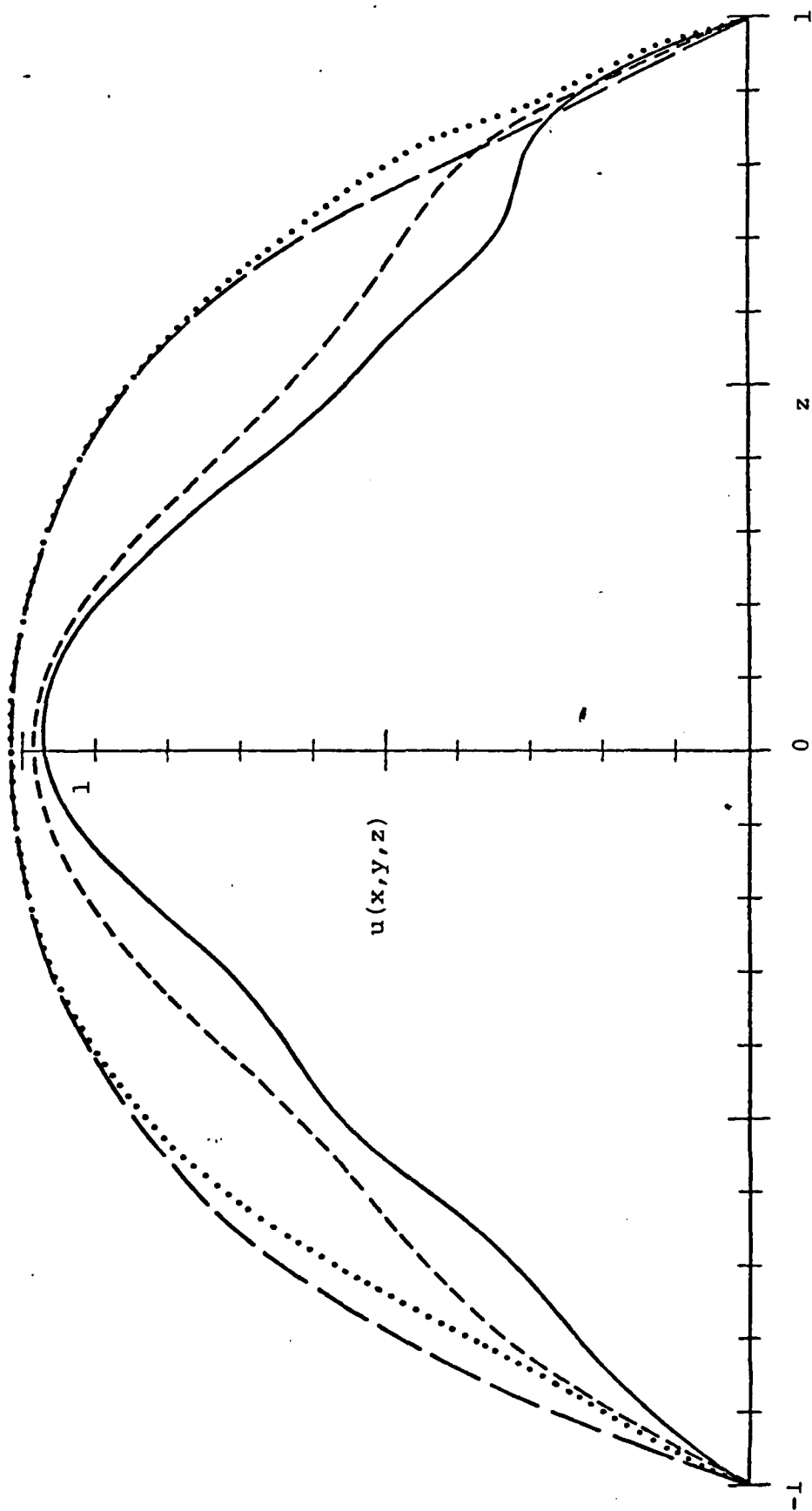
Figure 17
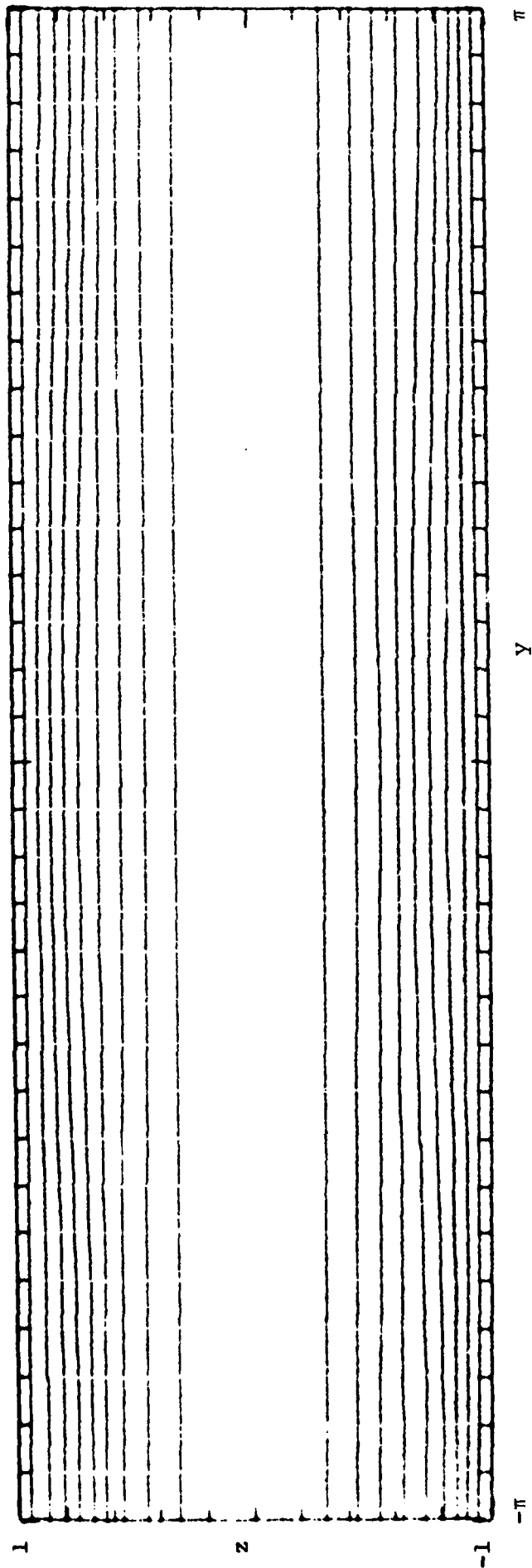
Figure 18(a)
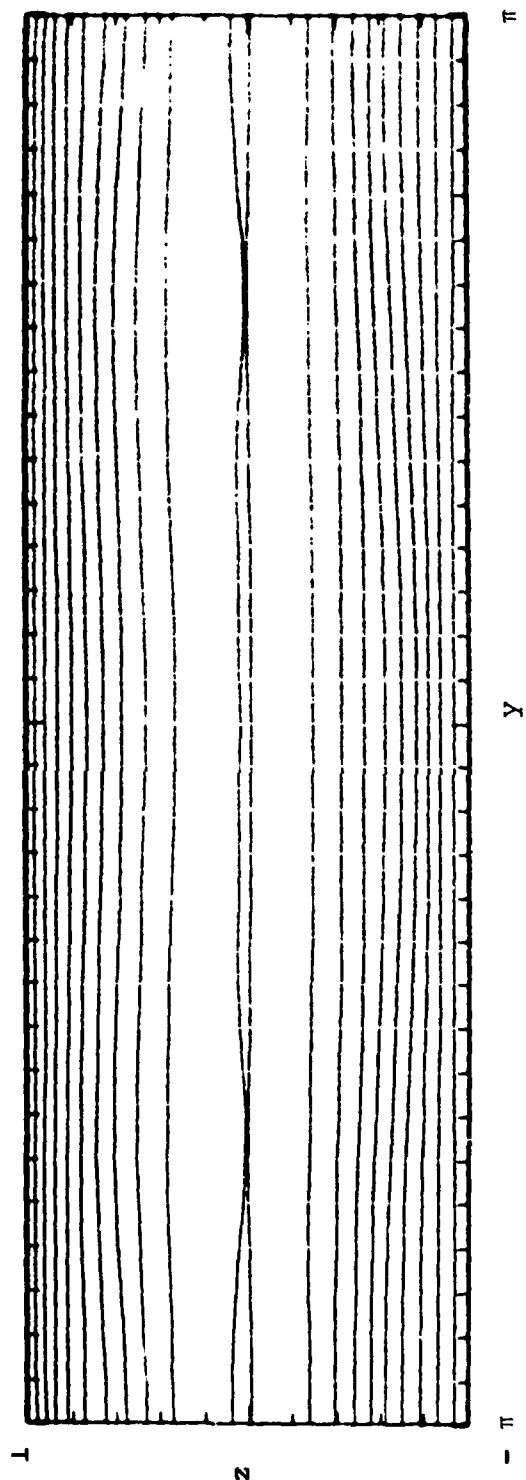
Figure 18(b)
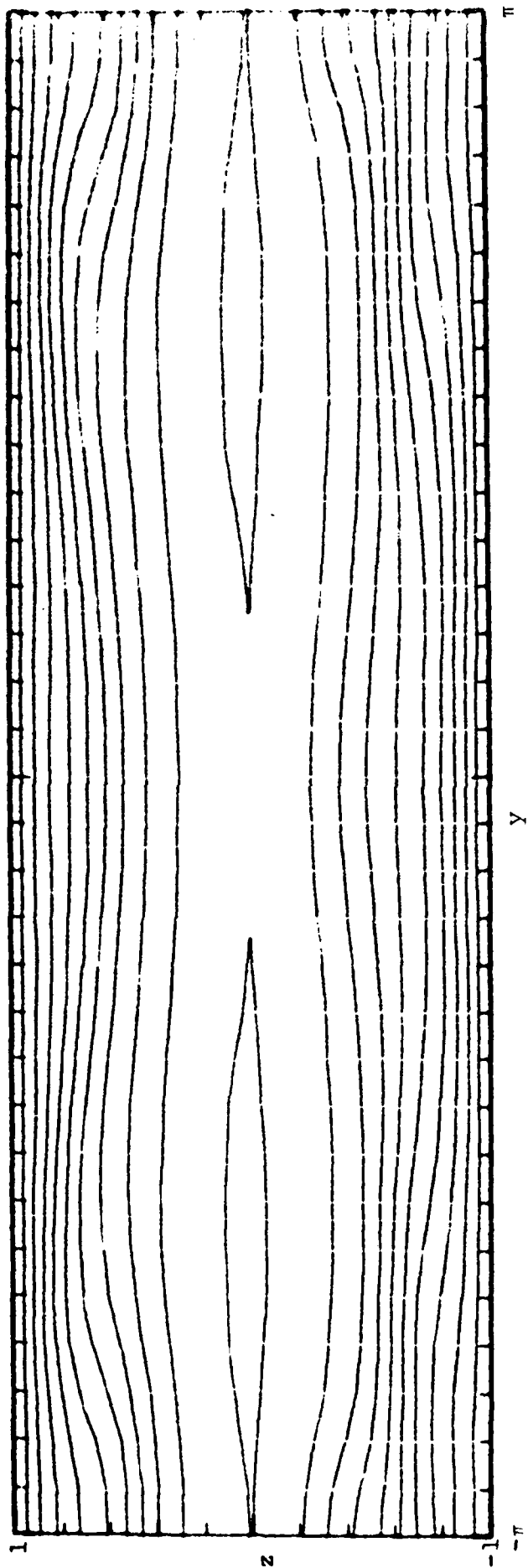
Figure 18(c)
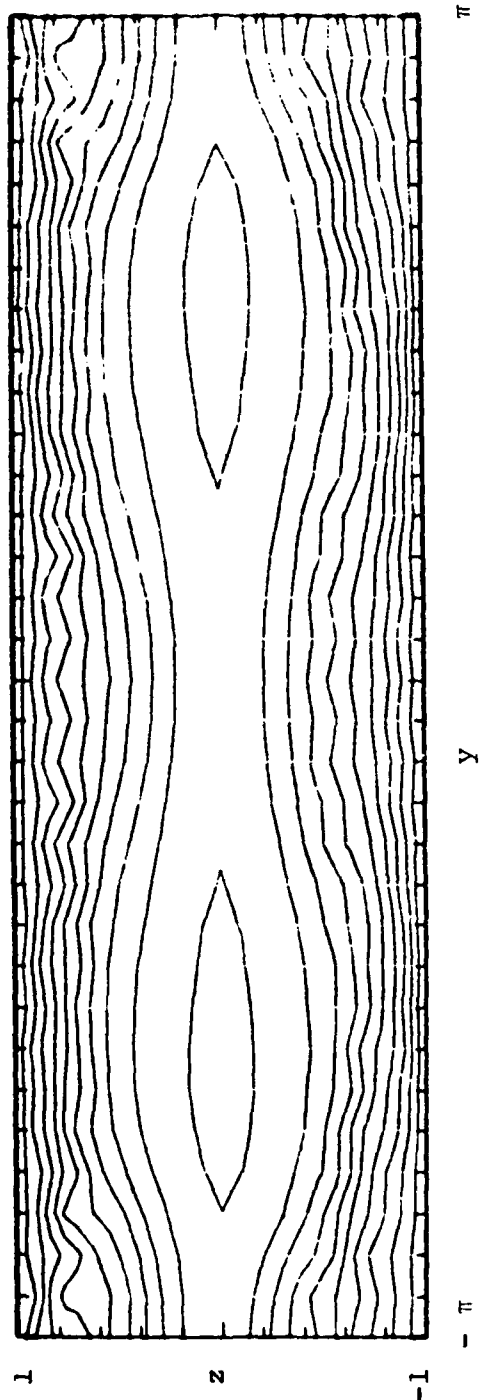
Figure 18(d)
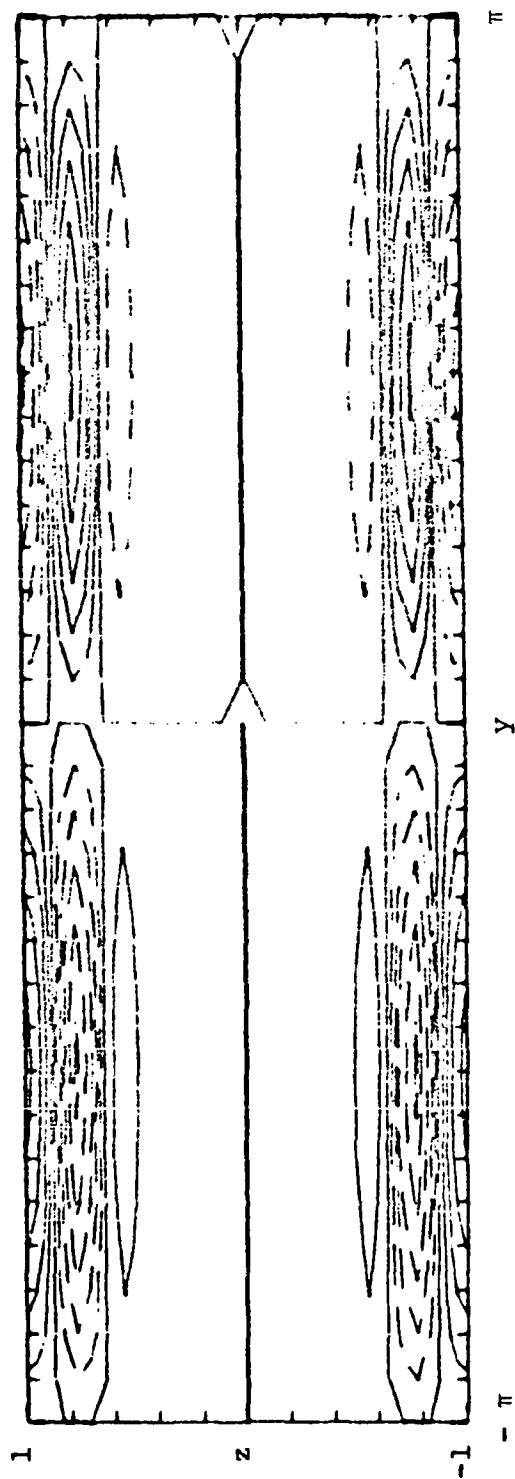
Figure 19(a)
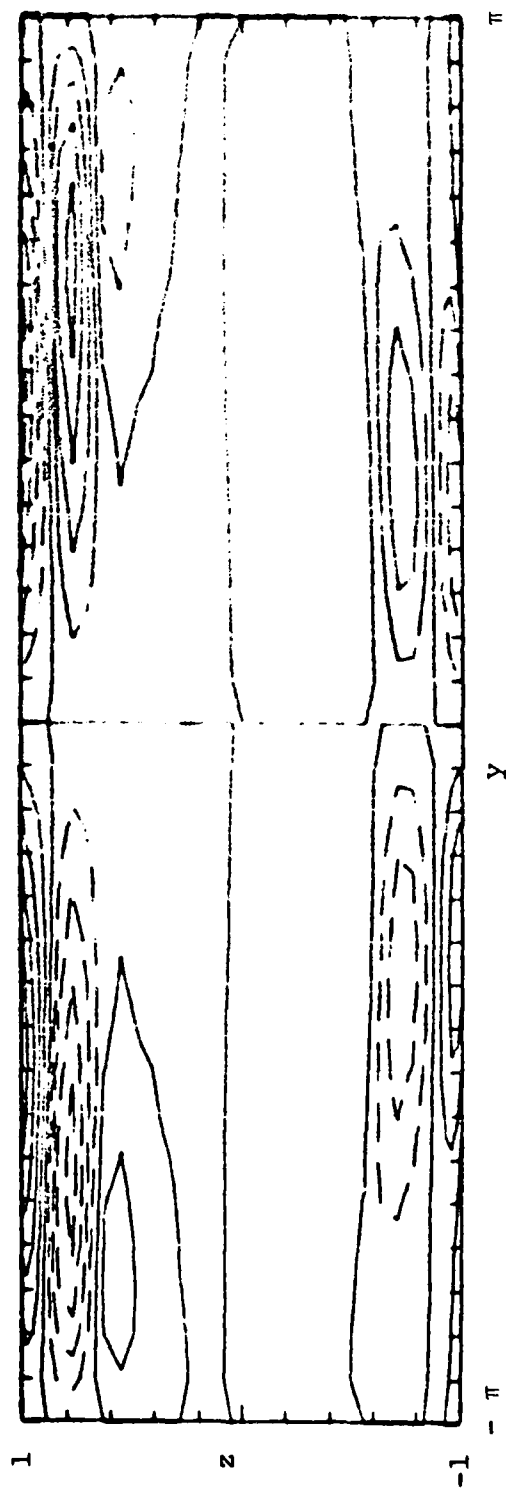
Figure 19(b)
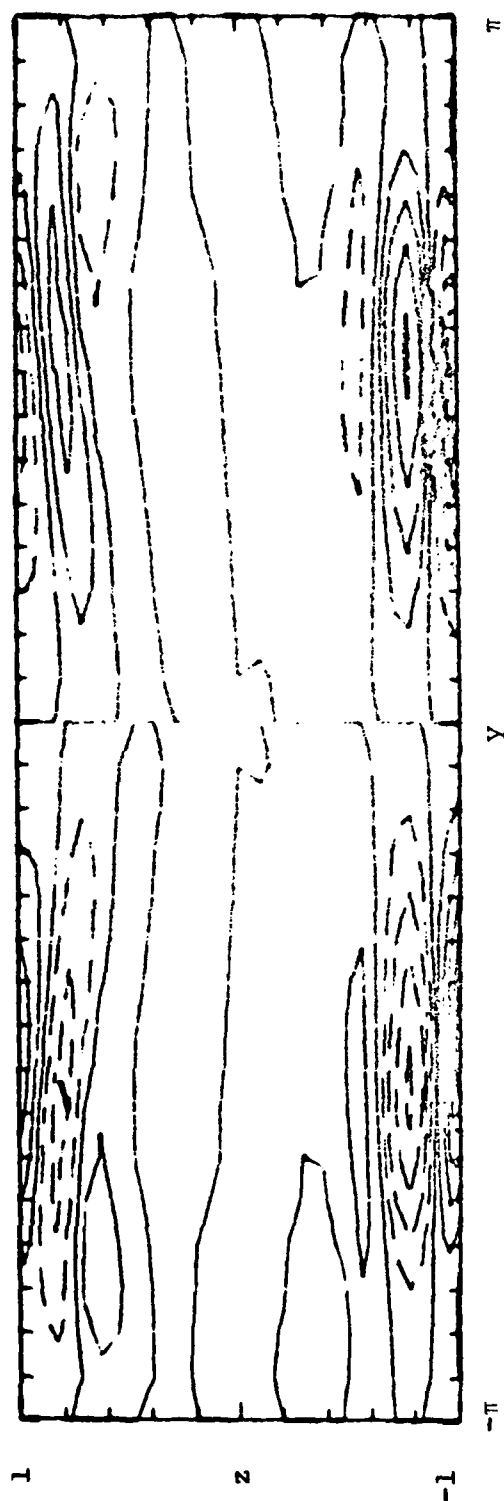
Figure 19(c)
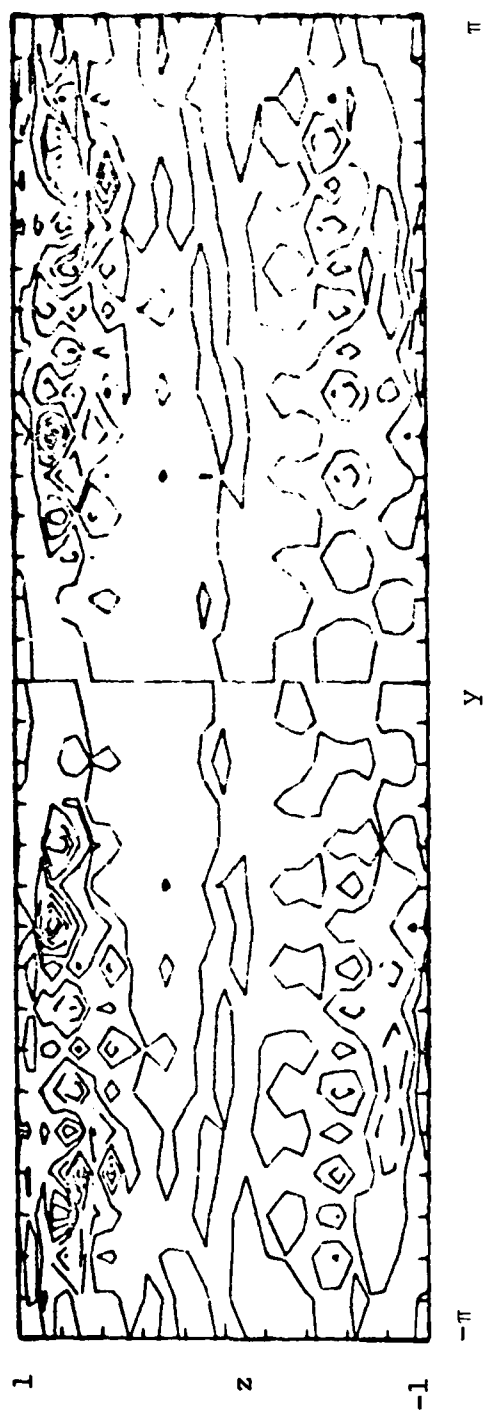
Figure 19(d)
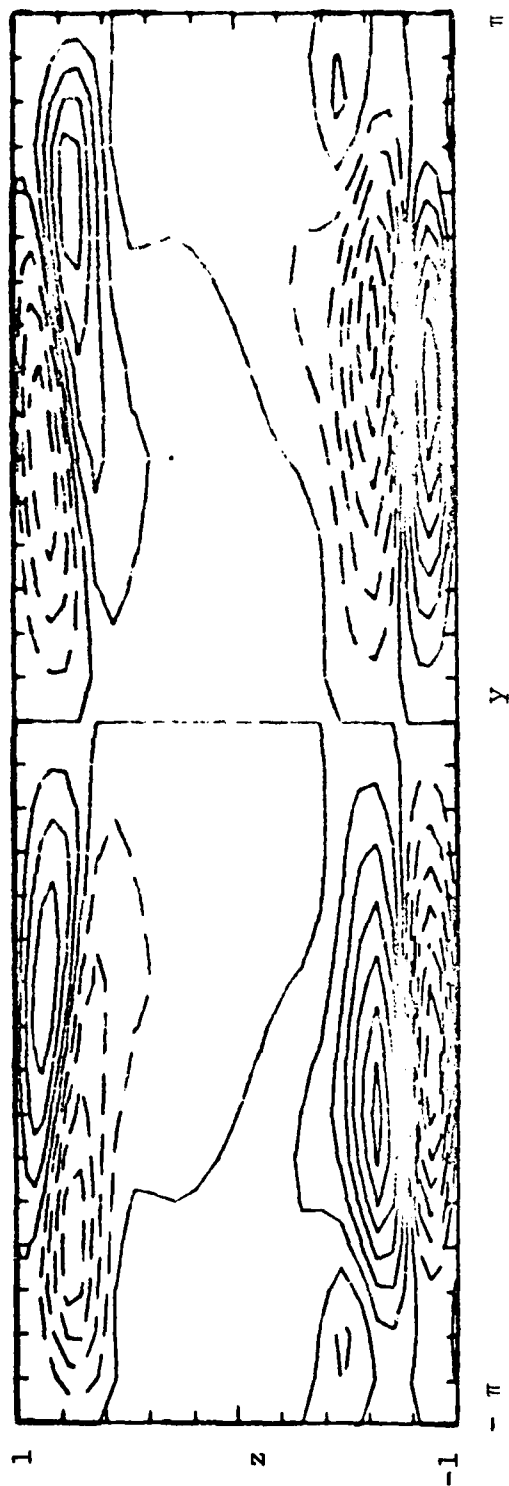
Figure 20(a)
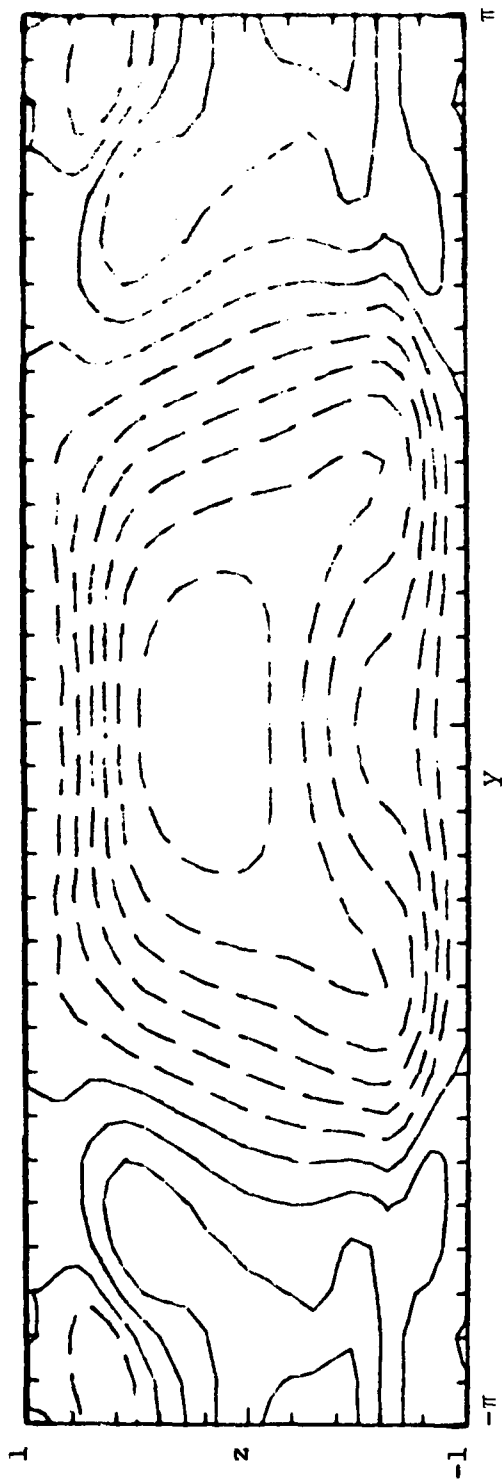
Figure 20(b)

END
DATE
FILMED
1-85
DTIC
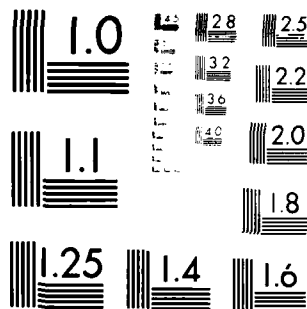
MICROCOPY RESOLUTION TEST CHART

NATIONAL BUREAU OF STANDARDS 1963 A
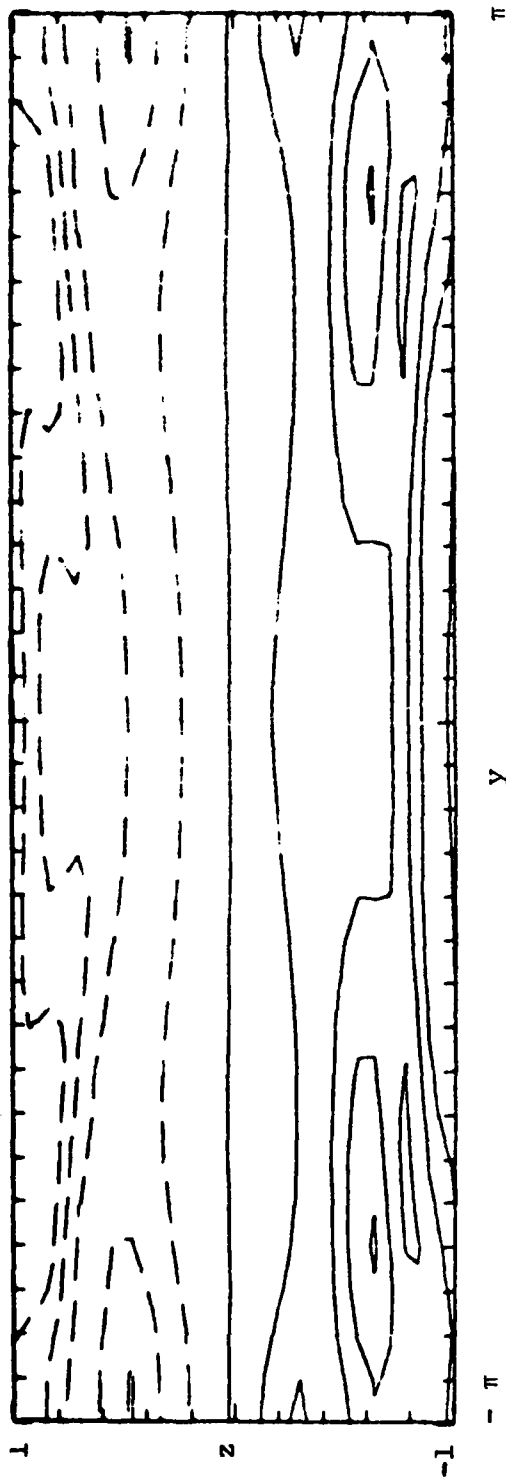
Figure 20(c)
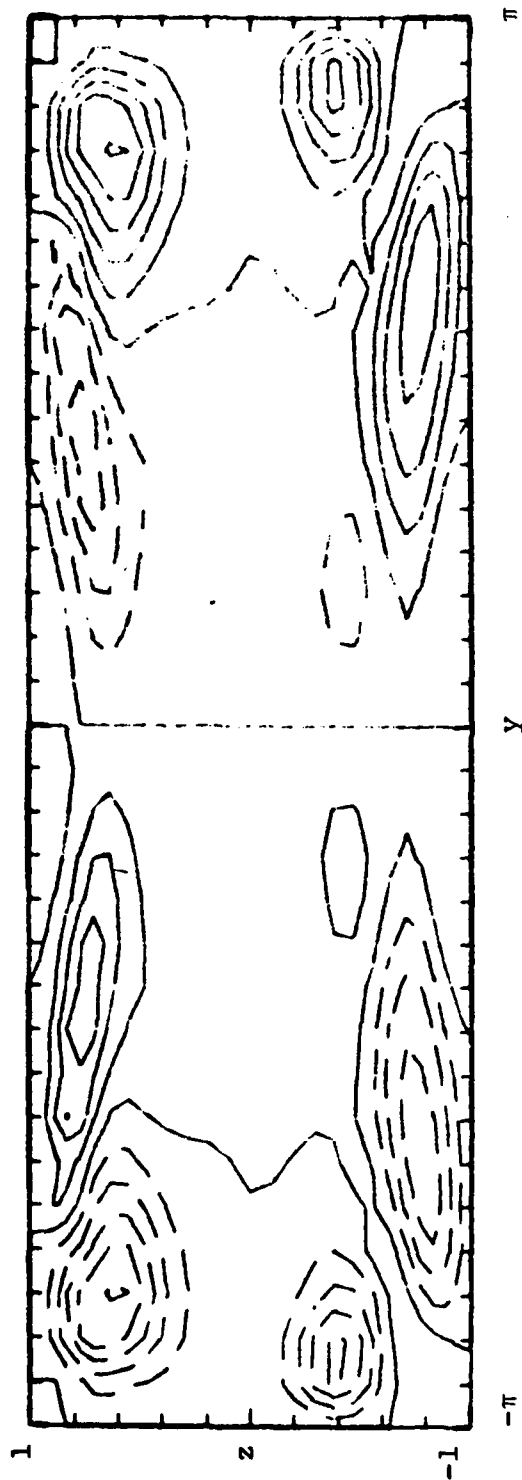
Figure 20(d)
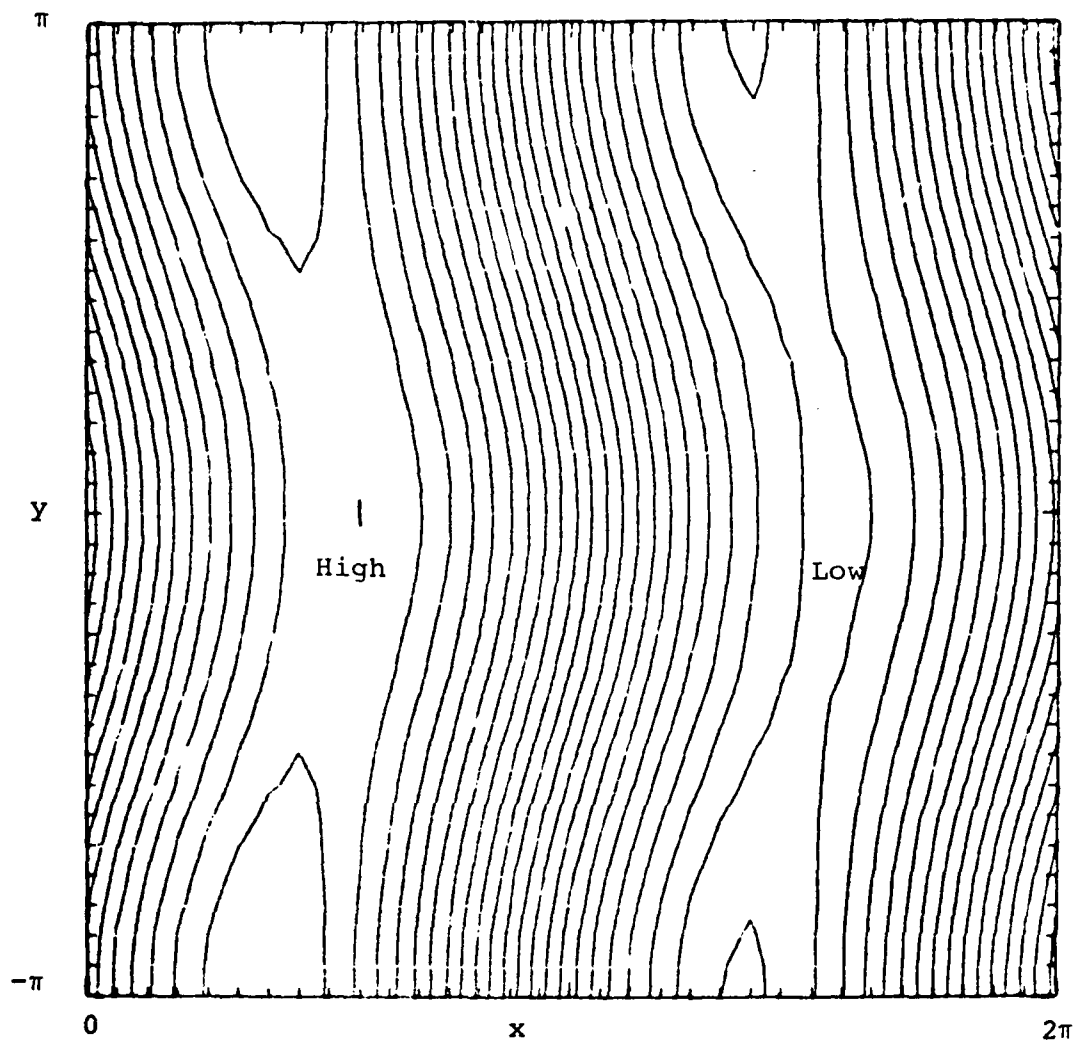
Figure 21(a)
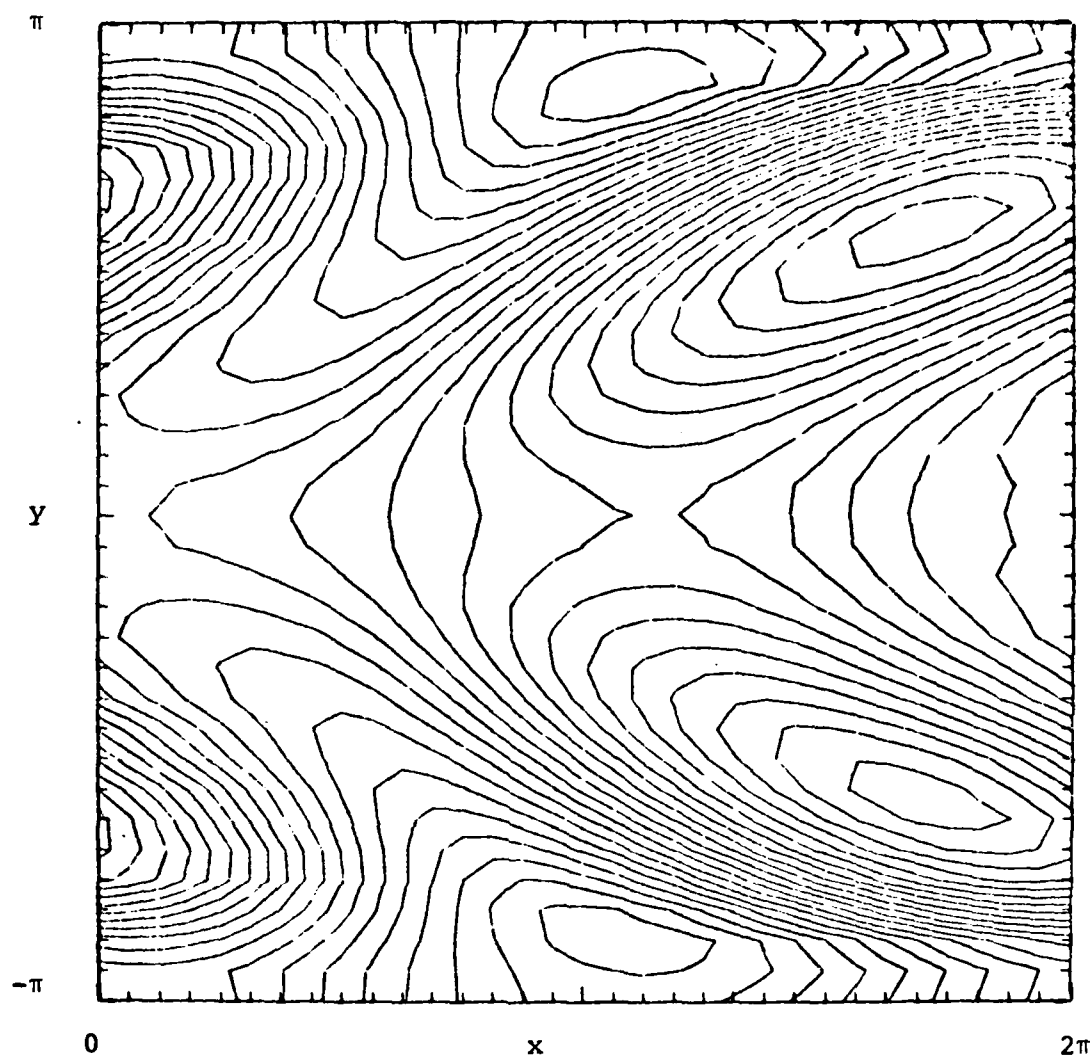
Figure 21(b)
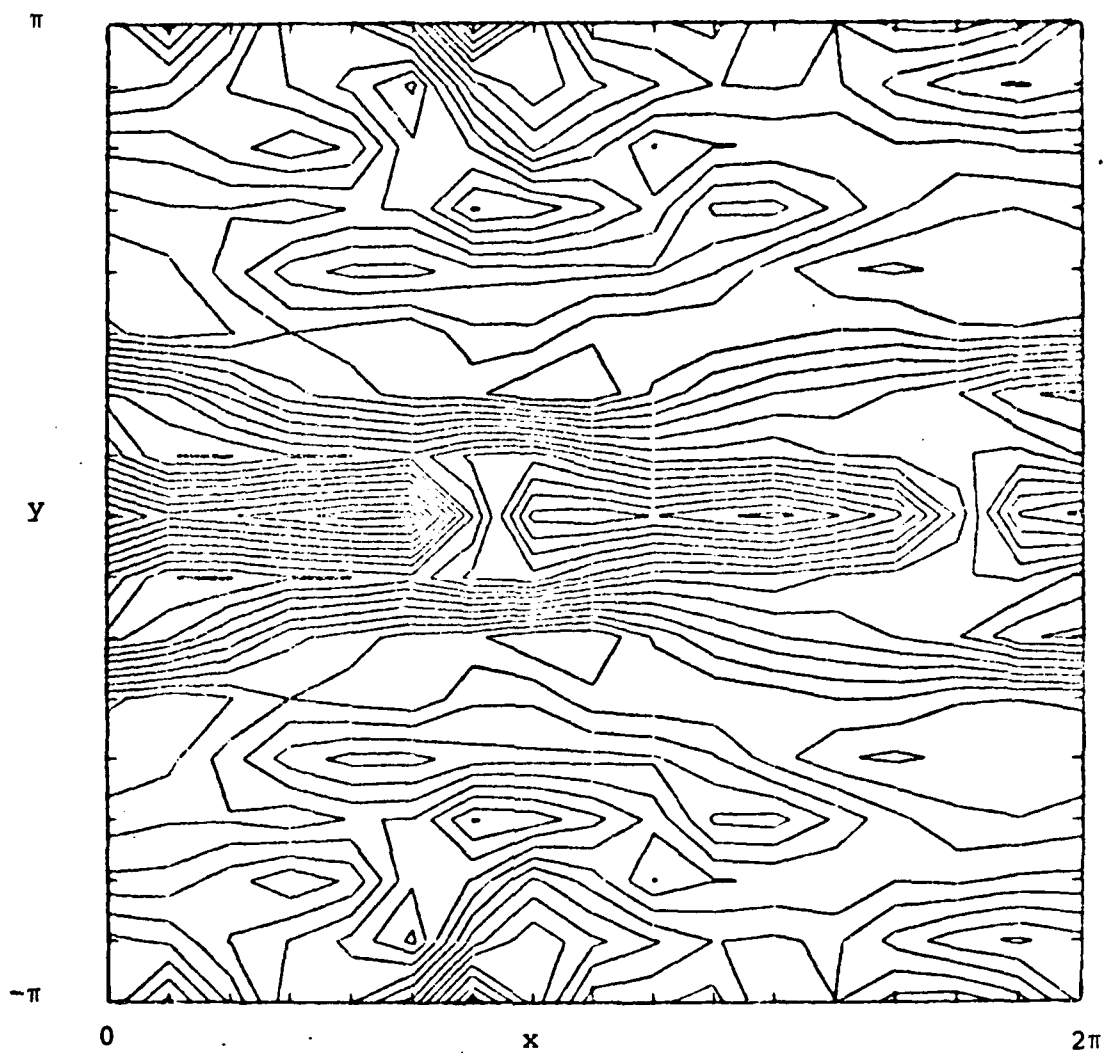
Figure 21(c)
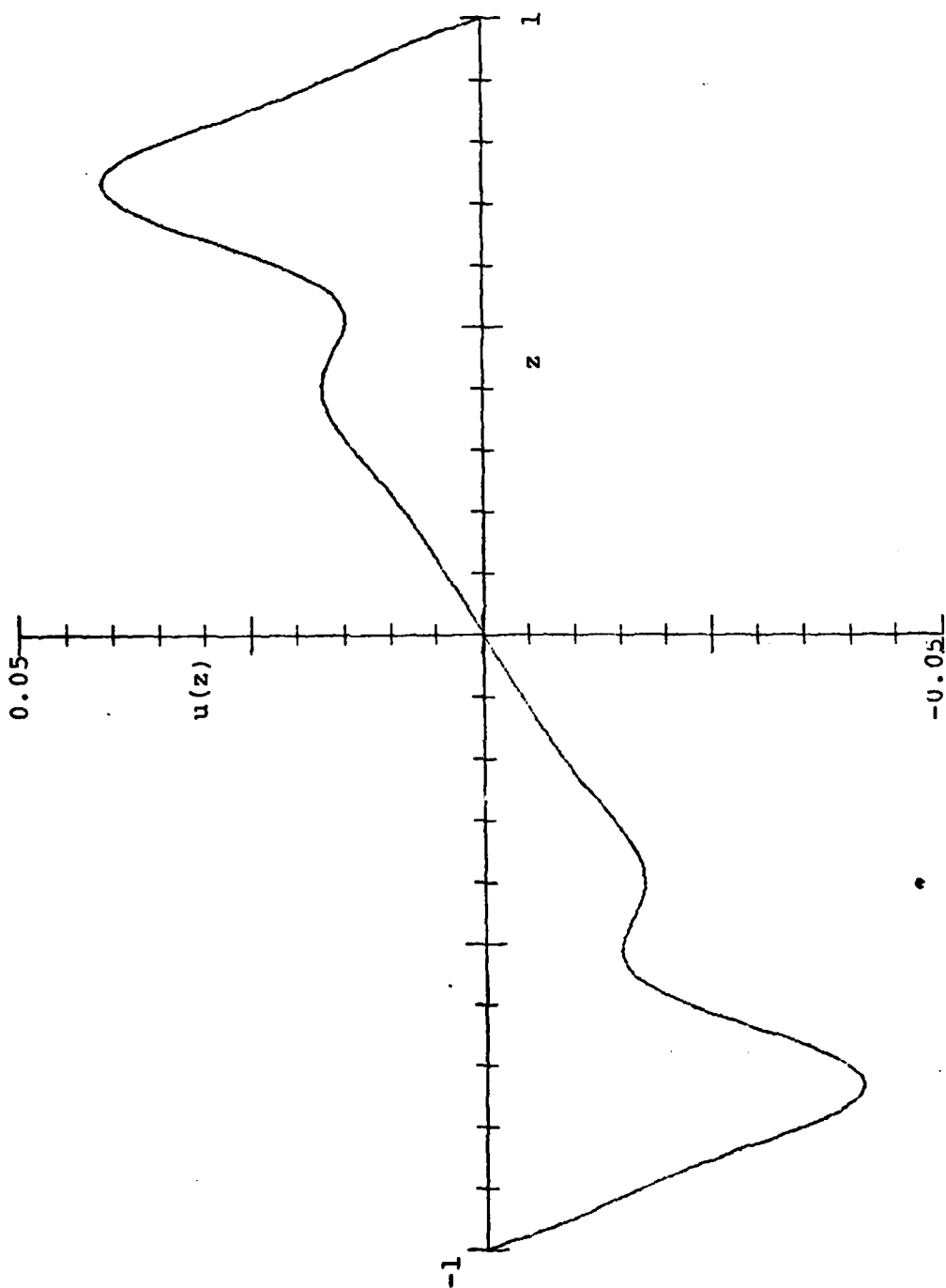
Figure 22(a)
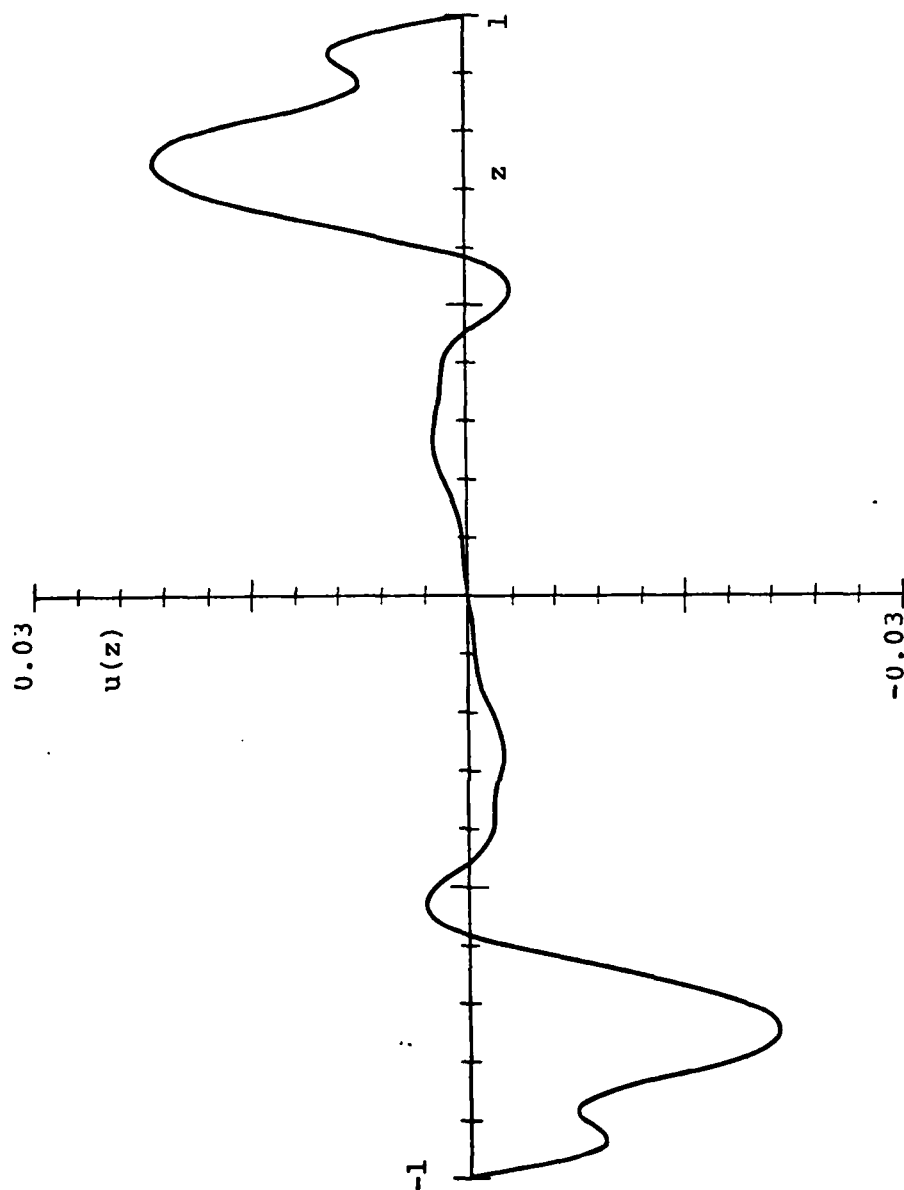
Figure 22 (b)
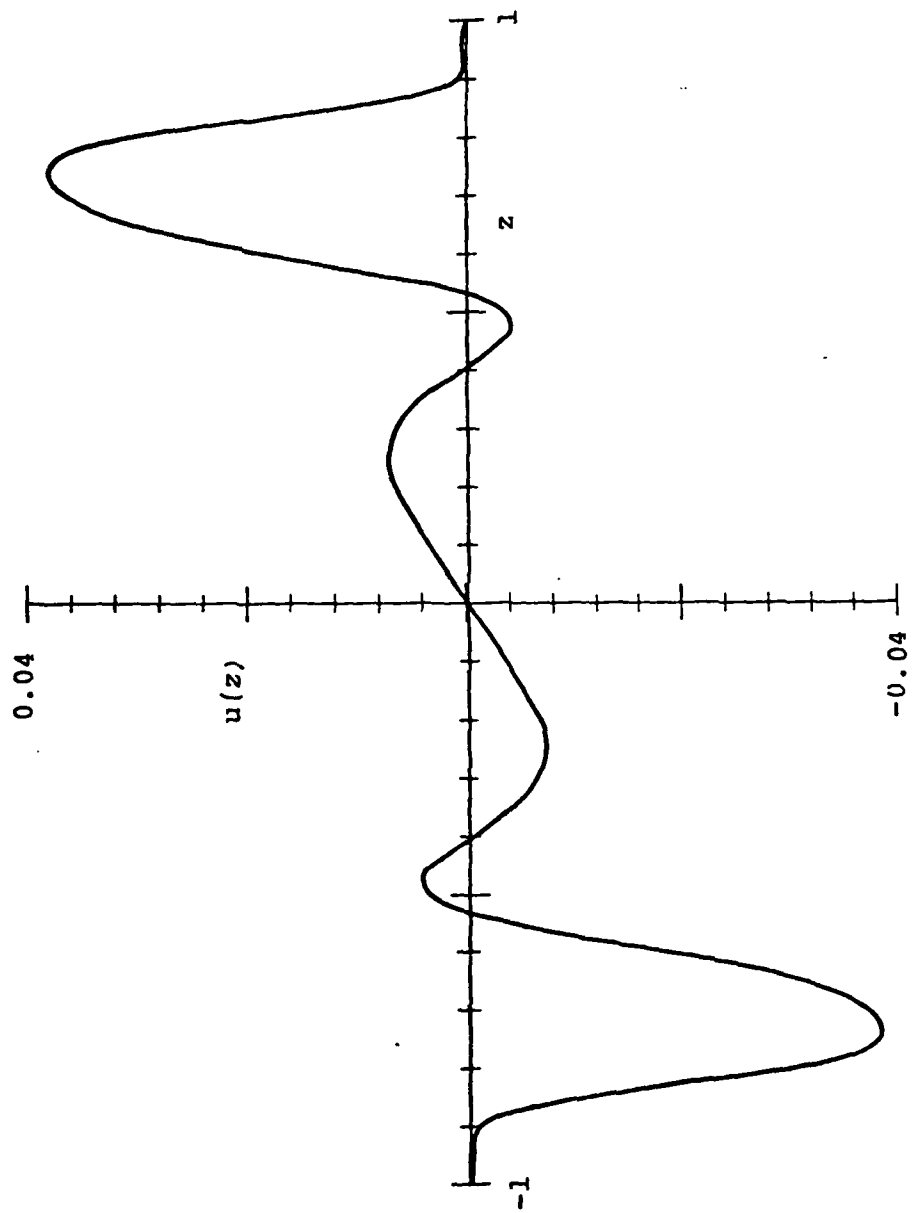
Figure 23

Figure 24

Figure 25

Figure 26

Figure 27

Figure 28

Figure 29

Figure 30

Figure 31

Figure 32

Figure 33

Figure 34

Figure 35

Figure 36

Figure 37